On the determination of diffusion coefficients in bone

Shokry, Abdallah

2015

Department of Construction Sciences
Solid Mechanics

ISRN LUTFD2/TFHF-15/1052-SE(1-132)
ISBN: 978-91-7623-313-9
ISBN: 978-91-7623-314-6

ON THE DETERMINATION OF DIFFUSION COEFFICIENTS IN BONE

Doctoral Thesis by

Abdallah Shokry Mahmoud Ali

Printed by Media-Tryck AB, Lund, Sweden
For information, adress:
Division of Solid Mechanics, Lund University, Box 118, SE-221 00 Lund, Sweden
Homepage: http://www.solid.lth.se

Preface

The work presented in this thesis is the outcome of my Ph.D. studies, which started in autumn 2011 and was performed at Division of Solid Mechanics at Lund University.

I would like to thank Erasmus Mundus Action 2 and Division of Solid mechanics at Lund University for financial support. Also, I would like to thank the Industrial Engineering Department at Fayoum University that gave me the opportunity to pursue my Ph.D. at Lund University.

Special thanks and sincere appreciations to Professor Per Ståhle, Division of Solid Mechanics, Lund University for his main supervision, fruitful assistance, continuous motivation and valuable advices. Likewise, I am thankful to Assistant Professor Ingrid Svensson, Department of Biomedical Engineering, Lund University for her assistant supervision, kind advices and encouragement throughout this work.

I would like to express my appreciation to Professor Abd El Khalik Radwan, Professor Mohammad Megahed, Department of Mechanical Design and Production Engineering, Faculty of Engineering, Cairo University, Professor Mohamed El-Shennawy, Mechanical Engineering Department, Faculty of Engineering, Helwan University and Doctor Mohammad Attia, General Electric Global Research, Niskayuna, USA for their support and encouragement.

I am grateful to my colleagues and all members of the Division of Solid Mechanics, Lund University for their kind help and support during my studies. A big thanks to my Egyptian friends in Lund, Tarek Selim, Ahmed Fawzy, Mohamed Abellah, Wael Awad, Mostafa Fekry, Ahmed Mohsen, Abdelrazek Mousa, Mohamed Hagras, and Wael Mubarak for the nice time that I have spent with them.

A great thanks to my mother, Samira, who sacrificed a lot to see me at a higher rank, my sister, Reda and her husband, Mohamed, and my brother, Mahmoud, for their support and encouragement. Finally, a warmest thanks to my beloved wife, Fathya, and my lovely kids, Gehan, Mahmoud, and Mostafa, for their support and inspiration during these years.

Lund University, April 2015

Abdallah Shokry Mahmoud Ali

Abstract

Diffusion in bone is needed for bone remodeling and bone healing. Understanding the phenomenon is often important for comprehension bone diseases. Mathematical modeling of the diffusion processes is a required prerequisite in the study of this important physical process in living bone tissue. A proper model is crucial in order to obtain realistic results. An easily accessible method to measure the diffusion coefficient in bovine bone is used in this work. In short, cortical bovine bone samples, that are saturated with potassium chloride are put in distilled water. The escaping chloride and potassium ions increase the conductivity of the water and the increase is registered over time.

In a first model, for simplicity, bone is regarded as a homogeneous material with position independent diffusion properties. However, it is well known that the bone structure in the shafts of the long bones is an in-homogeneous material with higher porosity closer to the medullary cavity and becomes denser closer to the outer surface. Because of this, a position dependent diffusion parameter is introduced in a second model. This improves the simulation model, and provides more realistic results. To determine the diffusion coefficients with good accuracy, an inverse method, a Kalman filter, is used to extract the diffusion coefficients from experiments for both constant diffusion and position dependent diffusion. The Kalman filter takes both measurement noise and material parameters noise into account. The results from the Kalman filter process are sensitive to the selection of initiation parameters, that have to be chosen carefully to avoid false local attractors or divergence. In this context, a method to determine diffusion coefficients is suggested together with recommendations on how to select the initiation parameters. To qualify the method a Kalman filter is applied on generated measurements with added noise . Finally, a method to determine the diffusion coefficient and the elastic properties of porous bone samples is derived. The method is based on a superposition principle, that employed dimensional scaling and established shape factors. The latter are found using finite element calculations for a few classes of characteristic pore shapes. The method is evaluated regarding both diffusion and mechanical behaviour on two real cases.

Abstract (Arabic)

ملخص

يعتبر الانتشار في العظام أمراً أساسياً في كلٌ من إعادة بناء العظام والتئام العظام. غالباً ما يعتبر تحليل هذه الظاهرة أمراً هاماً في معرفة أمراض العظام. تمثل النمذجة الرياضية لعمليات الانتشار متطلباً هاماً وذلك بالنسبة لدراسة العملية الفيزيائية التي تحدث في أنسجة العظام الحية. يعتبر النموذج الجيد بالغ الأهمية من أجل الحصول على نتائج حقيقية. وقد تم في هذا البحث استخدام طريقة بسيطة لقياس معاملات الانتشار في العظم البقري. باختصار، يتم وضع عينات من العظام القشرية للبقر المشبعة بكلوريد البوتاسيوم في الماء المقطر؛ حيث يزيد انتشار شاردات الكلوريد والبوتاسيوم من توصيلية الماء مع مرور الزمن.

في نموذج أول وللبساطة، تم اعتبار العظم كمادة متجانسة بخواص انتشار غير مرتبطة بالموقع، غير أنه من المعروف جيداً بأن بنية العظم في محاور العظام الطويلة مادة غير متجانسة ذات نفاذية متزايدة وذلك بالقرب من التجويف المتوسط وتصبح أكثر كثافةً بقرب السطح الآخر. ومن اجل ذلك تم إضافة معامل انتشار مرتبط بالموقع وذلك في نموذج ثاني؛ مما يؤدي إلى رفع جودة المحاكاة و الحصول على نتائج أكثر واقعية. لقد تم استخدام طريقة عكسية تسمى كالمان فلتر من اجل الحصول على معاملات انتشار في حالتي الانتشار الثابت والانتشار المرتبط بالموقع بدقه عاليه. تأخذ طريقة كالمان فلتر أخطاء القياس وأخطاء المعاملات بعين الاعتبار؛ كما تعتبر نتائجها ذات حساسية مرتبطة باختيار القيم البدائية للمعاملات والتي يجب أن تقترح بعناية لتجنب الانحراف وعدم التقارب. وفي هذا الإطار، تم اقتراح طريقة لتحديد متغيرات الانتشار مصحوبة بتوصيات لكيفية اختيار القيم البدائية. تم تقييم هذه الطريقة باستخدام كالمان فلتر اعتماداً على قياسات مولدة و مقرونة بالاضطرابات. وأخيرا تم اشتقاق طريقة لتحديد معامل الانتشار وخواص المرونة في عينات العظام؛ حيث تعتمد هذه الطريقة على مبدأ التنضيد وفيه يتم استخدام عوامل مرتبطة بالشكل والأبعاد. وقد تم إيجاد هذه العوامل باستخدام طريقة العناصر المحدودة وذلك لبعض الأشكال من الفجوات. تم تقييم هذه الطريقة لكلٌ من الانتشار والسلوك الميكانيكي بتطبيقها على حالتين حقيقيتين.

sammanfattning

I Sverige drabbas årligen så många som 100.000 personer av benbrott, höftfrakturer och sjukdomar, som kan kopplas till benskörhet. Under normalt åldrande ändras benets struktur och täthet vilket ökar risken för benbrott. Man vet att förändringarna förorsakas av förändringar i skelettets förmåga att ombildas. Under hela livet byts benvävnaden successivt ut och ersätts av ny och balansen regleras den kemisk-fysiska miljön som omger bencellerna. När man blir äldre störs balansen så benvävnaden in återskapas i samma takt som den gamla dras tillbaka. Den kemiska miljön uppstår och underhålls genom transport av näringsämnen och signalsubstanser genom benvävnaden. Transporten sker genom diffusion, som pådrivs på ett eller annat sätt, av gradvisa skillnader sk. gradienter i koncentration, mekanisk töjning, elektro-kemi eller temperatur för att nämna de flesta fenomen som kan vara aktuella. Diffusionen utan någon annan pådrivande mekanism än koncentrationsgradienten har visat sig vara otillräcklig åtminstone för transport av näringsämnen genom den relativt täta benvävnaden.

En pådrivande faktor som ligger nära till hands är de töjningsgradienter som uppstår vid mekanisk belastning. Det är känt att motion ökar tätheten hos benvävnaden och ökar skelettets hållfasthet. Ihärdigt tuggande med nya tandimplantat stärker tandens infästning i käkbenet. Man har också sett hur felkonstruerade tandimplantat gjort att benet runt implantatet har dragit sig tillbaka och skapat en glugg mellan implantatet och käkbenet. I teorier som tagits fram tidigare har vi kunnat visa att diffusionen, som normalt är riktad bort från delar där koncentrationen är hög utan särskild annan riktning, vid mekanisk belastning styrs mot ställen i skelettet där belastningen är hög. Experiment på motionerande kalkoner visar att bentillväxten sker på just dessa ställen. För att förklara fenomenet har det framförts en lång rad av förklaringar, från sådana som är mer eller mindre välgrundade till sådana som är minst sagt korkade.

En avgörande brist för utveckling och verifiering av ny teori är frånvaron av uppmätta materialegenskaper. Det är här den föreliggande avhandlingen kommer in. Det finns gott om matematiska modeller som beskriver diffusion men precis som all annan fysik är modellerna empiriskt baserade. dvs modellens parametrar måste bestämmas genom experiment. Avhandlingen beskriver en relativt enkel metod för att mäta diffusionshastigheten i ett benprov. Metoden baseras på att man mäter joner som diffunderar genom benprovet och passerar ut i ett omgivande vattenbad. I vattenbadet kan konduktiviteten mätas med hög noggrannhet. Mätningen pågår tills jämvikt har uppnåtts.

För att ta fram materialdata från mätningarna har en invers metod, Kalman filtrering, som har flera fördelar som att den är rekursiv, kan optimeras för olinjära material och lämpar sig väl för beräkningar av parametrar i olinjära modeller. I det senare fallet används en sk Lagrangeinterpollering baserad på en mindre serie av finita-elementberäkningar använts. Diffusionsmodeller för material med diffusionskoefficienter som varierar gradvis mellan benets inner och ytteryta kräver flera parametrar för sin beskrivning. Resultatet visar att man kan bestämma hur diffusionskoefficienten varierar inne i benet. I avhandlingen har också en superpositionsteori för styvhet och diffusion i porösa material tagits fram. Teorin bygger på den energifrigörelse som ett en adderad por innebär. Med hjälp av metoden kan

man enkelt räkna ut elasticitetsmodul och diffusionskoefficient för ett material. Teorin är begränsad till material som har en volymsandel som är mindre än ca 20%.

List of appended papers

This doctoral thesis is based on the following manuscripts:

Paper A
G. Lindberg, A. Shokry, W. Reheman and I. Svensson (2014)
Determination of diffusion coefficients in bovine bone by means of conductivity measurement.
International Journal of Experimental and Computational Biomechanics, volume 2, issue 2, pages 324-342.

Paper B
A. Shokry (2015)
A methodology for using Kalman filter to determine material parameters from uncertain measurements.
Submitted for international publication.

Paper C
A. Shokry, P. Ståhle and I. Svensson (2015)
Determination of spatially dependent diffusion parameters in bovine bone using Kalman filter.
Submitted for international publication.

Paper D
A. Shokry, G. Lindberg, G. Kharmanda, and P. Ståhle (2015)
Superposition principles for calculation of diffusion and elastic parameters of sparsely porous materials.
Submitted for international publication.

Own contributions
The author of this thesis was responsible for writing and performing the Kalman filter part in paper A. In paper C, the author has taken the main responsibility for doing the experiments, developing the theories, and writing the paper. Further, the author was responsible for doing the calculations, planning and preparing, and taking part in writing paper D in collaboration with the co-authors.

Contents

1 Introduction

The diffusion process is defined as movement of matter such as ions or molecules from a high concentration area to a low concentration area in the absence of a bulk motion. The process describes an important physical phenomenon that can be observed in liquid, gas, and solid phases. In the solid phase, the diffusion process occurs on the atomic or molecular length scale while liquid and gas phases might involve a variety of length scales (Glicksman, 2000).

Physically, diffusion in bone is an important process for studying bone functions. In bone, the diffusion has a clear impact on the transportation of substances from the medullar cavity to the outer surface of the skeletal bone. Substances that promote bone growth are possibly among these (Banks-Sills et al., 2011; Lindberg et al., 2013). The diffusion of substances at the cellular level also needs to be understood. This is required in studies of the interactions taking place in the bone structure, and to improve the cellular environment that is from the medullar cavity to the outer surface of the skeletal bone. Input regarding diffusion in bone can probably fill a gap in the existing mathematical models for bone remodeling and bone healing.

There is a large variety of techniques that can be used to study diffusion. Accessibility, complexity and cost varies. Also the need for sample preparation, specific technician skills and experience varies. The ability to study different diffusing substances such as, large molecules, small molecules, atoms, ions also is more or less limited. Among the more complex but more direct, in the sense that the diffusing substance and its spatial distribution may be observed, are computed tomography (CT) and different techniques using magnetic resonance (MR). The fact that these techniques have a focus on producing high resolution images on the expense of accuracy is disadvantage when precise model parameters are sought. Measurements using neutron diffraction and synchrotron light can also be used to study diffusion. A general problem is the accessibility and in many facilities the resource allocation system is a problem to say the least.

In addition to this, there is also a large variety of inexpensive methods that focuses on the resolution of measurements. One such method is used in this work. In brief, the increase of the conductivity when potassium chloride (KCl) ions escape into distilled water is measured over time. The diffusion coefficients are then determined inversely by using a mathematical model based on Fick′s law of diffusion.

Experimental results are always related to more or less noise. The noise can be in the form of measurement noise or parameter noise. The measurement noise might be associated with, e.g., external influence, instrumentation or calibration while thermal fluctuations or in-homogeneous structure might be reasons for parameter fluctuations, here termed as parameter noise. The conventional methods that commonly are used to determine material parameters, such as non-linear least squares method do not take noise directly into account. The Kalman filter, a method to determine material parameters from indirect and uncertain measurements can be effectively used, just because it takes noise of both the parameters and measurements into consideration (Kalman, 1960). Also, it speeds up the rate of convergence.

In this thesis, the first paper deals with determination of diffusion coefficients on bovine bone using conductivity measurements. A Kalman filter is used to obtain the diffusion coefficients. Because of problems with convergence and a sensitivity to initial conditions that was encountered, the second paper focuses on the Kalman filter description, and presents a method that improves the stability and robustness of the Kalman filter to determine diffusion coefficients from uncertain measurements. The third paper presents a model for linear position dependent diffusion, and successfully uses the Kalman filter to determine diffusion coefficients at endosteal and periosteal surfaces in bone. The technique from paper two is used and the problem with divergence is found to be almost absent. Finally, the fourth paper presents a superposition method to compute the diffusion coefficient and elastic modulus in a bone sample that contains irregular pores. The basis for the method is a series of finite element calculations of the changed flux or stress due to individual pores.

2 Diffusion theory

A mathematical representation for diffusion as a physical process is extensively helpful. It quantifies the behaviour of the diffusive substance in tissue materials and organs, which can be helpful for studying and simulating their functions.

The diffusive behaviour in many materials are sufficiently accurately described by Fick′s laws for diffusion. In these, the rate of matter that passes through a unit area is proportional to the concentration gradient normal to this area, which mathematically represented the Fick′s first law for diffusion as

$$J = -D\nabla C \tag{1}$$

where J is the flux vector that represents the rate of matter transfer per unit area, D is the diffusion coefficient, C is the concentration, and ∇ is the gradient vector in a Cartesian coordinates system,

$$\nabla = \left(\frac{\partial}{\partial x}, \frac{\partial}{\partial y}, \frac{\partial}{\partial z}\right). \tag{2}$$

Mainly, the diffusion process needs time to be completed. The rate of change of the matter concentration with respect to time is given by Fick′s second law for diffusion as

$$\frac{\partial C}{\partial t} = -\nabla \cdot J = \nabla(D\nabla C) \tag{3}$$

where t is the time.

The diffusion coefficient in Eqs. (3) and (1) may be dependent of position, concentration, time, etc.

Many solutions to Eq. (3) for homogeneous and in-homogeneous materials for different initial and boundary conditions were presented over the years (cf. e.g. Crank (1975)).

Both diffusion mobility and solubility may be affected by the material structure. Consequently, the accuracy of Fick′s laws become less accurate and may even not at all be described as Fickian diffusion. Collectively these diffusion processes are so called non-Fickian

diffusion. Several authors have studied non-Fickian diffusion using non-linear partial differential equations (Peppas and Reinhart, 1983) or statistical mechanics to study the so called Fokker–Planck diffusivity (Van Milligen et al., 2005). Onsager introduced other driving forces for diffusion than the concentration gradient (Onsager, 1931). Among other phenomena, this theory may be used for studies of diffusion driven by mechanical stresses (Banks-Sills et al., 2011)

3 Diffusion in bone

The transport of substances from the endosteal surface on the inner boundary near the medullar cavity to the periosteal outer surface of long bones, is here described as a diffusion process. The transport mechanism is important for the bone metabolism, and creates a good environment for healthy bone. Bone remodeling, in which old bone tissue is replaced by new tissue, is a natural process that continuously takes place in living bone tissues. Also, bone healing, in which repairing of the bone structure after fracture is a process relaying on a good bone environment. Knowing more about the diffusion process and a numerical value for the diffusion coefficients is important to build mathematical models of both bone healing and bone remodeling processes.

Knowledge about diffusion in bone may be useful for understanding diseases that attack the bone such as metastatic bone cancer, the spread of cancer in bone after triggering in organs, and myeloma, a cancer that starts in the plasma cells in the bone marrow and affects the bone tissue. The metastatic and myeloma bone cancer make the bone weak and susceptible to fracture (Messiou and Desouza, 2010). Osteoporosis is a bone disease, in which both bone mass and density are decreased, which deteriorate the bone health and increase the risk of fracture. As for patients with metastatic or myeloma cancer, patients with osteoporosis show higher diffusivity than normal diffusivity in the bone marrow (Yeung et al., 2004).

Cortical bone forms around 80% of the bone mass (Wang et al., 2010). Functionally, it protects the other, cancellous, e.g. more spongy parts of the skeleton and supports the whole body because cortical bone is dense and strong. Also, a large number of pores and canals are located in cortical bone, in which blood vessels pass through, which allows nutrients and oxygen to move from the blood vessels to the bone. The porosity in the cortical bone, i.e. the volume fraction of the pores, ranges from 5-10% with different pores shape and size. Fig. 1 shows a CT image for a compact bovine bone sample that taken in the shaft from a femur bone.

4 Diffusion measurements

An experimental technique where the diffusing matter can be followed in time and space is required in order to determine the diffusion coefficients. Several techniques can be found in the literature, some of the them are complex and expensive while others are more

straightforward.

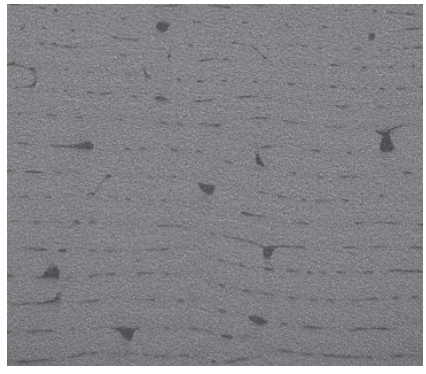

Fig. 1. CT image for a bovine cortical bone shows different pores size and shape (4 μm resolution), c.f. (Ståhle et al., 2013)

Nuclear magnetic resonance (NMR) can be used to investigate the physical and chemical properties of atoms and molecules using the magnetic properties of a specific nuclear spin (Stejskal and Tanner, 1965). It has been used extensively for measuring diffusion coefficients in biology and biomedical fields (Burstein et al., 1993; Fernandez-Seara et al., 2002). The NMR measures the atoms motion. The motion is monitored by measuring spatial positions for atoms or molecules with the specific nuclear spin at two different times. The NMR method can be used for following diffusion processes during a long period of time but the method is not easily accessible.

Diffusion magnetic resonance imaging (dMRI) is presented as a new application of the NMR technique (Merboldt et al., 1985). The dMRI technique is based on the characterization of water diffusion properties for each pixel in an image. In fact, the diffusivity of water is quite high in some organs such as the brain. Consequently, the technique can be used to study the structure properties in specific organs, in addition to measurements of the diffusion coefficient.

Fluorescence intensity, the escaped light from a substance that absorbed light, is the core of fluorescence correlation spectroscopy (FCS). It is firstly presented by Magde et al. (1972). In this technique, a tiny substance emits fluorescence into a solution that contains small fluorescent particles. The particles randomly move, and consequently fluctuate the fluorescence intensity. The fluorescence is followed over time. The diffusion coefficient can be determined from fluorescence time.

A less complex method and for quantitative determination probably more accurate method is used in this work to measure the diffusion coefficients. The method starts by putting a bone sample into a solution of potassium chloride for sufficient time to be close to fully saturated. After that, the samples are quickly rinsed in distilled water, and molded in polyester to close axial and tangential directions leaving only the radial direction opened. Finally, the conductivity of the escaped ions from the sample when placed in distilled water is followed over time. Fig. 2 shows three different stages for sample preparations and

a conductivity measurement.

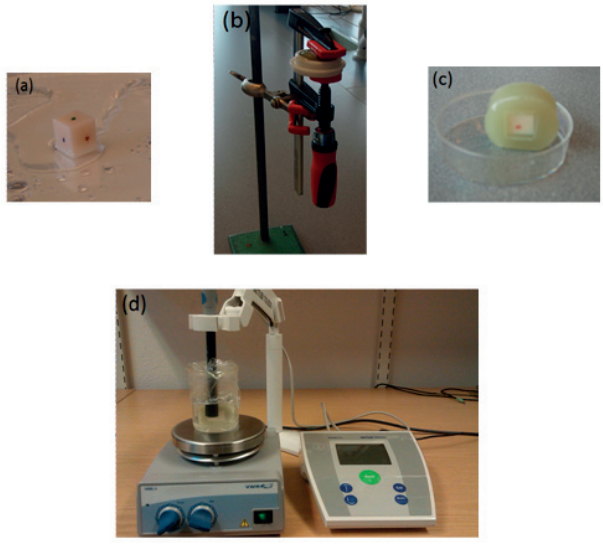

Fig. 2. (a) Cubic bovine bone sample with around 1 cm edge length, (b) the bone sample is hold in a clamp when the polyester is curing, (c) after the polyester has cured, it is now sealed in the axial and tangential directions and open in radial direction, (d) conductivity measurement using a SevenEasy S30 conductivity meter from Mettler Toledo.

The diffusion coefficient in one dimension can be determined by constituting the relation between the concentration and the conductivity as

$$\xi = A + \frac{B}{L}\int_0^L C(x,t) \tag{4}$$

where ξ is the conductivity, A and B are two constants that constitute the relation between the concentration and the conductivity, and L is the bone wall thickness. The concentration, C, is obtained by solving Eq. (3) with proper initial and boundary conditions. In the experiment, the initial conditions are

$$C(x,0) = C_0, \qquad \text{for} \quad 0{<}x{<}L \quad \text{at} \quad t{=}0, \tag{5}$$

where C_0 is the initial concentration, and t is the diffusion time. The boundary conditions are

$$C(0,t) = C(L,t) = 0, \qquad \text{for} \quad t{\geq}0\,. \tag{6}$$

The solution for $C(x,t)$ for constant diffusion is given by Crank (1975) as

$$C(x,t) = \frac{4C_0}{\pi}\sum_{n=0}^{\infty}\frac{1}{2n+1}\exp\{-D(2n+1)^2\pi^2 t/L^2\}\sin\frac{(2n+1)\pi x}{L}. \tag{7}$$

The solution for $C(x,t)$ for linear position dependent diffusion is given in Paper C, where $D(x)$ is assumed to be linear with

$$D(x) = D_o(1 - \frac{x}{L}) + D_1\frac{x}{L}\,, \tag{8}$$

with $D_o > 0$ and $D_1 > 0$, where D_0 and D_1 represent the diffusion coefficients at the endosteal and periosteal surfaces respectively.

5 Kalman filter technique

The technique is obtained by Kalman and presented in 1960 (Kalman, 1960). A Kalman filter is a competitive computational inverse method to extract variables such as position, temperature, time, etc from noisy experimental data. Here, the Kalman filter is applied to extract the diffusion coefficients. Mainly, the Kalman filter consists of two processes, prediction and correction. A loop starts with the prediction of the parameters and ends with the correction of the parameters, until convergence, i.e. the corrected parameters are sufficiently equal to the predicted parameters. The details of the Kalman filter equations can be found in e.g. Brown (1983).

The corrected parameters are given by

$$x_{k+1} = x_k + \mathbf{K}_k\{z - \zeta(x_k)\} \tag{9}$$

where x is an $n \times 1$ vector that represents the sought parameters, z is an $N \times 1$ vector that contains the measurements, ζ is an $N \times 1$ vector that introduces predicted measurements using the predicted parameters, x, k is a time step, and $\mathbf{K}_k$ is denoted the Kalman gain that is derived to minimize the covariance error of the parameters. The Kalman gain is given by

$$\mathbf{K}_k = P_k\mathbf{H}_k^{\mathrm{T}}(\mathbf{H}_k P_k \mathbf{H}_k^{\mathrm{T}} + R)^{-1} \tag{10}$$

where P_k is an $n \times n$ matrix that introduces the covariance error of the parameters, R is an $N \times N$ matrix that represents the covariance error of the measurements, $\mathbf{H}_k$ is an $N \times n$ Jacobian matrix that represents variation of predicted measurements with respect to changes in the desired parameters

$$\mathbf{H}_k = \begin{bmatrix} \frac{\partial \zeta_1}{\partial x_1} & \cdots & \frac{\partial \zeta_1}{\partial x_n} \\ \vdots & \vdots & \vdots \\ \frac{\partial \zeta_N}{\partial x_1} & \cdots & \frac{\partial \zeta_N}{\partial x_n} \end{bmatrix}. \tag{11}$$

The P_k is updated as

$$P_{k+1} = (\boldsymbol{I} - \mathbf{K}_k\mathbf{H}_k)P_k + Q \tag{12}$$

where Q is the covariance error of the parameters noise. Values of both x_0 and P_0 are initially required. The suggested values for x_0 and P_0 is based on the *a priori* available information of the parameters. Values have to be chosen carefully for good convergence. The initial values of R and Q have to be chosen based on measurements and parameters noise. The choice is influenced by the initial range of the parameters, x, and affects the rate of convergence (c.f. Paper B for more details about the Kalman filter description and derivation).

6 Results and discussions

In this section, a summary for the appended papers are presented. Also, the outcomes of the papers are introduced and discussed.

6.1 Paper A: Determination of diffusion coefficients in bovine bone by means of conductivity measurement

In Paper A, the diffusion coefficient in bovine bone is modeled as a constant, using Fickian diffusion. To measure the diffusion coefficient, an experimental set-up is designed. Using this set-up, the conductivity of potassium chloride ions that escape from a saturated bovine bone sample into surrounding distilled water is followed over time. A linear relation between the conductivity and the concentration is used. The diffusion coefficient is determined using the Kalman filter technique.

The diffusion coefficient, D, is determined for 14 different bovine bone samples. The sample size is approximately 10 mm cubic length. The analytical solution for the Fickian boundary value problem includes two constants A and B apart from the diffusion coefficient D that have to be experimentally determined (see Eq. (4)). The two constants A and B are assumed to be related at $t = 0$, which means B and D have to be determined. The Kalman filter is applied to determine the two constants using four different initial suggested ranges, starting with a large range and ending with a narrow range. (c.f. Paper A for more details).

Figure 3 shows the convergence of D and B for a bovine bone sample that are extracted using the Kalman filter and the last initial selected range after 1, 2, 10, and 40 iterations. It is clearly seen that the initial selected constants converged around a curve after only 1 iteration as in Fig. 3a. Then, it starts to converge to smaller area on this curve as shown in Fig. 3c, b, and d. It has been confirmed manually that the mean square error between the measurements and the predicted measurements is located on this curve. The values of D that are obtained using the Kalman filter are in good agreement with the previous work.

The analytical results for D and B, obtained using Kalman filter for two bovine bone samples plotted with the respective experimental data are shown in Fig. 4. The figure shows a good fitting between the analytical results and the experimental data for both samples. The values of D and B for the 14 different samples have a large variation. This is

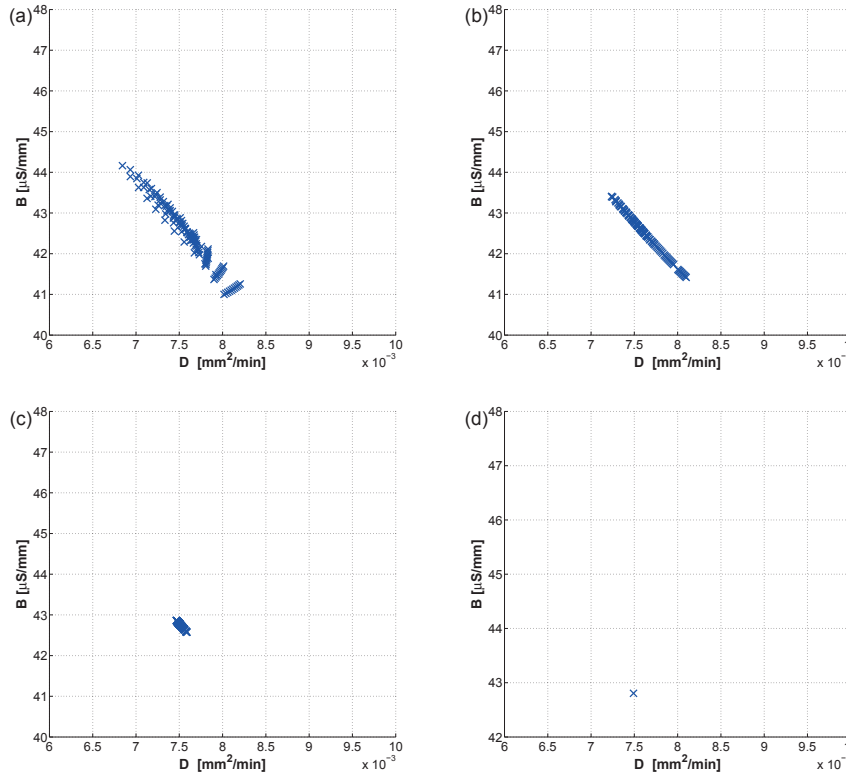

Fig. 3. Convergence of D and B for a bovine bone sample for the final range of initial parameters after (a) 1 iteration, (b) 2 iterations, (c) 10 iterations, and (d) 40 iterations.

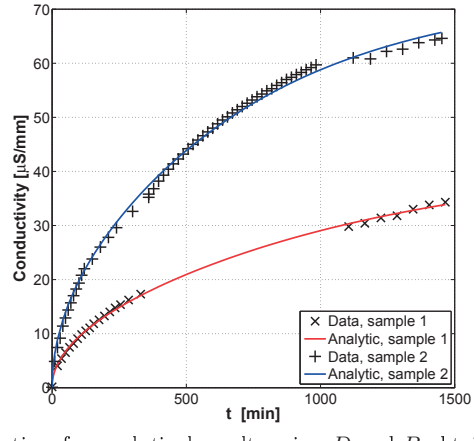

Fig. 4. Conductivity versus time for analytical results using D and B obtained by Kalman filtering for two samples. Experimental data for both samples are also included in the graph.

however not a big surprise since bone is known to have a large scatter of material properties in general.

An average value the of diffusion coefficients for the 14 samples is found to be 0.011 mm^2/min with standard deviation of 0.0069 mm^2/min. The obtained diffusion coefficients agree with previous work taking different methods and mammals into consideration (c.f. Paper A).

6.2 Paper B: A methodology for using Kalman filter to determine material parameters from uncertain measurements

In Paper B, the Kalman filter method is further investigated and refined. Focus is on the initial parameters and the covariance errors of both measurements and parameters that are required for using the Kalman filter. The first part of the study suggests a method to choose the initial suggested parameters. The second part results in a method to choose the covariance errors for both measurements and parameters. The third part is a case study where the methods from the first and second parts are applied to determine the diffusion coefficients in bovine bone using the diffusion model that has been presented in Paper A.

The effect of the covariance errors for both measurements, R, and parameters, Q, is investigated using generated data with different noises from 10% to 100%. Large R values give a small Kalman gain step as expected from Eq. (10), which means that the process becomes more stable. The effect of changing Q based on convergence, standard deviations and mean values for the obtained D for large R is shown in Fig. 5. As shown in Fig. 5a the

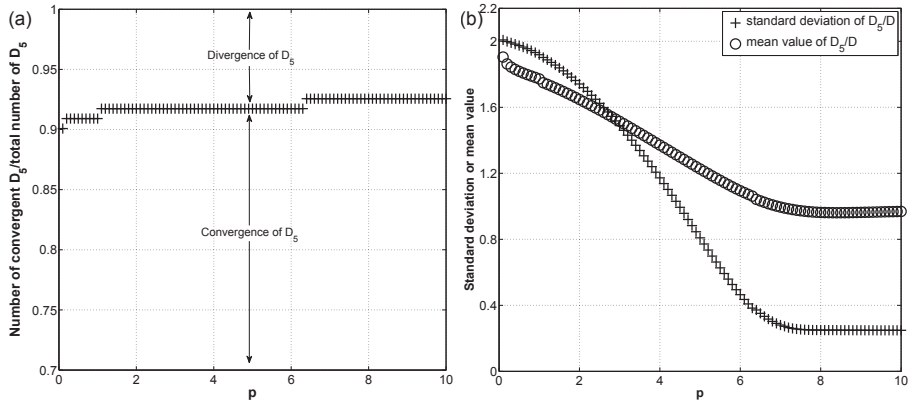

Fig. 5. (a) Effect of Q on obtained D_5/D using Kalman filter, the subscript denotes the number of iteration. D is the true diffusion coefficient. Generated data with 5% for parameters and 10% noise for measurements are used, Q is chosen to be p (*apriori* estimated relative variance) multiplied with a constant noise . (a) convergent results, (b) standard deviations and mean values.

convergent results increase as the Q increases. Further, the standard deviation decreases as the Q increases as shown in Fig. 5b, which increase the rate of convergence. One possible reason is that a large Q gives a large Kalman gain step, and the proposed combination

between large R and large Q leads to a moderate Kalman gain step, which increases the number of convergent results and increases the rate of convergence.

The determined diffusion coefficients using: (1) the Kalman filter with large R and Q, values are compared to the values that are obtained by using: (2) the Kalman filter with $Q = 0$ and (3) the Kalman filter with a "good guess" for Q based on the generated data. Also, results are compared with the diffusion coefficients that are obtained by using (4) the non-linear least squares method (see Paper B for more details). Fig. 6 shows a color plot of the obtained D_{50}/D for the four different methods. Also, it shows the convergence of D_{50}/D and B_{50}/B, where the subscript denotes the number of iterations. As shown in

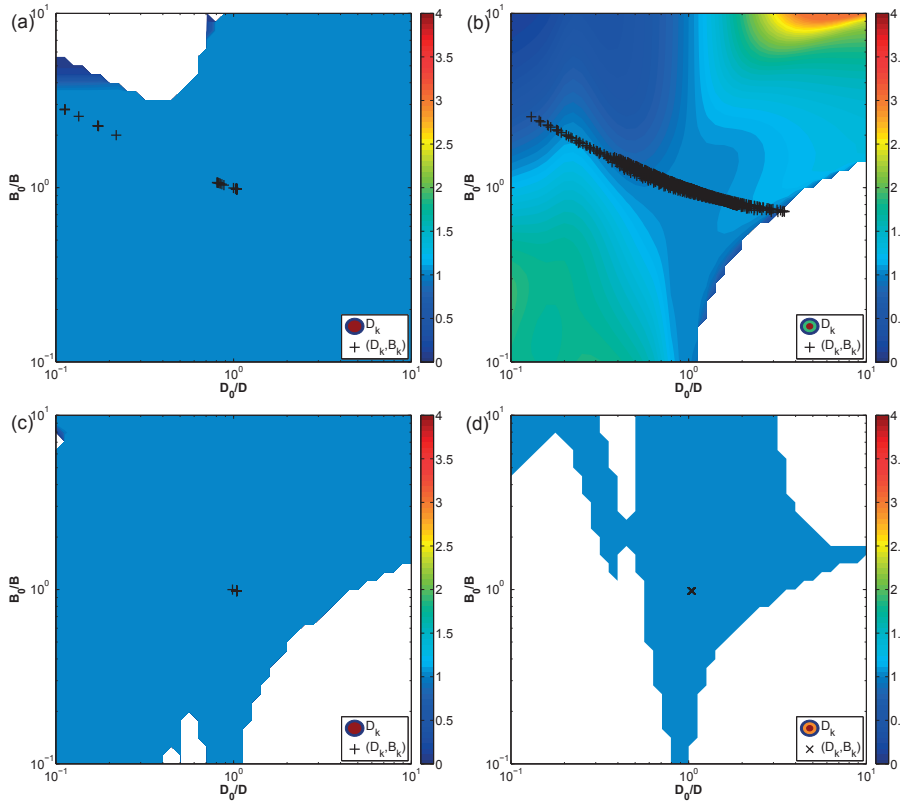

Fig. 6. Color plot for D_{50}/D merged with convergence plot between (D_{50}/D,B_{50}/B) for initial starting points D_0/D and B_0/B after 50 iterations for: (a) Kalman filter with large R and large Q, (b) Kalman filter with $p = 0$, (c) Kalman filter with $p = 0.01$, and (d) non-linear least square method. All results are for generated data with a noise of ±5% for parameters and ±10% for measurements.

the figure, the convergent results of the obtained parameters using the Kalman filter with large R and Q values (around 92.09%) are larger than those obtained from the methods 2, 3, and 4 (from 40.93% to 80.19%).

Around 98.3% from the obtained parameters using Kalman filter with large R and Q

values are converged to the true parameters after 50 iterations, while the 1.7% converged to the true parameters after 180 iterations. 100% from the converged results is converged to the true parameters using Kalman filter with $p = 0.01$ and non-linear least squares method after 50 iterations. In summation, the Kalman filter with large R and Q values can be used to determine the diffusion coefficients with high probability for convergence and also with a high rate of convergence in the case of rare information about the searched parameters. On the other hand, the Kalman filter with the Q that comes from a good assumption of the value for the parameter noise and the non-linear least squares method could be used if there is good information about the searched parameters.

6.3 Paper C: Determination of spatially dependent diffusion parameters in bovine bone using Kalman filter

In Paper C, a model for Fickian diffusion with position dependent parameters is presented. Analytical solutions are derived for a diffusion parameter that is linearly dependent on the coordinate across the bone wall thickness, c.f. Eq. (8). The experimental set-up that was used in Paper A is also used here along with the Kalman filter process to determine the linear position dependent diffusion coefficients.

The motivation for the study is that in previous studies, linear regressions between the bone wall thickness and results of how porosity decreases from the endosteal to the periosteal surface have been shown in the literature (Baron, 2012). In this context, it is believed that the diffusivity is increasing with the porosity, which means the diffusion rate is decreasing from the endosteal surface to the periosteal surface.

The diffusion coefficients D_0 and D_1 at the endosteal and the periosteal surfaces respectively are determined using Kalman filter method assuming linear position dependent diffusion as in Eq. (8) (c.f Paper C for more details). Fig. 7 shows the analytical results using the converged parameters obtained by the Kalman filter process using three different assumed initial parameter ranges for one bone sample. As a comparison, the experimental data for the sample is also presented in Fig. 7. As it can be seen in the figure, the analytical calculations give a curve closer to the experimental data as the initial range for the parameters is decreased. A possible reason for that is the using of interpolation function to predict conductivity using 27 Lagrange interpolation points, is improved when the range is narrowed in. The Lagrangian interpolation replace the analytical solution in order to save computer time. A very good fitting between the analytical results and the experimental data is found.

The convergent results for both D_0 and D_1 obtained by Kalman filter for the final range are shown in Fig. 8. The figure shows that D_0 converges to 0.00568 mm^2/min, Fig. (8a) and D_1 converges to 0.0020 mm^2/min, Fig. (8b) as the number of iterations increases. It can be seen that D_1 decreases in the beginning as the number of iterations increases, then increases again until convergence occurs. This surprising behaviour might be due to choice of the covariance of the errors of the initial parameters, P_0. Personal experience has indicated that this might be a reason. Regarding the diffusivity values, it can bee noticed

that the diffusivity decreases from the endosteal surface to the periosteal surface as it has been hypothesized in this work.

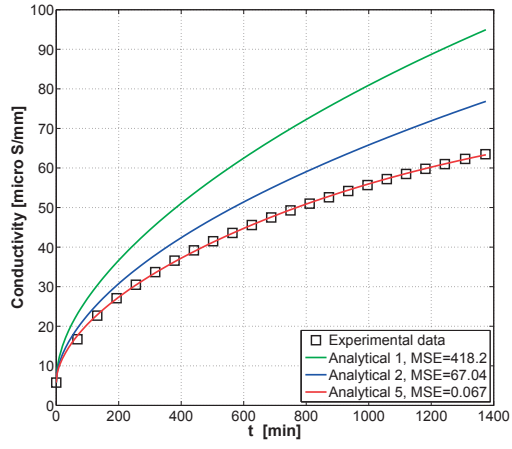

Fig. 7. Analytic results using the parameters obtained from Kalman filter using first, second, and fifth initial suggested parameters range for one sample. Experimental results for the sample is also presented in the figure. The mean square error (MSE) is included.

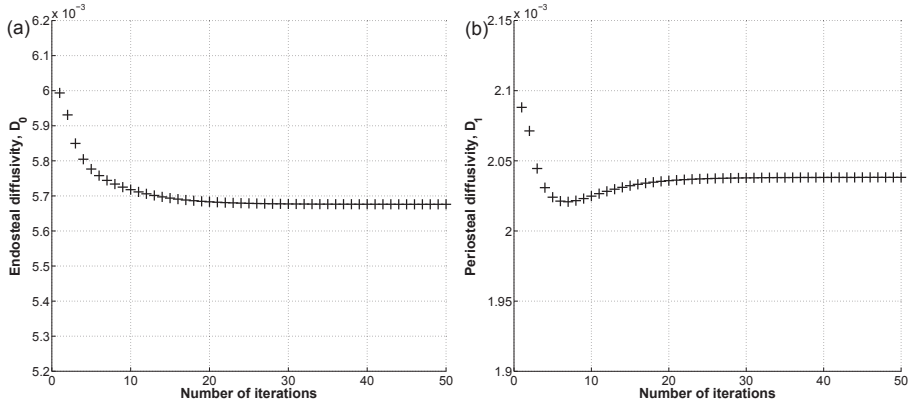

Fig. 8. (a) Diffusivity versus number of iterations. (a) endosteal diffusivity, D_0, and (b) periosteal diffusivity, D_1.

Figure 9 shows the linear position dependent diffusion that determined by Eq. (8) in the bone wall thickness, using D_0 and D_1 that are obtained by the Kalman filter for four bovine bone samples. The figure shows that the diffusivity inside the bone wall thickness is more accurately modeled as position dependent diffusion. Also, it supports a hypothesis that the diffusivity correlate directly with the porosity in the bone wall thickness. i.e. the larger porosity the higher diffusivity and vice versa. The average diffusivity in the middle

of the bone wall thickness agrees well with the findings for assumed position independent diffusion coefficients in previous work (c.f. Paper C for more details).

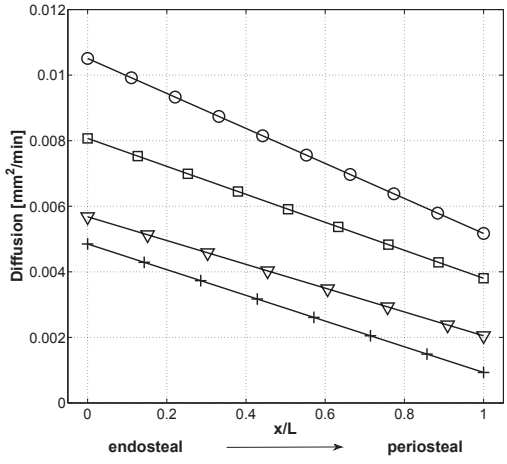

Fig. 9. Linear position dependent diffusion coefficients versus positions in the bone wall for four samples. The markers are merely identifying the specified samples.

6.4 Paper D: Superposition principles for calculation of diffusion and elastic parameters of sparsely porous materials

In Paper D, a method to determine a realistic diffusion coefficient and elastic modulus in bone in the presence of irregular pores using superposition and finite element calculations is presented. The method is based on the calculated correction factor for infinitesimal pore sizes for a few classes of pore shapes.

Figure 10 shows a small region of a bone sample that taken from a bovine cortical bone. A correction factor is obtained for pores A, B, C, and D using finite element calculations. The hypotheses assumes that the pores that almost have the same shape have the same correction factor, it also assumes that the pores do not interact with each other (see Paper D for more details).

The results show that the correction factor for the diffusion process decreases as the pore size increases (see Fig. 11a). As shown in Fig. 11b, the correction factor for the mechanical stiffness part increases as the pore size increases. In both cases, i.e. diffusivity and elastic modulus, the correction factors show dependent results on the shape of the pore. Here, the correction factors are obtained in bone related radial, x_1 direction, and tangential, x_2 direction, for different pore sizes with a and b in x_1 and x_2 directions respectively. The a versus b is the pore side ratio.

The superposition method is applied for a region with pore marked D and 1 to 11 in Fig. 10 to compute the diffusivity and the elastic modulus as a benchmark example. The results show that the difference between the change in the calculated diffusivity using finite

element calculations and the change of the calculated diffusivity using superposition are 9% and 4% in the radial and the tangential directions respectively. In case of elastic modulus, 6% and 14% in the radial and the tangential directions respectively are the differences. Here, the change is considered as the difference between the obtained diffusivity or elastic modulus for the region with pores and the diffusivity or the elastic modulus for the region without pores.

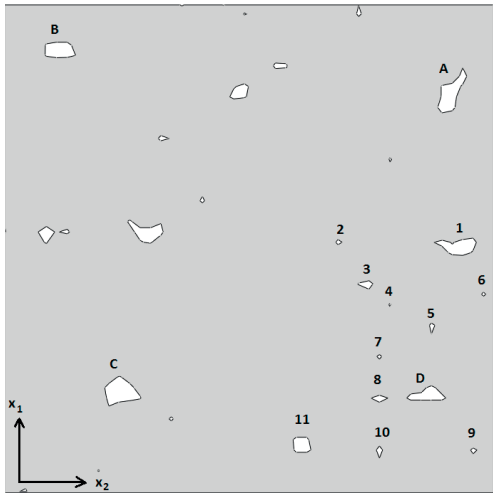

Fig. 10. A region from bone sample contains irregular pores. The region constructs a square with 94 pixels length from an image taken by CT technique.

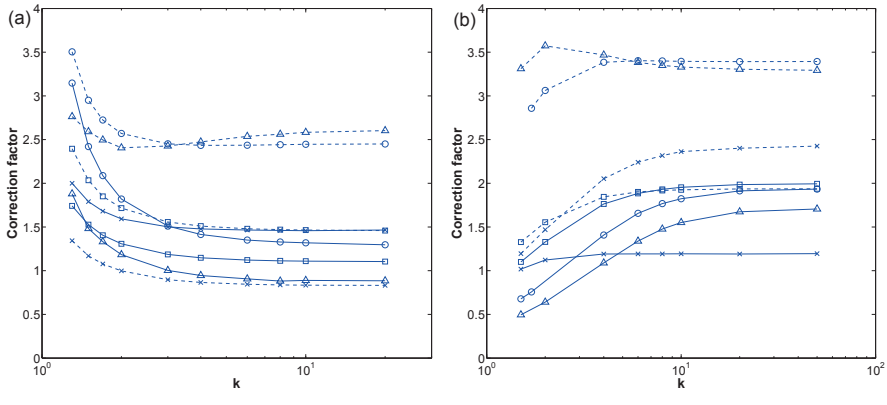

Fig. 11. Influence of correction factor for different pore sizes, k, in the x_1-direction (solid lines) and in the x_2-direction (dashed lines) for pores A ($\times$) , B ($\circ$), C ($\square$) and D ($\triangle$) for different pore sizes (a) correction factor for diffusivity (b) correction factor for elastic modulus.

7 Conclusions

The thesis, shows that a conductivity method can be used to measure the diffusivity of potassium chloride ions in bovine bone. A postulated relation between the concentration and the conductivity may be assumed. The diffusion coefficient is modeled both as a constant and as a linear position dependent parameter with good results. Using the linear position dependent diffusion parameter even improves the result. The results show that the position dependent diffusion parameter decreases as the porosity decreases, from the endosteal surface to periosteal surface. An agreement between the constant diffusion results and the linear position dependent diffusion results is found.

The thesis demonstrates how the Kalman filter, can be successfully used for extracting diffusion coefficients from noisy conductivity measurements. A method is suggested of how to make the initial assumption of the parameters in the Kalman filter procedure. A scheme is proposed that covers a wide range of initial filter parameters and increases the rate of convergence.

Finally, an analytical model of diffusion and mechanical deformation of porous materials are derived to obtain the effect of an infinitesimal pore. A size scaling and interaction is obtained. The method has been used, with good accuracy, to compute the diffusivity and the elastic modulus in the bovine bone samples based on the superposition principle and the finite element calculations for bone sample with irregular pores.

References

Banks-Sills, L., Ståhle, P., Svensson, I., Eliaz, N., 2011. Strain driven transport for bone modeling at the periosteal surface. Mathematical biosciences 230 (1), 37–44.

Baron, C., 2012. Using the gradient of human cortical bone properties to determine age-related bone changes via ultrasonic guided waves. Ultrasound in medicine & biology 38 (6), 972–981.

Brown, R. G., 1983. Introduction to random signal analysis and Kalman filtering. Vol. 8. Wiley New York.

Burstein, D., Gray, M. L., Hartman, A. L., Gipe, R., Foy, B. D., 1993. Diffusion of small solutes in cartilage as measured by nuclear magnetic resonance (NMR) spectroscopy and imaging. Journal of orthopaedic research 11 (4), 465–478.

Crank, J., 1975. The mathematics of diffusion. Oxford: Clarendon.

Fernandez-Seara, M. A., Wehrli, S. L., Wehrli, F. W., 2002. Diffusion of exchangeable water in cortical bone studied by nuclear magnetic resonance. Biophysical journal 82 (1), 522–529.

Glicksman, M. E., 2000. Diffusion in solids. Wiley Interscience, New York.

Kalman, R. E., 1960. A new approach to linear filtering and prediction problems. Journal of Fluids Engineering 82 (1), 35–45.

Lindberg, G., Banks-Sills, L., Ståhle, P., Svensson, I., 2013. A two-dimensional model for stress driven diffusion in bone tissue. Computer methods in biomechanics and biomedical engineering 18 (5), 457–467.

Magde, D., Elson, E., Webb, W. W., 1972. Thermodynamic fluctuations in a reacting system—measurement by fluorescence correlation spectroscopy. Physical Review Letters 29 (11), 705.

Merboldt, K.-D., Hanicke, W., Frahm, J., 1985. Self-diffusion NMR imaging using stimulated echoes. Journal of Magnetic Resonance (1969) 64 (3), 479–486.

Messiou, C., Desouza, N., 2010. Diffusion weighted magnetic resonance imaging of metastatic bone disease: A biomarker for treatment response monitoring. Cancer Biomarkers 6 (1), 21–32.

Onsager, L., 1931. Reciprocal relations in irreversible processes. I. Physical Review 37 (4), 405.

Peppas, N. A., Reinhart, C. T., 1983. Solute diffusion in swollen membranes. Part I. A new theory. Journal of membrane science 15 (3), 275–287.

Ståhle, P., Isaksson, P., Persson, C., Shokry, A., 2013. CT scanned cross section of bovine ulna. Researchgate.
URL http://dx.doi.org/10.13140/RG.2.1.3961.8082

Stejskal, E., Tanner, J., 1965. Spin diffusion measurements: spin echoes in the presence of a time-dependent field gradient. The journal of chemical physics 42 (1), 288–292.

Van Milligen, B. P., Bons, P., Carreras, B. A., Sánchez, R., 2005. On the applicability of fick′s law to diffusion in inhomogeneous systems. European journal of physics 26 (5), 913.

Wang, X., Nyman, J., Dong, X., Leng, H., Reyes, M., 2010. Fundamental biomechanics in bone tissue engineering. Vol. 2. Morgan & Claypool Publishers.

Yeung, D. K., Wong, S., Griffith, J. F., Lau, E., 2004. Bone marrow diffusion in osteoporosis: evaluation with quantitative MR diffusion imaging. Journal of Magnetic Resonance Imaging 19 (2), 222–228.

Paper A

G. Lindberg, A. Shokry, W. Reheman and I. Svensson (2014)

Determination of diffusion coefficients in bovine bone by means of conductivity measurement

International Journal of Experimental and Computational Biomechanics, volume 2, issue 2, pages 324-342

Determination of diffusion coefficients in bovine bone by means of conductivity measurement

Gustav Lindberg[a], Abdallah Shokry[a,b], Wureguli Reheman[a] and Ingrid Svensson[c]

[a] *Division of Solid Mechanics, Lund University, 22100 Lund, Sweden*

[b] *Industrial Engineering Department, Fayoum University, 63514 Fayoum, Egypt*

[c] *Department of Biomedical Engineering, Lund University, 22100 Lund, Sweden*

Abstract

Measuring the diffusivity of various substances in cortical bone is in general difficult. For instance, making use of micro computed tomography requires agents that can be separated from bone, blood and other substances that exist in cortical bone. Here a more easily accessible method is presented. A series of cortical bovine bone samples were put in a saturated solution of potassium chloride for a time period that was long enough for the samples to be regarded as saturated. The samples were removed from the solution and molded in polyester leaving only the radial directions open. In the next step, the bone samples were put in distilled water and the conductivity of the water was registered over time. An analytical model fulfilling Fick′s law was introduced and by means of Kalman filtering an estimation for the diffusion coefficient of potassium chloride in bovine bone is presented.

1 Introduction

It is well known that bone, like other living tissue, has the function of self-repairing and can adapt its size and external shape, internal structure and mass density according to mechanical environment and hormonal changes. The modelling and remodelling is a dynamic process that involves removal of old bone tissue, resorption and formation of new tissue. This process is dominated by the activity of bone cells such as osteoblasts, osteoclast, osteocytes and bone lining cells. The cause of activation of these cells is widely discussed, and several hypotheses exist. A number of studies focus on the shear forces that arise due to the fluid flow in the bone matrix when exerted to mechanical loading. The hypothesis is that activation of the bone building osteocytes is directly or indirectly depending on shear forces, see for instance Weinbaum et al. (1994). The studies of Cardoso et al. (2013) and Fritton and Weinbaum (2009) nicely summarise some of the research carried out this far. In a recent published article by Lindberg et al. (2013a) a theory is tested which suggests that the nutrients which are important for bone building are moved through the bone matrix by means of stress driven diffusion, here having a special focus on the mathematical modelling of the process. A similar theory using strain driven diffusion in bone tissue is presented by Banks-Sills et al. (2011). Tate et al. (2000) hypothesize that load-induced fluid flow enhances the transport of key substances for bone remodelling throughout the bone matrix. Kufahl and Saha (1990) developed a mathematical model to study stress-induced fluid flow in the lacunar-canalicular system in an osteon, suggesting that it is possible that such stress-induced flow may be important in bone remodelling, and that lack of such flow may be one cause for producing osteoporosis due to immobilization. Some investigations show that molecules with lower molecular weight are dominantly transported through diffusion, while a pumping effect caused by mechanical load mainly controls the transportation of higher molecular weight solutes (Bali and Shukla, 2001; Tandon and Agarwal, 1989). In other studies, it is shown that there is a strong correlation between diffusion coefficients and healthiness of bone, and it is found that the diffusivity in degenerated bone is significantly lower than in normal bone, (Kealey et al., 2005).

Because of its complex micro and macro structure, and due to the minute size and inaccessibility of the lacunar-canalicular system that serves as a transportation network, the study of diffusion in bone is quite complicated. The mechanisms of diffusion of substances in the bone matrix, and the effects of mechanical load triggering bone cells to remodel, are poorly understood. The diffusion based magnetic resonance image (MRI) and nuclear magnetic resonance (NMR) methods have been used to characterize the structure, and evaluate the composition of bone (Burstein et al., 1993; Sigmund et al., 2008). Several studies have investigated the mechanisms of how solutes transport in bone, and how the removing of the waste products that are stored in skeletal tissue is accomplished. It was understood that one of the important mechanisms is diffusion, which plays an essential role in accomplishing these transports and also in the removal of waste products (Fernandez-Seara et al., 2002; Maroudas, 1979; Maroudas et al., 1992). Better understanding of the diffusion in bone is needed in biomedical research and medical application in order to study bone diseases, like osteoporosis, and the degradation of bone and fracture healing.

For the various models that exist, using mechanical loading, the diffusion coefficient for the nutrient-bone system has to be determined in order to make exact recommendation of load amplitude and frequency in order to maximize remodelling of bone. What kind of nutrients that are involved must of course also be determined, and research is ongoing. In *vivo* studies by Jee et al. (1990) showed that prostaglandins stimulate osteoblast activity and Fan et al. (2004) found that nitric oxide can prevent bone resorption since it decreases the recruitment of bone resorbing osteoclasts.

To directly study transport of matter through the complicated cellular structure of the bone matrix requires access to technically complicated instruments (e.g. NMR, CT scanners etc). To make research of such kind more accessible an experiment was set up in this study to investigate diffusion in bone by measuring electrical conductivity using a more common equipment, namely a conductivity meter. The diffusion parameters are extracted from the experimental result by using Kalman filtering, see Kalman (1960). This is a recursive method, here based on an analytical solution, for extracting values of unknown parameters from noisy input data. The mathematical analysis assumes that the bone is homogeneous.

Bone growth takes place at the outer bone surface, the periosteum. This study focuses on the diffusivity properties in the radial direction going from the nutrient rich bone marrow inside the bone out to the periosteum. It is believed that the diffusivity parameters of potassium chloride, KCl, in bovine bone found in this study may serve as an average over the bone cross-section and may be used to compute the transport in radial direction of the nutrients trigging bone growth at the periosteum.

2 Method

The right side femur of a 15 month old male bovine of type Charolais was step by step cut in to small bone cubes approximately of size 1 cm^3, see Table 1, giving a total of 16 pieces. The femur was cut up four days after slaughter, and up until then it had been stored in a fridge with the meet not yet removed.

Table 1: The mean values and standard deviations for the side lengths for all samples

Direction	*Mean value [mm]*	*Standard deviation [mm]*
Axial	9.97	0.38
Radial	9.70	0.65
Tangential	9.74	0.84

An important part of the process was, all the time, to keep track of the three axial directions (axial, radial and tangential) and where exactly on the femur each piece was taken from. The 16 pieces were taken from four places over the cross-section, see Fig. 1.

At each location two pieces were taken above the midplane and two below the midplane, see Fig. 1. In each row the samples were numbered from 1 to 4, where 1 is the sample

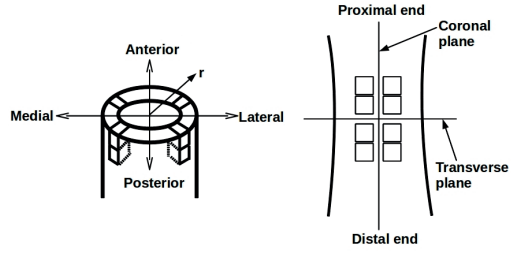

Fig. 1. Location of samples

closest to the proximal end and 4 closest to the distal end. Eight pieces were taken from the lateral side (outside), where four of them were located slightly towards the anterior side (front side) and the other four were located slightly towards the posterior side (back side). The other eight were taken from the medial side (inside), where four of them were located slightly towards the anterior side and the other four were located slightly towards the posterior side. During the process the pieces were kept in a freezer overnight holding a temperature of minus 2 degrees Celsius, making the bone barley freeze.

On the day of experiment each set of samples was taken from the freezer and kept in room temperature for an hour, after which each piece was put in a beaker with saturated KCl solution which had been prepared by stirring 37 grams of KCl in 100 grams of distilled water. KCl was chosen since it has a high ability to conduct electricity, hence being suitable to use in conductivity measuring giving a strong read, along with the linear relationship between concentration and conductivity giving an easy mathematical approach. Although salts may affect the tissue, it is here believed that the mass transfer ability of the bone samples is not affected. The bone pieces were put in the beakers for 24 hours exposing them to a very high concentration, after which they were quickly rinsed with distilled water, lightly wiped with paper and then molded in polyester in order to close the axial and tangential directions leaving only the radial direction ends opened, see Fig. 2. The choice of 24 hours was based on the assumption that this was enough to make the samples saturated. This is discussed further down.

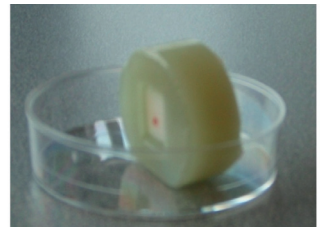

Fig. 2. Polyester closing axial and tangential directions of bone sample

The polyester was left to dry for 60 minutes, after which the measurements started. The polyester did not give any conductivity increase for water when tested. During the

experiments measurements were taken for samples that had been completely molded in with polyester after being in the salt solution, i.e. all six sides were closed. After 48 hours the conductivity had increased about 1 μS/mm. By that it was decided that the diffusion through the polyester from the closed sides could be neglected.

To measure the conductivity the instrument SevenEasy S30 from Mettler Toledo was used along with a cell that had two electrode plates. The samples were put in beakers with 100 ml distilled water where the ions that came from the KCl in each sample diffused into the water and changed its conductivity. The increased conductivity was registered over time, and measurements went on for 24 hour for each sample. Before each measurement the beakers were stirred in order to obtain a homogeneous concentration. During night time automatic measuring was done for one sample taking values every second. The other three samples were not measured during night, here assuming that the progress behaves in the same manner for all samples. An overview of the experimental set-up for the measurements is shown in Fig. 3.

Fig. 3. The conductivity measurement

In general conductivity is measured in Siemens per length unit, normally μS/cm where μ is the prefix for 10^{-6}. The conductivity ξ of a solution is determined as

$$\xi = G\,K = \frac{1}{\rho}\,K\,, \tag{1}$$

where G [S] is the conductance of the sample, which is the inverse of the resistance ρ [Ω]. The cell constant, or probe constant, K [cm^{-1}] is specific for the used cell, and consists of the ratio of the distance between the electrodes and the area of the electrodes. The cell constant must be determined which is done by calibrating the base unit for the used cell.

The experiments took place in a temperature controlled room, holding a constant temperature of 22 degrees Celsius. However, to be sure that the measurements did not get affected by some temporary temperature change, the in-built temperature compensation

was used. Since pre-trials showed that the conductivity would be above 10 μS/cm, except for in the very beginning, but still not becoming strongly conductive the temperature dependence was assumed to be linear and so the conductivity is determined as (Down and Lehr, 2005)

$$\xi_{ref} = \frac{1}{1 + (\alpha/100)(T_{ref} - T)} \frac{K}{\rho} \,. \tag{2}$$

Here α is the temperature correction factor, T_{ref} is the chosen reference temperature and T is the actual temperature of the sample. If α is set to zero the actual conductivity of the sample is given, compare Eq. (1). The correction factor is determined as

$$\alpha = \frac{(\xi_{T2} - \xi_{T1})100}{(T_2 - T_1)\xi_{T1}}, \tag{3}$$

and was for this experiment determined to α=0.021 meaning an error of 2.1% of the relative correction per centigrade.

3 Theory

3.1 Governing equations

The flux vector $\bar{J}$ of a selected substance in the bone environment becomes, due to differences in concentration of matter,

$$\bar{J} = -D\bar{\nabla}c \,. \tag{4}$$

Here D is the diffusion coefficient of the substance-bone system and $\bar{\nabla}c$ is the gradient vector of the concentration where

$$\bar{\nabla} = (\frac{\partial}{\partial x}, \frac{\partial}{\partial y}, \frac{\partial}{\partial z}) \tag{5}$$

in a Cartesian coordinate system. Matter is assumed to be conserved and therefore the divergence of the flux $\bar{J}$ relates to the concentration as

$$\bar{\nabla}\bar{J} = -\dot{c} \,, \tag{6}$$

where the dot indicates the derivative with respect to time. If $\bar{J}$ is eliminated by using Eq. (4), the divergence of Eq. (6) becomes

$$\dot{c} = \bar{\nabla}(D\bar{\nabla}c) \,. \tag{7}$$

If the diffusion coefficient D is assumed not to be dependent of the current concentration nor explicitly dependent of spatial coordinates Eq. (7) now changes to

$$\dot{c} = D\Big(\frac{d^2c}{dx^2} + \frac{d^2c}{dy^2} + \frac{d^2c}{dz^2}\Big) \,, \tag{8}$$

which is the partial differential equation to solve. Here x, y and z are serving as Cartesian coordinates. There is, of course, an option to choose a polar coordinate description, however with greater mathematical complexity. The cross-section of the long bone is not a perfect circle, but rather quite irregular. By that shifting to the standard cylindrical coordinate system is believed to be irrelevant. The bone pieces were hence chosen to be cut out as cubes so that the Cartesian coordinate system could be used. For each sample the coordinate system is placed so that the x-axis runs from the endosteum out to the periosteum, i.e. in the radial direction. To clarify that, x is replaced by r and Eq. (8) is written as

$$\dot{c} = D\Big(\frac{d^2c}{dr^2} + \frac{d^2c}{dy^2} + \frac{d^2c}{dz^2}\Big) \,. \tag{9}$$

4 Mathematical model

A solution to the one-dimensional Fick′s second law with a constant diffusion coefficient can be

$$C(r,t) = X(r)T(t) \,, \tag{10}$$

where the most general solution is readily given as (Crank et al., 1975),

$$C(r,t) = \sum_{m=1}^{\infty} \Big(A_m \sin(\lambda_m r) + B_m \cos(\lambda_m r)\Big) e^{(-\lambda_m^2 Dt)} \,. \tag{11}$$

In the experiment each sample had a volume of $1/100$ of the surrounding water. By that the concentration increase in the water was ignored, and the boundary conditions were regarded as constant. See Lindberg et al. (2013b) for a comparison with the case where the increase of concentration at the boundaries is compensated for.

For a one-dimensional slab having an initial concentration of C_0 at $t = 0$ for $0 < r < a$ and the constant boundary conditions $C = 0$ at the boundaries $r = 0$ and $r = a$, see Fig. 4, the solution becomes

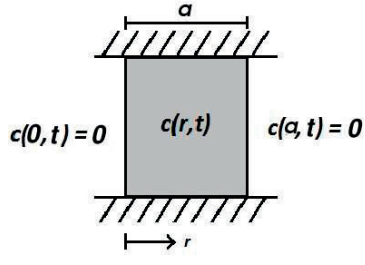

Fig. 4. One-dimensional slab

$$C(r,t) = C_0 \sum_{n=1}^{\infty} e^{-\lambda_n^2 Dt} A_n \sin\Big[\lambda_n r\Big] \,, \tag{12}$$

where

$$A_n = \frac{4}{\pi}\frac{1}{(2n-1)} \tag{13}$$

and

$$\lambda_n = (2n-1)\frac{\pi}{a}\,. \tag{14}$$

More details about analytical diffusion problems can be found in e.g. the rigorous book by Glicksman (2000). The mean value $\tilde{C}_b$ of the concentration in the bone sample is given by taking the integral of Eq. (12) over r and then divide it by the integration length a which is expressed as

$$\tilde{C}_b(t) = C_{b0}\frac{1}{a}\sum_{n=1}^{\infty} e^{-\lambda_n^2 Dt} A_n \int_0^a \sin(\lambda_n r)dr\,, \tag{15}$$

where index b is for bone. Deriving the integral the mean value of the concentration in the bone sample becomes

$$\tilde{C}_b(t) = C_{b0}\sum_{n=1}^{\infty} e^{-((2n-1)\frac{\pi}{a})^2 Dt}\frac{8}{\pi^2(2n-1)^2}\,. \tag{16}$$

From the experiments the conductivity ξ in the distilled water surrounding the bone sample was registered over time. The relationship between conductivity and concentration for a KCl solute is almost ideally linear. The relation between concentration and conductivity for a KCl solute is described by

$$C = \frac{\xi}{\varrho V}\,, \tag{17}$$

where V $[l^3]$ is the volume of the solute, ϱ has the unit S/l mole and l is the used length unit. The product ϱV [S l^2/mole] is the molar conductivity of the solute. The concentration C [mole/l^3] of matter in the solution may be described by the number of existing moles of matter m_i divided by the volume of the solution. The decrease of the concentration of KCl in the bone sample once put in the distilled water may hence be described by

$$\Delta\tilde{C}_b = \frac{-\Delta m_i}{V_b}\,. \tag{18}$$

Since the same amount Δm_i of KCl has diffused out to the distilled water, the increase of concentration of KCl in the water becomes

$$\Delta\tilde{C}_w = \frac{\Delta m_i}{V_w}\,, \tag{19}$$

where index w is for water. Using Eqs. (17), (18) and (19) the change of conductivity of the water can be expressed as

$$-\Delta\tilde{\xi}_w = \varrho_w V_b \Delta\tilde{C}_b \,. \tag{20}$$

The mean conductivity $\tilde{\xi}_w$ of the distilled water may hence be modelled by

$$\tilde{\xi}_w(t) = A - B\sum_{n=1}^{\infty} e^{-((2n-1)\frac{\pi}{a})^2 Dt}\frac{8}{\pi^2(2n-1)^2}\,. \tag{21}$$

Here A $[\mathrm{S}/l]$ is the final value of the conductivity, i.e. the conductivity after infinity of time, since the dimensionless summation converges towards zero. $A - B$ is the start value, i.e. $\xi_{t=0}$, since the summation equals 1 for $t = 0$. It is by that very interesting to determine the constant B $[\mathrm{S}/l]$ as well as the diffusion coefficient D. If B is determined it can be calculated what the very end value A of the conductivity will be, and by that the measurements can be much more time effective.

4.1 Kalman filtering

In order to extract the diffusion coefficient a Kalman filter is used. The technique has several advantages; The random noise from the measurements and other process parameters is included into the equations and a non-linear behaviour can be included. The technique has shown very good results, which is obtained due to minimization of the mean square root of the difference between the measured conductivity and the model.

The Kalman filter is a versatile estimator and the algorithm operates recursively and results in an incrementally improved estimate of the model parameters D and B, whereas $A - B$ is obtained directly from a measurement immediately before the experiment starts. An introduction to the Kalman filter is, e.g., found in Brown (1983). Kalman filter recursive equations are expressed as

$$\hat{x}_k = \hat{x}_k^- + K_k[z - h(\hat{x}_k^-)], \tag{22}$$

$$K_k = P_k H_k^T R^{-1}, \tag{23}$$

and

$$P_k = \left[(P_k^-)^{-1} + H_k^T R^{-1} H_k\right]^{-1}. \tag{24}$$

Here $\hat{x}_k = [D_k \quad B_k]^T$ is an *a posteriori* estimate vector of the state that contains the two unknown parameters D and B at increment k. The vector $\hat{x}_k^-$ is an *a priori* estimate vector for the state at increment k and K_k is denoted the optimal Kalman gain. It is introduced to minimize the error of the *a posteriori* estimate at increment k. The vector z contains the measured conductivity at times t_i. The vector $h(\hat{x}_k^-)$ is a function that contains the analytical result, i.e. Eq. (21), using the *a priori* estimated parameters $\hat{x}_k^-$ at times t_i.

The Kalman gain K_k is defined in Eq. (23) using P_k, a matrix containing the *a posteriori* estimate of the error, and R, which is a scalar giving the maximum difference between the

measurement z and the predicted result, as explained in more detail below. The matrix H_k is the derivatives with respect to B and D of $h(\hat{x}_k^-)$ at increment k and at times t_i.

The predicted non-linear conductivity function $h(\hat{x}_k^-)$ is a bi-quadratic form approximating Eq. (21). The interpolation is performed for D and B in the region $D^{(1)} \leq D \leq D^{(3)}$ and $B^{(1)} \leq B \leq B^{(3)}$, where $D^{(1)}$, $D^{(3)}$, $B^{(1)}$ and $B^{(3)}$ are selected to give a sufficient span so that the given space includes the expected D and B. The remaining values $D^{(2)} = (D^{(1)} + D^{(3)})/2$ and $B^{(2)} = (B^{(1)} + B^{(3)})/2$. To be able to catch any possibly present local convergence sets for D and B, the algorithm is executed for many starting values $\hat{x}_0$. The initial state values $\hat{x}_0 = [D_0 \quad B_0]^T$ are chosen as $11 \times 11 = 121$ equidistant values in the range $D^{(1)} \leq D \leq D^{(3)}$ and $B^{(1)} \leq B \leq B^{(3)}$. The predicted non-linear conductivity functions are computed using rectangular nine set Lagrange interpolation as

$$\left[h(\hat{x}_k^-)\right]_i = \sum_{p=1}^{3}\sum_{q=1}^{3}\left[\left(\prod_{m=1\neq p}^{3}\frac{D_k - D^{(m)}}{D^{(p)} - D^{(m)}}\right)\left(\prod_{n=1\neq q}^{3}\frac{B_k - B^{(n)}}{B^{(q)} - B^{(n)}}\right)\xi_{pq}\right], \tag{25}$$

where $\left[h(\hat{x}_k^-)\right]_i$ is element i, for time $t = t_i$, of $h(\hat{x}_k^-)$. Further, ξ_{pq} is the analytically calculated conductivity for $D = D^{(p)}$ and $B = B^{(q)}$, at time $t = t_i$ according to Eq. (21). The matrix H_k is obtained by taking the derivative of the interpolated conductivity function and is expressed as

$$H_k = \left[\frac{\partial h(\hat{x}_k^-)}{\partial D_k}, \frac{\partial h(\hat{x}_k^-)}{\partial B_k}\right]. \tag{26}$$

A single iteration requires hours of computing time on a standard desktop computer using the analytical derivative of the model for 1000 terms while only a few seconds are required using the interpolation algorithm in Eq. (25). Therefore, a little decrease of accuracy is accepted for a considerable saving of computer time.

The quantity R, being a difference between measurement and prediction, is computed as the largest difference in the entire set of measurements, i.e.

$$R = max_{i=1,2,..}\left(\left|\left(z - h(\hat{x}_0^-)\right)_i\right|\right), \tag{27}$$

where the index i denotes vectorial element i, which corresponds to measurement and prediction at time $t = t_i$. The error R is usually an updated quantity. However, in the present case the result was found to be very insensitive to reasonable variations of R. Therefore R is chosen as the error according to Eq. (27) as the value for the best out of all 121 initial state values for $\hat{x}_0$ that is used for analysing each experiment. The error R differs from one bone piece to another.

The Kalman filter update equations are given as

$$\hat{x}_{k+1}^- = \hat{x}_k \tag{28}$$

and

$$P_{k+1}^- = P_k + Q, \tag{29}$$

where Q is selected to be the unit matrix (Brown, 1983).

The initial value of the *a posteriori* estimate error is selected to be

$$P_0 = \begin{bmatrix} 100 & 0 \\ 0 & 100 \end{bmatrix}. \tag{30}$$

The process of extracting the unknown parameters is repeated for different ranges of initial state values ranging from larger range to smaller range until a good fitting between the measured conductivity and the model is obtained. The standard deviation σ_e of the difference between the experimental data and the obtained approximated Kalman data is determined according to

$$\sigma_e = \sqrt{\tfrac{1}{N}\sum (z - h(\hat{x}_k^-))_i^2}, \tag{31}$$

where N is the number of measurements. In Table 3 the final σ_e for each sample is shown.

5 Analysis and Results

The determination of the diffusion coefficient D and the constant B for the second bone sample from the medial posterior side, MP_2, is explained but the process for all bone samples follow the same strategy. The units used during the experiment were for convenience millimetres and minutes. The initial eleven different state values of D_0 were at first placed in the interval 0.0001 to 0.1001 mm^2/min with the midpoint 0.0501. For B_0 the initial eleven different state values were placed in the interval 10 to 90 $\mu S/mm$ with the midpoint 50. These values were chosen to introduce an initially large range, and are based on experimental and preliminary curve fitting result.

The calculations were repeated with smaller range of initial state values until a sufficiently small standard deviation between the model and measured conductivity was found. The ranges and results are shown in Table 2.

Table 2: Values of D, B, and σ_e for four different initial ranges for sample MP_2

Range for D_0 *[*mm^2/min*]*	*Range for* B_0 *[*$\mu S/mm$*]*	D *[*mm^2/min*]*	B *[*$\mu S/mm$*]*	σ_e *[*$\mu S/mm$*]*
0.0001-0.1001	10-90	0.00030	334.86	11.90
0.0010-0.0410	10-90	0.00212	94.087	4.010
0.0010-0.0110	10-90	0.00760	41.911	0.411
0.0060-0.0100	40-48	0.00749	42.805	0.298

The combinations of D and B in $\hat{x}_0$ converged to one single point after some different iterations for the first, second, and fourth range but they converged towards two different points for the third range.

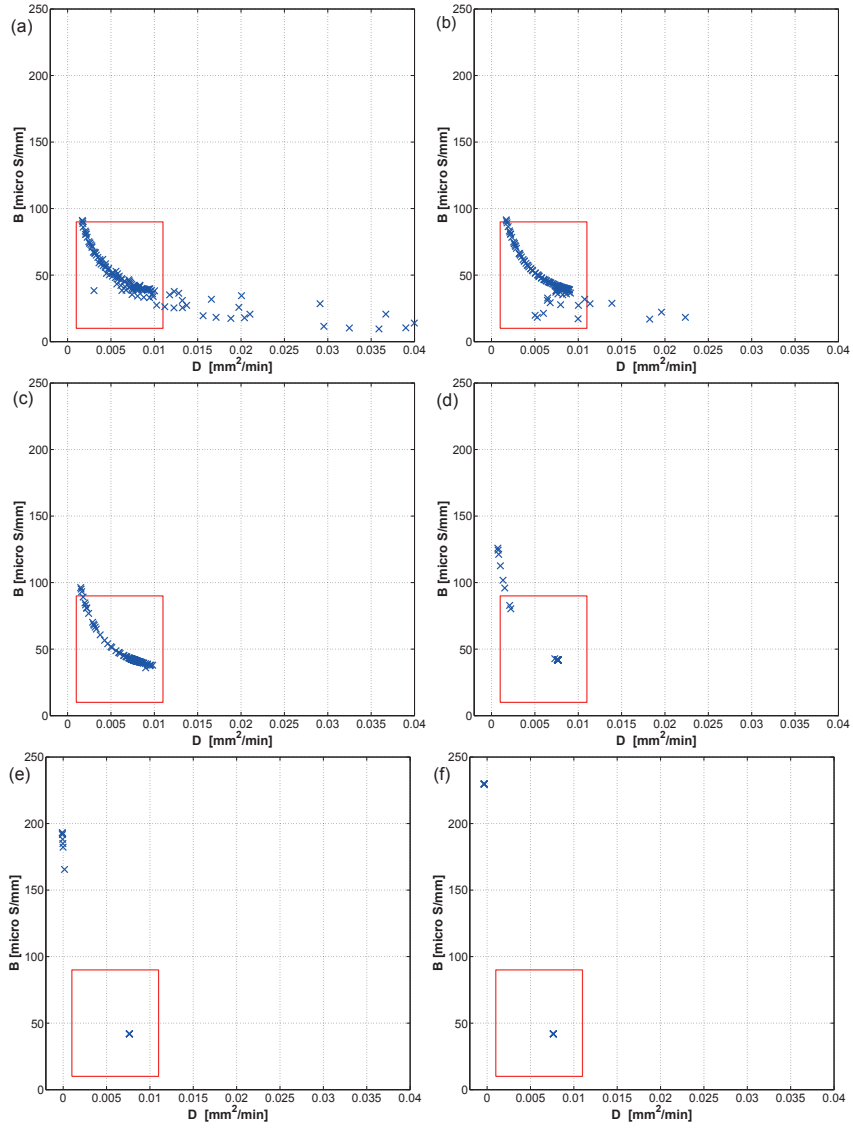

Fig. 5. Convergence between D [mm^2/min] and B [µS/mm] after six different iterations for sample MP_2 using range 3, (a) convergence after 1 iteration for MP_2 (b) convergence after 2 iterations for MP_2 (c) convergence after 10 iterations for MP_2 (d) convergence after 40 iterations for MP_2 (e) convergence after 120 iterations for MP_2 (f) convergence after 500 iterations for MP_2. The initial state borders are marked by the square.

Here 114 combinations of D and B converged to the point that fits well with the experimental data and seven combinations converged to another one that does not and can be excluded because it gave negative value for D with no physical meaning. Fig. 5 shows the process of convergence between D and B after 1, 2, 10, 40, 120, and 500 iterations for sample MP_2 for the third range. The rectangle shows the border of the initial state range.

A study was performed to investigate how many terms n that should be used in the summation operator in the model, see Eq. (21). It showed that consistency can be reached after 10 000 terms. Extrapolation from this value to infinity of terms showed that the value for the diffusion coefficient changed by less than $5 \cdot 10^{-6}$ mm^2/min. Hence summation over 10 000 terms are used in this study.

The four different initial state ranges are figured with the experimental data for sample MP_2 in Fig. 6.

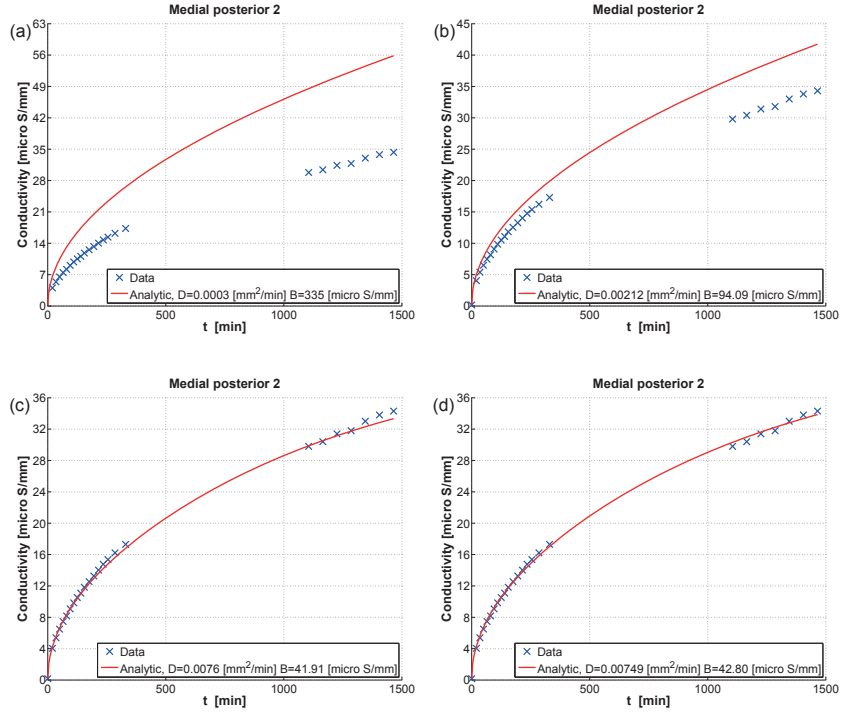

Fig. 6. Kalman approximated conductivity versus data for the four different ranges in Table 2 for sample MP_2, (a) model vs exp. data for the first range in Table 2 (b) model vs exp. data for the second range in Table 2 (c) model vs exp. data for the third range in Table 2 (d) model vs exp. data for the fourth range in Table 2.

Table 2 along with Fig. 6 show that the best approximated values that were achieved by the Kalman filter for D and B are 0.0074906 mm^2/min and 42.8049 μS/mm respectively

for the MP_2 sample.

The process was performed in the same way for all samples. For the lateral posterior sample no 1, LP_1, the diffusion coefficient was for instance found to be 0.014360 mm^2/min and for sample no 2 from the lateral anterior side, LA_2, it was determined to 0.010660 mm^2/min. These results are plotted in Fig. 7 and as can be seen the model has a good match with the experimental data.

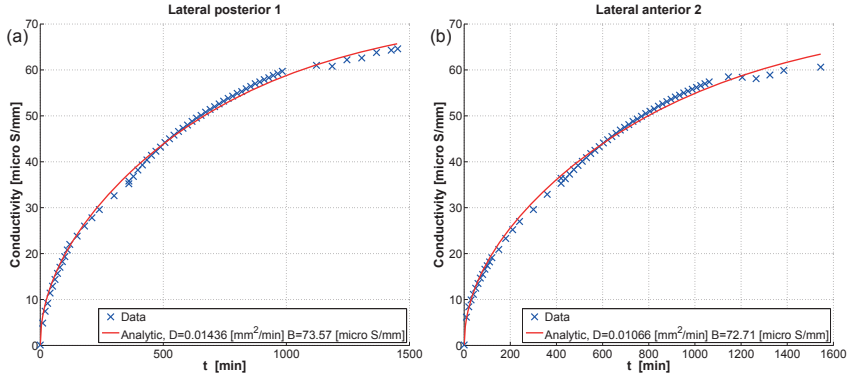

Fig. 7. Experimental data and analytical function for samples from the lateral (a) posterior and (b) anterior side.

One observation is that the experimental data seems to behave more linear rather than exponential at the end of the measuring. The reason for this is unclear. It is possible that the real inhomogeneity of the bone tissue has a greater effect when the concentration in the bone samples starting to get lower. In Table 3 all the obtained values from the Kalman filter can be found. The average value and the standard deviation of the bone samples become $D = 0.0110 \pm 0.0069$ mm^2/min. These values are derived using the final diffusion coefficient D for each sample.

6 Discussion

An experimental study determining the diffusion coefficient for KCl in bovine bone was performed using easily accessible equipment in form of a conductivity meter. The study was focused on the diffusion in radial direction, i.e. between the endosteum and the periosteum. The diffusion was described in mathematical terms using a Fourier series expansion and the diffusion coefficient was obtained from the experimental data using Kalman filtering. An average value and a standard deviation of D of the bone samples from the same animal can be computed from the values in Table 3 and become $D = 0.0110 \pm 0.0069$ mm^2/min. The distribution of the value of the diffusion coefficient for the samples is quite large. This can be explained through both bovine bone being an inhomogeneous material and limitations in the experimental method. The experiment includes several steps, as described in the

Table 3: Diffusion coefficient D, the constant B and σ_e for all series

Sample	D $[mm^2/min]$	B $[\mu S/mm]$	σ_e $[\mu S/mm]$
MP1	0.001762	90.892	0.391
MP2	0.007491	42.805	0.298
MP3	0.006860	46.116	0.223
MP4	0.010631	42.551	0.332
MA1	0.020988	39.925	3.300
MA2	0.001666	57.780	0.476
MA3	0.001685	71.022	0.513
MA4	0.015418	23.181	0.323
LA1	0.011802	65.384	0.419
LA2	0.010660	72.713	0.983
LA3	0.008483	86.706	0.835
LA4	0.025767	73.503	1.127
LP1	0.014360	73.573	0.935
LP2	0.016701	61.779	0.862

Method section, which are executed as equally as possible for all samples. But each step is a possible source for differences between the samples. The solution was stirred before each measurement but still, the distribution of the KCl might not be homogeneous. This and any other noise introduced during the measurements such as temperature change or any inaccuracy of the instrument is captured by the Kalman filter. The standard deviation σ_e of the difference between the experimental data and the obtained approximated Kalman data for each sample, as defined in Eq. (31), is included in Table 3. No significant difference between the different locations from which the bone samples were taken was achieved in the study.

The results could be compared to the findings of Patel et al. (2004). They used FRAP, Fluorescence Recovery After Photobleaching, to measure the diffusion coefficient in bovine bone. They found that the permeability of cortical bone differs extensively depending on what length scale and direction that is studied, having values for D in the longitudinal direction in the range of 94.20 ± 5.23 to $6.11 \cdot 10^{-6} \pm 2.37 \cdot 10^{-7}$ mm^2/min. The FRAP technique was also used by Wang et al. (2005). They measure the diffusion of fluorescein in cortical bone of mice and present a value of $D = 0.0198 \pm 0.0036$ mm^2/min, here using sodium fluorescein which has a molecular weight of 376 Da. In the study of Li et al. (2009), further results are presented using the FRAP technique. They report diffusion coefficients of five different exogenous fluorescence tracers in mice bone. Values range from $D = 0.0039 \pm 0.0013$ for Ovalbumin, 43 000 Da, to $D = 0.0177 \pm 0.0028$ mm^2/min for sodium fluorescein, 376 Da. It is also interesting to notice that they also have quite big standard deviations. The comparison should be done keeping in mind that the fluorescence tracers are much bigger molecules than KCl. The fluorescein tracers have a molecular weight from 376 to 43 000 Da compared to 74 Da for KCl. A summary of the here discussed studies is

presented in Table 4.

Table 4: Summary of comparable studies for femoral cortical bone

Study	*Species*	*Direction*	*Tracer [Da]*	*D [mm²/min]*
Patel et al. (2004)	Bovine	Transverse	300	4.2e-4±3.6e-7
Patel et al. (2004)	Bovine	Longitudinal	300	6.0e-6±1.2e-6
Wang et al. (2005)	Mice	Transverse	376	0.0198±0.0036
Li et al. (2009)	Mice	Transverse	376	0.0177±0.0028
Li et al. (2009)	Mice	Transverse	43 000	0.0039±0.0013
Current study	Bovine	Transverse	74	0.0110±0.0069

The assumption that 24 hours in the KCl solution was enough to make the bone samples saturated can be easily checked using the calculated diffusion coefficient inserted in Eq. (12). Although Eq. (12) must first be modified for three dimensions since all sides were open when the samples were in the KCl solution. If this is done the results show that the value in the middle of the samples is about 95% of the value of the boundaries after 24 hours. I.e. the samples were close to saturated. As earlier explained the end value of the conductivity will be the constant A, see Eq. (21). The start value can be expressed as $A - B$. Since this study uses distilled water, the start value of the conductivity in each measurement is very low, close to zero. By that $A \approx B$, meaning that B can here be regarded to be the end value. As can be seen in Table 3 the end value differs some from sample to sample. The reasons for this are several. One reason is that the volume of the samples differs a few per cent. In general a larger volume indicates a larger amount of KCl and hence a higher end value of conductivity. For some samples this was not the case. One explanation for this could be that the density over the bone might vary, indicating that more or less salt water could be trapped inside the bone samples.

It would be interesting to study samples of different sizes in future studies. A variation of the dimensions could reveal possible size effects, possible statistical variation, deviation of the assumed uniaxial flux and end effects that arise when the area of the open ends is small compared to the length in the direction of the flux.

Besides the 16 samples some measurements were performed for bone pieces that had not been in the KCl-solution before going into the distilled water. After 24 hours the conductivity in the distilled water had reached about 5.5 μS/mm for these samples, i.e. about 7-13 % of the end values shown in Table 3. By that the diffusion coefficients calculated here cannot be said to be for purely KCl through bone tissue, but rather KCl mixed with a small part of bone substances moving through the bone tissue.

7 Conclusions

The idea of this study is that determination of diffusion coefficients and material constants in bone tissue will be more easily accessible. Since the calculated values of the diffusion coefficients are in line with other studies, as discussed in previous section, this method could

be considered as an option for avoiding using more advanced and expensive equipment. Even so, the experiment should be further evaluated and developed. More test samples should be used and it would be interesting to use a mathematical model which considers the inhomogeneity of bone tissue.

Acknowledgements

The authors would like to acknowledge the anonymous reviewers and the editor of this journal. Further G. Lindberg, I. Svensson and W. Reheman would like to acknowledge the Swedish Research Council for funding this research. Likewise A. Shokry would like to thank the Erasmus Mundus Action 2 Project. A special thanks to Prof. Per Ståhle at the Division of Solid Mechanics, Lund University, for his valuable comments and insights. Finally the authors would like to thank Ekerödsrasten, Hörby, Sweden for their donations of bovine bone.

References

Bali, R., Shukla, A., 2001. Rheological effects of synovial fluid on nutritional transport. Tribology Letters 9 (3-4), 233–239.

Banks-Sills, L., Ståhle, P., Svensson, I., Eliaz, N., 2011. Strain driven transport for bone modeling at the periosteal surface. Mathematical biosciences 230 (1), 37–44.

Brown, R. G., 1983. Introduction to random signal analysis and Kalman filtering. Vol. 8. Wiley New York.

Burstein, D., Gray, M. L., Hartman, A. L., Gipe, R., Foy, B. D., 1993. Diffusion of small solutes in cartilage as measured by nuclear magnetic resonance (NMR) spectroscopy and imaging. Journal of orthopaedic research 11 (4), 465–478.

Cardoso, L., Fritton, S. P., Gailani, G., Benalla, M., Cowin, S. C., 2013. Advances in assessment of bone porosity, permeability and interstitial fluid flow. Journal of biomechanics 46 (2), 253–265.

Crank, J., et al., 1975. The mathematics of diffusion. Vol. 2. Clarendon press Oxford.

Down, R. D., Lehr, J. H., 2005. Environmental instrumentation and analysis handbook. John Wiley & Sons.
URL `http://eu.wiley.com/WileyCDA/Wiley-Title/productCd-0471473324,descCd-ebook.html(Accessed05August2013)`.

Fan, X., Roy, E., Zhu, L., Murphy, T. C., Ackert-Bicknell, C., Hart, C. M., Rosen, C., Nanes, M. S., Rubin, J., 2004. Nitric oxide regulates receptor activator of nuclear factor-κB ligand and osteoprotegerin expression in bone marrow stromal cells. Endocrinology 145 (2), 751–759.

Fernandez-Seara, M. A., Wehrli, S. L., Wehrli, F. W., 2002. Diffusion of exchangeable water in cortical bone studied by nuclear magnetic resonance. Biophysical journal 82 (1), 522–529.

Fritton, S. P., Weinbaum, S., 2009. Fluid and solute transport in bone: flow-induced mechanotransduction. Annual review of fluid mechanics 41, 347.

Glicksman, M. E., 2000. Diffusion in solids. Wiley, New York.

Jee, W., Mori, S., Li, X., Chan, S., 1990. Prostaglandin E 2 enhances cortical bone mass and activates intracortical bone remodeling in intact and ovariectomized female rats. Bone 11 (4), 253–266.

Kalman, R. E., 1960. A new approach to linear filtering and prediction problems. Journal of Fluids Engineering 82 (1), 35–45.

Kealey, S. M., Aho, T., Delong, D., Barboriak, D. P., Provenzale, J. M., Eastwood, J. D., 2005. Assessment of apparent diffusion coefficient in normal and degenerated intervertebral lumbar disks: Initial experience 1. Radiology 235 (2), 569–574.

Kufahl, R. H., Saha, S., 1990. A theoretical model for stress-generated fluid flow in the canaliculi-lacunae network in bone tissue. Journal of biomechanics 23 (2), 171–180.

Li, W., You, L., Schaffler, M. B., Wang, L., 2009. The dependency of solute diffusion on molecular weight and shape in intact bone. Bone 45 (5), 1017–1023.

Lindberg, G., Banks-Sills, L., Ståhle, P., Svensson, I., 2013a. A two-dimensional model for stress driven diffusion in bone tissue. Computer methods in biomechanics and biomedical engineering 18 (5), 457–467.

Lindberg, G., Ståhle, P., Svensson, I., 2013b. A perturbation analysis of non-linear diffusion from a permeable solid into a finite volume containing a liquid. LUTFD2/(TFHF-3088)/1-8/(2013).

Maroudas, A., 1979. Physicochemical properties of articular cartilage. Adult articular cartilage 2, 215–290.

Maroudas, A., Schneiderman, R., Popper, O., 1992. The role of water, proteoglycan, and collagen in solute transport in cartilage. Articular cartilage and osteoarthritis, 355–371.

Patel, R., O'Leary, J., Bhatt, S., Vasnja, A., Knothe Tate, M., 2004. Determing the permeability of cortical bone at multiple length scales using fluorescence recovery after photobleaching techniques. In: Proc 51st Annual ORS Meeting. Vol. 141.

Sigmund, E., Cho, H., Chen, P., Byrnes, S., Song, Y.-Q., Guo, X., Brown, T., 2008. Diffusion-based MR methods for bone structure and evolution. Magnetic Resonance in Medicine 59 (1), 28–39.

Tandon, P., Agarwal, R., 1989. A study of nutritional transport in a synovial joint. Computers & Mathematics with Applications 17 (7), 1131–1141.

Tate, M. K., Steck, R., Forwood, M., Niederer, P., 2000. In vivo demonstration of load-induced fluid flow in the rat tibia and its potential implications for processes associated with functional adaptation. Journal of Experimental Biology 203 (18), 2737–2745.

Wang, L., Wang, Y., Han, Y., Henderson, S. C., Majeska, R. J., Weinbaum, S., Schaffler, M. B., 2005. In situ measurement of solute transport in the bone lacunar-canalicular system. Proceedings of the National Academy of Sciences of the United States of America 102 (33), 11911–11916.

Weinbaum, S., Cowin, S., Zeng, Y., 1994. A model for the excitation of osteocytes by mechanical loading-induced bone fluid shear stresses. Journal of biomechanics 27 (3), 339–360.

Paper B

A. Shokry (2015)

A methodology for using Kalman filter to determine material parameters from uncertain measurements

Submitted for international publication

A methodology for using Kalman filter to determine material parameters from uncertain measurements

Abdallah Shokry[a,b]

[a] *Division of Solid Mechanics, Lund University, 22100 Lund, Sweden*

[b] *Industrial Engineering Department, Fayoum University, 63514 Fayoum, Egypt*

Abstract

A Kalman filter can be used to determine material parameters using uncertain experimental data. However, starting with inappropriate initial values for material parameters might include false local attractors or even divergence. Also, inappropriate choices of covariance errors of initial state, present state, and measurements might affect the stability of the prediction. The present method suggests a simple way to predict the parameters and the errors, required to start Kalman filter based on known parameters that are used to generate the data with different noises used as "measurement data". The method consists of two steps. First, an appropriate range of parameter values is chosen based on a graphical representation of the mean square error. Second, the Kalman filter is used based on the selected range and the suggested parameters and errors. The method of the filter significantly reduces the iteration time, and covers a wide range of initial suggested values for the parameters compared with the standard Kalman filter. When the methodology is applied to real data, very good results are obtained. Diffusion coefficient for bovine bone is chosen to be a case study in this work.

1 Introduction

The Kalman filter is an inverse method to determine variables or parameters using input data with more noise and get output data with less noise. It is firstly presented by Kalman (1960). Kalman filter has the advantages of taking the random noise for state and measurements into consideration, also it is an optimal estimator for linear models because it minimizes the mean square error between the state. In addition, it converges quickly. A more complete introduction to the Kalman filter is given by Brown (1983). The Kalman filter can be found under different updated forms that used in many different fields such as tracking objects (Siouris et al., 1997; Weng et al., 2006; Antonov et al., 2011), control systems (Ahn and Truong, 2009; Shi et al., 2009), and weather forecast (Mitchell and Houtekamer, 2009; Wu et al., 2010; Miyoshi and Kunii, 2012).

Nomenclature

α_{ij}	elements of covariance matrix of stochastic vectors a, and b.
$\boldsymbol{P}_k^-$, $\boldsymbol{P}_k$	variance errors of the parameters before and after iterative update at iteration k
$\boldsymbol{Q}_k$, $\boldsymbol{Q}$	covariance error of the parameters at iteration k, constant covariance
$\boldsymbol{R}_k$, $\boldsymbol{R}^{(i)}$	covariance error for measurements at iteration k, constant covariance at initial parameters i
$\hat{x}_k$	vector of estimated state variables at iteration k
$\mathbf{H}$, $\mathbf{H}_k$	matrix of derivatatives of h, at iteration k
$\mathbf{K}_k$	$n \times N$ matrix represents Kalman gain
$\mathcal{M}(\hat{x})$	mean square error between z and h
ν, ν_k	vectors of N errors of the measurements, at iteration k
Φ	sum of the squared residuals between z and h
ϑ_i	elements of noise vectors w, and v
$\zeta(t)$	conductivity of escaped ions at time t
a, b	two stochastic vectors
A, B, R	three constants
D, D_k	diffusion parameter, at iteration k
h	vector of N predicted measurements
L	side length of bone sample
N, n, M	number of measurements, state variables, iterations
p	a priori estimated relative variance
T	transpose
t	time
w, w_k	vectors of n perturbations of the state variables, at iteration k
w_D, w_B	noise of parameters D, and B
x, $\bar{x}$, x_0	vectors of n unknown, perturbed, initial state variables
z, z_k, z_{av}	vectors with N measurements, at iteration k, avergare z

Kalman filter can be used to determine material parameters from uncertain and inaccurate measurements. Aoki et al. (1997) used Kalman filter to identify Gurson's model constant. They found that the accuracy of parameters prediction is affected by both specimen geometry and measurement type, and the shape of the tested specimen affects the convergence of the parameters. Also, they noticed that the rate of convergence can be improved by combining measurements of two different specimens in shape. The identification of Gurson–Tvergaard material model parameters via Kalman filtering technique is studied by Corigliano et al. (2000). They stated that the estimated values of the parameters are in well agreement with those obtained in previous work, but the initial suggested values for the seeking parameters affects the estimated parameters.

Nakamura and Gu (2007) implemented Kalman filter to determine elastic−plastic anisotropic parameters for thin materials using instrumented indentation. They observed that the initial chosen values for the parameters converged to a specific small area, but not to one point. Also, based on the convergence intensity, the parameters are determined. The same findings are obtained by using Kalman filter to determine the nonlinear properties of thermal sprayed ceramic coatings (Nakamura and Liu, 2007). Bolzon et al. (2002) used Kalman filter to identify parameters of a cohesive crack model. They reported that almost a linear correlation between convergent parameters is found, and the reason for the multiple local minimum might be related to using the linear Kalman filter for non-linear model.

Vaddadi et al. (2003) used Kalman filter to determine critical moisture diffusion parameters for a fiber reinforced composite. They estimated the parameters from the intensity of the convergence, which found to be in consistent with known values. Another study made by Vaddadi et al. (2007) to determine hygrothermal properties in fiber reinforced composite using Kalman filter. The parameters are extracted by reading the intensity of convergence plot.

Kalman filter is an efficient way to filter noisy experimental data for determination of material parameters. However, the initial suggested parameters required for Kalman filter should be chosen carefully, to avoid false local attractor. Also, the covariance error for the parameters noise almost assumed to be zero, which slow the rate of convergence and might lead to more than one intensity area for the predicted parameters.

In this study, a methodology will be applied for using Kalman filter to determine material parameters using uncertain measurements. The methodology starts by a way based on the mean square error to choose appropriate initial suggested parameters required for Kalman filter, and followed by a suggested way to choose the covariance errors for both state and measurements. The determination of diffusion coefficients in bovine bone for generated data with different noises scatter from known parameters will be applied as a case study. A real measurements will be used also.

2 Methods

2.1 The Model

Assume that an experiment resulted in N measurements obtained at different times, locations, temperatures etc. These are collected in a vector, z, with N measurements. Measurements and all other data are available *a priori*.

In an attempt to predict the measurements a model, $h = h(x)$ is used, with h being a vector of N predictions of observations. Further, x is a vector of n unknown parameters defining the model based on variables such as position, temperature, time, etc. The unknown model parameters may describe the state of the system regarding, material, geometry or similar. In the present study, x is limited to parameters describing the material.

Measurements always include systematic and non-systematic errors due to instrumentation, indirect observations, gauges sensitive, irrelevant external influence, and similar. Material parameter is sought but the experimental method may require a state parameters to be determined as well. Further, material parameters contain non-systematic errors due to thermal fluctuations, unstable structural configurations such as mobile dislocations, impurities, inclusions, unstable chemical composition, etc. Also inevitably, there is a difference between model and reality while a model never gives an exact description of the physical processes. Under ideal conditions the model would perfect in the sense that $z = h(x)$. Here, only non-systematic errors or noise is considered. The model is defined for measurement i as

$$z = h(\bar{x}) + v\,, \tag{1}$$

where v is a vector with N errors due to inaccurate measurements z. The instant parameter $\bar{x}$ corresponding to the individual measurement i includes noise according to

$$\bar{x}{=}x + w\,, \tag{2}$$

where w is a vector with n errors caused by the parameter deviations. The elements of v and w are assumed to be uncorrelated. All elements of w and v are supposed to be random, having the same respective stochastic distribution and for both a vanishing mean value is expected, cf. (Brown, 1983).

Assuming that a set of parameters $\hat{x}_k$ is an estimate in the neighborhood of x, an improved estimate $\hat{x}_{k+1}$ may be obtained by using linearized using a Taylor series which gives

$$h(\hat{x}_{k+1}){\approx}h(\hat{x}_k) + \mathbf{H}(\hat{x}_k)(x - \hat{x}_k)\,, \tag{3}$$

where quadratic and higher order terms of x are neglected. On matrix form involved variables are

$$h(x){=}\begin{bmatrix} h^{(1)} \\ \vdots \\ h^{(N)} \end{bmatrix},\ \mathbf{H}(x){=}\begin{bmatrix} \dfrac{\partial h^{(1)}}{\partial x_1} & \cdots & \dfrac{\partial h^{(1)}}{\partial x_n} \\ \vdots & \ddots & \vdots \\ \dfrac{\partial h^{(N)}}{\partial x_1} & \cdots & \dfrac{\partial h^{(N)}}{\partial x_n} \end{bmatrix},\ x = \begin{bmatrix} x_1 \\ \vdots \\ x_n \end{bmatrix}. \tag{4}$$

Here, $\mathbf{H}$ is an $N \times n$ a Jacobian matrix.

2.2 Least-Squares

The system is supposed to be overdetermined, meaning that the number of measurements N exceeds the number of unknown parameters n. The best fit in the least-squares sense minimizes the sum of squared residuals with a residual being the difference between an observations z and the predictions $h(x)$. The unknown x is obtained in a series of iterative improvements of the approximation $x \approx \hat{x}_k$, where k is the iteration number. The initial parameters x_0 may be an educated guess based on previous measurements, data from resembling materials or other similar expectations.

Solutions for non-linear systems (see Appendix A) may be obtained iteratively. As an example, the Newton-Raphson method applied to these solutions gives the following recursive scheme,

$$\hat{x}_{k+1} = \hat{x}_k + (\mathbf{H}_k^{\mathrm{T}}\mathbf{H}_k)^{-1}\mathbf{H}_k^{\mathrm{T}}\{z - h(\hat{x}_k)\}, \tag{5}$$

where $\mathbf{H}_k$ is an $N \times n$ matrix and a function of $\hat{x}_k$. If convergence is reached, a local minimum of the sum of squared residuals has been found. To find global minimum, additional steps have to be taken. The drawback of the method is that convergence is not necessarily reached and is less likely if the *a priori* information of x is vague, unreliable or even misleading. This is especially accentuated when the measurements are noisy. Further, all data have to be present *a priori*. Modifications have been developed that allow an incremental treatment, which may be useful if data is continuously added, cf. (Plackett, 1950).

2.3 Kalman Filter

The method of least-squares does not take the properties of the noises v and w as regards expected mean value and distribution into account. Opposed to that, the Kalman filter is developed to use information about the noise *a priori* or as the measurements are assembled. The filter is an improvement of the least-squares method as it recursively optimizes the unknown model parameters in search for least sum of squared errors. The method is developed with the particular endeavor to effectively handle noisy input data (Brown, 1983). It is also operating incrementally so that new may be added as they appear in during ongoing measurements without loss of accuracy. However, in the present study all measurements are supposed to be available when the optimization is initiated. The Kalman method is generally assumed to be an effective method to filter noisy data combined with a high convergence rate. The derived algorithm is taking the character of the noise into consideration. The expected vanishing mean values for ν and w are explicitly utilized.

Assuming that the measured data is the predicted data based on the optimum material parameters with the addition of noise, as given by Eq. (1) it is here assumed that the noise ν a distribution with a zero mean value.

Initially a set of parameters x_0 is selected based on *a priori* information from other measurements under same or similar conditions or otherwise known data. From this, the

parameters are iteratively updated using an algorithm on the same form as the least-squares algorithm (cf. Eq. 5) as follows

$$\hat{x}_{k+1} = \hat{x}_k + \mathbf{K}_k\{z_k - h(\hat{x}_k)\} \qquad \text{for} \qquad k{=}0, 1, 2, ...M\,, \tag{6}$$

where $\mathbf{K}_k$ is an $n \times N$ matrix denoted the Kalman gain, and M is the number of iterations. In Eq. (6). Normally the Kalman algorithm operates on single measurements one by one so that the Kalman gain is updated for every new measurements. This may be necessary for interactive processes where the action requires knowledge of the instantaneous state of the system. In the present study, iterations are simultaneously utilizing all measurements. The derivation of the Kalman gain (see Appendix B) is based on measurements added recursively as in the original form of the filter.

The optimal $\mathbf{K}_k$ that minimizes the mean square error is given by

$$\mathbf{K}_k = \boldsymbol{P}_k^- \mathbf{H}_k^{\mathrm{T}} (\mathbf{H}_k \boldsymbol{P}_k^- \mathbf{H}_k^{\mathrm{T}} + \boldsymbol{R}_k)^{-1}\,, \tag{7}$$

where $\boldsymbol{P}_k^-$ is the variance of the errors of the parameters before the iterative update, and $\boldsymbol{R}_k$ is $N \times N$ matrix introduces the covariance error of the measurements that computed as

$$\boldsymbol{R}_k = \mathrm{Var}(v_k)\,. \tag{8}$$

The $\boldsymbol{P}_{k+1}^-$ is expressed as

$$\boldsymbol{P}_{k+1}^- = (\boldsymbol{I} - \mathbf{K}_k \mathbf{H}_k)\boldsymbol{P}_k^- + \boldsymbol{Q}_k\,, \tag{9}$$

where $\boldsymbol{Q}_k$ is an $n \times n$ matrix represents the covariance errors for the state parameters that is computed as

$$\boldsymbol{Q}_k = 2\mathrm{Var}(w_k). \tag{10}$$

The derivation of $\mathbf{K}_k$, $\boldsymbol{P}_k^-$, $\boldsymbol{R}_k$, and $\boldsymbol{Q}_k$ are given in details in Appendix B.

The algorithm involves recursive use of the Eqs. (6), (7) and (9). The measurements considered in each recursive cycle may be everything from a single measurement to all measurements. For non-linear problems, each cycle may be repeated until convergent results are obtained. As an alternative, the entire recursive scheme may be restarted and the resulting parameters x_n, $\boldsymbol{P}_n^-$, from previous application of the scheme are used as initial parameters. Also $\boldsymbol{Q}_k$ and $\boldsymbol{R}_k$ may be adjusted based on the improved information that is obtained. In the present study, all measurements are placed in a single set with N measurements, meaning that $z_k = z$ is a constant vector with N elements. The number of recursive cycles is M and $k = 1, 2, ..., M$ where M is prescribed or conditional. The recycling is performed to achieve a converged result for a non-linear problem. In each cycle, x_k, $\mathbf{H}_k$, $\boldsymbol{P}_k$ and therefore $\mathbf{K}_k$ is updated.

By putting $\boldsymbol{R}_k = R\boldsymbol{I}$ in Eq. (7) and then taking the limiting result as $R \to 0$ one obtains $\mathbf{K}_k = \mathbf{H}_k^{\mathrm{T}}(\mathbf{H}_k\mathbf{H}_k^{\mathrm{T}})^{-1} = (\mathbf{H}_k^{\mathrm{T}}\mathbf{H}_k)^{-1}\mathbf{H}_k^{\mathrm{T}}$. After inserting this into Eq. (6) it is readily seen that the result is identical to that of the non-linear least squares method, cf. Eq. (5). The result is independent of $\boldsymbol{P}_k^-$ and consequently also independent of $\boldsymbol{Q}_k$.

3 Methodology

In Aoki et al. (1997), Nakamura and Gu (2007), and Vaddadi et al. (2007), the $\boldsymbol{R}_k$ was chosen to be a small percentage of the measured data, and the $\boldsymbol{Q}_k$ value was chosen to be zero. In a recent study, the $\boldsymbol{R}_k$ value was chosen as the difference between the measured data and a predicted data a round the measured data, and the $\boldsymbol{Q}_k$ was chosen to be unity (Lindberg et al., 2014).

To use the Kalman filter the parameters $\boldsymbol{Q}_k$ and $\boldsymbol{R}_k$, and initial values for $\hat{x}_0$ and $\boldsymbol{P}_0^-$ have to be defined. In the following, different strategies for choosing these values is described.

For common usage of the Kalman filter, the choice would be $\boldsymbol{R}_k = \mathrm{Var}(\nu_k)$ and $\boldsymbol{Q}_k = 2\mathrm{Var}(w_k)$ according to Eqs. (8) and (10). These variations are assumed to be known *a priori*, at least approximately. The information may be based on expectation or derived from the present measurements, using a large variety of hypotheses. When the method is used recursively, the indices k allow for using $\boldsymbol{Q}_k$ or $\boldsymbol{R}_k$ or both as functions of time, position, etc.

The Kalman gain, given by Eq. (7), with the selected $\boldsymbol{Q}_k$ or $\boldsymbol{R}_k$, minimizes the squared error of the estimate $\hat{x}_k$ of x. A condition for the derivation is that $h(x)$ is a linear function of the parameters x. In the present study, $h(x)$ is a non-linear function of x. The aim is to formulate a strategy for selecting the free parameters $\boldsymbol{R}_k$ and $\boldsymbol{Q}_k$, not necessarily according to Eqs. (8) and (10), so that the square of the error

$$\mathcal{M}(x) = \frac{1}{N}\mathrm{Var}(z - h(x))\,, \tag{11}$$

is minimized. The study does not attempt to be exhaustive and the conclusions are empirical and based on a case study. The selection of method is primarily based on convergence rate. With a wide range of starting values, occasionally the estimate converges outside the range of interest and there is also the risk of failure in producing converging results at all. These, disadvantages are also considered in the selection of a suitable procedure for selecting $\boldsymbol{R}_k$ and $\boldsymbol{Q}_k$.

In the first part of the study, the initial parameters $\hat{x}_0$ are selected to cover a several orders of magnitude wide range of values. Under normal circumstances, this cannot be done for non-linear phenomena or realistic geometries or anything else for which an analytical solution cannot be found, which may be the general case. When the predictions are based on non-linear numerical calculations of field problems, e.g., using lengthy finite element analyses, usually only a few initial parameters $\hat{x}_0$ can be considered. Here however, a wide range of initial parameters is examined as regards the mean square error $\mathcal{M}(\hat{x}_0)$. The aim is to obtain an overall picture of the possibilities of fast convergence or difficulties because of present local minima, sadle points etc.

The second part is, the using of a suggested method and comparing the resulting convergence rate, the ability of producing convergent results, and the percentage of convergent results from a range of the initial parameters with three additional methods. All four methods are described in subsec. 3.1.

3.1 Selecting $\boldsymbol{Q}_k$ and $\boldsymbol{R}$

In the present study, the results of constant

$$\boldsymbol{Q}_k = 2p^2 x x^{\mathrm{T}} \quad \text{including} \quad \boldsymbol{Q}_k = 0, \tag{12}$$

are evaluated. The parameter p is an *a priori* estimated relative variance.

The relative variance p of the state parameters is a quantity that possibly can be guessed with more or less accuracy. Since the real state parameters x are not known *a priori* constant $\boldsymbol{Q}_k$ may be either too big or too small depending on how accurate initial guess of x_0 is. However, since the knowledge of the state variables increases as the iterations proceed, to stick a constant $\boldsymbol{Q}_k$ may unnecessarily slow down the convergence rate. As the iterations proceed, the estimate x_k is improved and a better estimate for $\boldsymbol{Q}_k$ can be used. Here, an updated $\boldsymbol{Q}_k$ is also evaluated. With the variation of x being $w_k = px$, the unknown x is here assumed to best approximated with x_k. The updated value given by Eq. (10) then becomes

$$\boldsymbol{Q}_k = 2p^2 \mathrm{Var}(x_k)\,. \tag{13}$$

The $\boldsymbol{R}_k$ taken as

$$\boldsymbol{R}^{(i)} = v^{(i)} I,\ i = 1, 2, ...U, \tag{14}$$

which is assumed to be a reasonable approximation of Eq. (8), where measurement noise $v^{(i)}$ is given by

$$v^{(i)} = \max|\mathrm{Var}(z_N - h_N(\hat{x}_0^{(i)}))|], \tag{15}$$

where max denoted to the maximum value, and U is the number of initial parameters.

In the suggested method, the $\boldsymbol{Q}_k$ and $\boldsymbol{R}^{(i)}$ are chosen for large values based on the evaluation according to Eqs. (7) and (9), cf. sec. 5 for explanation. There are additional two Kalman filter methods, one method uses $p = 0$ in Eq. (12), and the another method uses $p = 0.01$ that gives the smallest standard deviation and largest percentage of convergence among different values for p, the mean values are closest to each other (see Fig. 4). These two methods use $\boldsymbol{R}_k$ as

$$\boldsymbol{R} = [\max|\mathrm{Var}(z_N - h_N(x))|]I\ , \tag{16}$$

so, the $\boldsymbol{R}$ is the largest squared element for the variance of the difference between measured data, z, and predicted data with noise. Here, $\boldsymbol{Q}$ and $\boldsymbol{R}$ without k index denote constant covariances during iterations.

The fourth method is the non-linear least squares method, which is obtained by letting $\boldsymbol{R}_k \to 0$ as it is described in subsec. 2.3.

3.2 The Initial Predicted Parameters Error $\boldsymbol{P}_0^-$

The initial predicted parameters error $\boldsymbol{P}_0^-$ is an $n \times n$ matrix that contains the expected values for the errors between the unknown parameters x_k and the initial predicted parameters $\hat{x}_0$ before the first iteration (see Appendix B). $\boldsymbol{P}_0^-$ is chosen as

$$\boldsymbol{P}_0^- = \mathrm{Var}(\hat{x}_0^{(max)} - \hat{x}_0^{(min)}), \tag{17}$$

where $x_0^{(max)}$ and $x_0^{(min)}$ are the two vectors that contain maximum and minimum of the selected initial values for the parameters. The choice for $\boldsymbol{P}_0^-$ is the same in all cases in the present study. Only one large initial value is tested since the $\boldsymbol{P}_0^-$ introduces the variance between the seeking parameters and the initial parameters.

3.3 Summary of Methods

A summary for the four used methods with the percentage of convergent results over total results (D.N%) for each method is presented in Table 1.

Table 1: Methods used

Method	$\boldsymbol{Q}$	$\boldsymbol{R}$	$\boldsymbol{P}_0$	D.N%
Kalman filter 1 (suggested method)	$\boldsymbol{Q} = \boldsymbol{P}_0$ as in Eq. (23)	Eq. (26)	Eq. (17)	92.09
Kalman filter 2	Eq. (12) with $p = 0$	Eq. (16)	Eq. (17)	80.90
Kalman filter 3	Eq. (12) with $p = 0.01$	Eq. (16)	Eq. (17)	80.19
Non-linear least squares	–––	0	–––	40.93

4 Case Studies

The determination of the diffusion coefficient of mammal bone using uncertain data is chosen to be a case study. Diffusion has recently been suggested to play an important role in transporting substances from the inner boundaries to the outer boundaries of bone. Therefore, knowing the diffusion coefficients in human bone are important to give required information for design of individual exercise programs that maximizes bone remodeling and bone healing.

In the present study, the proposed four methods are applied to several simulated cases of generated data and the most effective method is applied to a case of real experimental data. The real experiment measures the amount of ions that leaves bovine bone samples that were put into a container with distilled water. During elapsing time the conductivity, $\zeta(t)$, of the water increases in proportion to the ionic concentration. The experiment is reported in Lindberg et al. (2014). Cubic bone samples with the side length L =10.1 mm from a bovine long bone were used. The concentration were measured using a SevenEasy

S30 conductivity meter from Mettler Toledo with an accuracy of $\pm 0.5\%$ of the measured value. Further details regarding the experiment is found in Lindberg et al. (2014).

The following model is suggested for the conductivity as a function of time, t,

$$\zeta(t) = A - B \sum_{m=1}^{M} \frac{8}{\pi^2(2m-1)^2} \exp\{-(2m-1)^2\pi^2 D \frac{t}{L^2}\} \,, \tag{18}$$

where D is the diffusion coefficient, and A and B are unknown constants. The model is based on Fick′s law using relevant boundary conditions.

The constants A and B provide the relation between the concentration in the bone sample and the conductivity in the distilled water. Putting $t = 0$ gives

$$A = \zeta(0) + B \,, \tag{19}$$

where $\zeta(0)$ taken to be the conductivity measured at $t = 0$. By using $h(t) = \zeta(t) - \zeta(0)$ as the measured quantity, the following model is obtained,

$$h(t) = B(1 - \sum_{m=1}^{M} \frac{8}{\pi^2(2m-1)^2} \exp\{-(2m-1)^2\pi^2 D \frac{t}{L^2}\}) \,. \tag{20}$$

The two remaining constants D and B are determined using the Kalman filter. More details are found in Lindberg et al. (2014).

To the experiment is added a Monte Carlo set of 250 fictive measurements where generated data is used as measurements. The measured data is generated using the exact model Eqs. (1) and (20) to compute the measurement vector z. To provide realistic conditions, a variation is added to the state parameters D and B and to the measurements. To this end, a random noise of 5%, i.e. $|w_D| < 0.05D$ and $|w_B| < 0.05B$, is added. In the same way, noises ν of 10%, 50% and 100% are included in the generated measurements z, i.e. $z = h(t) + \nu$, where $\nu = q\frac{1}{N}\sum h(t_i)$ and q equals 0.1, 0.5 and 1. Summation is performed for the 24 different times of measurement. Further, the w_D, w_B and ν are uncorrelated and the probability density is constant within the limits of the respective noise. Also the noises for each measurements are uncorrelated. Thus,

$$\mathrm{Cov}(\vartheta_i, \vartheta_j) = \begin{cases} \vartheta_i^2 & \text{if} \quad i = j \\ 0 & \text{if} \quad i \neq j \end{cases} \,, \tag{21}$$

where ϑ_i and ϑ_j represent the elements of each noise vector w_D, w_B and ν at individual measurements i and j.

As observed from Eq. (20), the only available time unit is provided by L^2/D. A typical experiment lasts for around 11.7 time units, i.e., $0 \leq t \leq 11.7L^2/D$ with generated measurements taken in time intervals of around $0.0032L^2/D$.

In an attempt to obtain less non-linear formulation of Eq. (20), a semi-linear model that is obtained after simplification and taking log of both sides of Eq. (20) one obtains

$$h^*(t) = B^* + f(D,t)\,, \tag{22}$$

where

$$h^*(t) = \log\{h(t)\}\,,\quad B^* = \log(B),$$

and

$$f(D,t) = \log\left(1 - \sum_{m=1}^{M} \frac{8}{\pi^2(2m-1)^2}\exp\{-(2m-1)^2\pi^2 D\frac{t}{L^2}\}\right),$$

which makes $h^*(t)$, a linear function of B^* while $f(D,t)$ is known to be rather small. Note that $\log(1-e^{-x}) \to e^{-x}$ as $x \to \infty$ and therefore $f(D,t)$ decays exponentially for large with increasing time which makes the linearization with respect to D undoable.

5 Results and Discussions

The accuracy of the series in Eq. (20) was studied in this work to reduce the computational time, it showed that the number of terms m may be chosen to be around 200 terms to obtain an accuracy of 99.9% in the middle of the sample at $t = 0$. Already at the second measurement at $t = 0.0003L^2/D$ only four terms are required to obtain the same accuracy. For systems with large amounts of data, a strategy for the selection of the number of terms in the series could save considerable computation time. However, here this is not the primary focus and the the calculations where not very much time consuming, which is why all calculations where made using $M = 200$ terms.

Measurements are generated from known D and B using $w_D = 0.1D$, $w_B = 0.1B$, and $v = 0.1z_{av}$ where z_{av} is the average of all generated measurements i.e $z_{av} = \frac{1}{N}\sum z_i$. Then the Kalman filer was used to obtain approximations of D and B. This was done first for the non-linear model Eq. (20), and then for the partly linearized model Eq. (22). To compare the accuracy in finding the least square error of the predicted measurements based on different state parameters found using model Eq. (20) and model Eq. (22) respectively, the least square error $\mathcal{M}(x)$ was calculated using Eq. (11). The non-linear model gave $\mathcal{M}(x) = 15\%$ while the partly linearized model gave 30%. For the reason of this, the partly linearized model is given up and the model Eq. (20) is used in the continued analysis.

Assuming that the information of the parameters D and B is uncertain, the Kalman filtering has to converge from initial values that are several orders of magnitudes different from the true values. To explore what this means, the mean square error is calculated for a very wide range of initial values. Mean square error here refers to the error of calculated estimates of the initial guesses D_0 and B_0 directly compared with the true values of D and B. No iterations are made. To cover a large variety of initial values a mesh 101 values for D and for each 101 values for B are used. The mesh covers values of D_0 ranging from $0.001D$ to $100D$ and values of B_0 from $0.01B$ to $100B$. Fig. 1 shows the mean square error for the initial values of D_0 and B_0 for the constructed mesh.

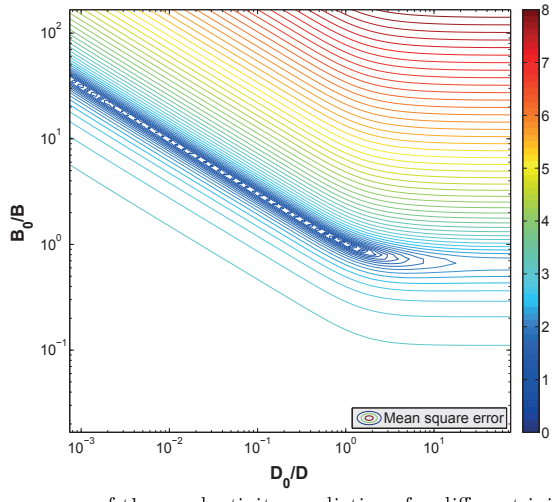

Fig. 1. The mean square error of the conductivity predictions for different initial values of the relative initial parameter values D_0/D and B_0/B. The noises are in the range $\pm 5\%$ for parameters and $\pm 10\%$ for measurements.

Regions with small gradients are found along a line for which D_0/D approximately equals $(B_0/B)^{-2}$. The several local minima along this trajectory correspond to the resolution of the grid and are merely graphical anomalities. Also in the region of small D_0 and large B_0 the gradient is very small. This makes the convergence rate of any gradient driven algorithm small. However, no local minimum seems to be present and convergence should be possible in entire range of initial values even if the convergence may be very slow in the above describe regions. A clear minimum mean square error is found around the close to D and B. The result is strongly influenced by the rapid changes due to the exponential behavior of Eq. (20).

For the study of the Kalman filter measurements z are generated for 250 measurements in the time interval $0 \leq t \leq 11.7L^2/D$. In this study, D and B are known parameters, but in a real case they are not known but believed to be in the neighborhood of the *a priori* guess. As it is suggested by Fig. 1, a very large variation of convergence rates are anticipated.

The Kalman filter is studied by gathering 10 generated experiments together, each experiment has 25 measurements, and each measurement has random noises of $\pm 5\%$ for parameters and $\pm 10\%$, $\pm 50\%$, and $\pm 100\%$ for measurements, which constructs a measurement vector z_i, i=1,2,3.....,250. The initial selected state variables are chosen from $0.1D$ to $10D$ for D_0 and from $0.1B$ to $10B$ for B_0.

The initial parameters error $\boldsymbol{P}_0^-$ is selected according to Eq. (17) as follows

$$\boldsymbol{P}_0^- = \begin{bmatrix} 9.9^2 D_0^2 & 0 \\ 0 & 9.9^2 B_0^2 \end{bmatrix}. \tag{23}$$

The $\boldsymbol{P}_k^-$ is updated using Eq. (9).

5.1 Different $\boldsymbol{R}$ and $\boldsymbol{Q}_k$

First $\boldsymbol{R}^{(i)}$ values are calculated as in Eq. (14). So, $\boldsymbol{R}^{(i)}$ is the squared largest element of the variance encountered so far, i.e. so far means before iteration k.

The effect of $\boldsymbol{Q}_k$ is studied by using,

$$\boldsymbol{Q}_k = \begin{bmatrix} (D_k - D_0)^2 & 0 \\ 0 & (B_k - B_0)^2 \end{bmatrix}. \tag{24}$$

This means that $\boldsymbol{Q}_k$ increases as the iterations proceed. The expected effect is that the convergence rate increases with increasing $\boldsymbol{Q}_k$. Which is selected to speed up the convergence rate.

Fig. 2a shows a color plot of the obtained values for D_1/D, here 1 is number of iterations. The markers ($\times$) that are included show the obtained values of D_1/D and B_1/B using Kalman filter, for 41×41 initial values D_0/D and B_0/B. The obtained (D_1/D,B_1/B) outside the selected range are excluded from convergence plot to make it in the same range as the color plot. The white areas in the figure give 21.5% of the obtained D_1/D that found to have negative values with no physical meaning. Consequently, this leads to divergent results in following iteration since the exponential term in the diffusion model would have large positive values. A large step for Kalman gain, $\mathbf{K}_k$, seems to be the reason, which can be forced to be small by assuming $\boldsymbol{R}$ large, but the rate of convergence would be slow.

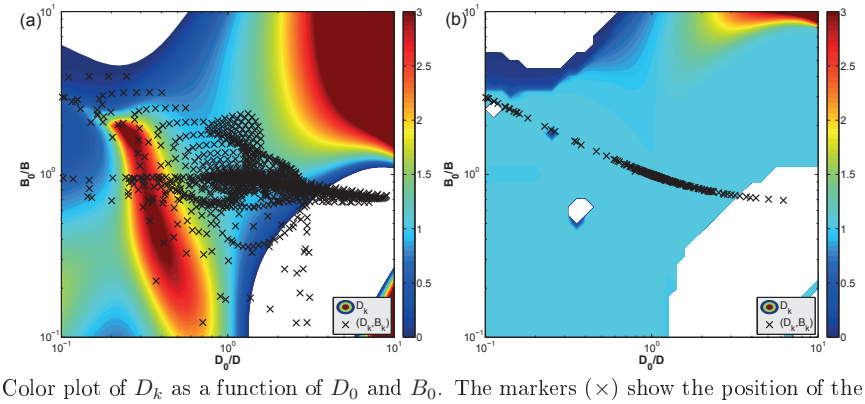

Fig. 2. Color plot of D_k as a function of D_0 and B_0. The markers ($\times$) show the position of the resulting D_k and B_k for the 1681 initial starting points in the range. (a) $k = 1$ iteration, and (b) $k = 20$ iterations. Noises are $\pm5\%$ for the parameters and $\pm10\%$ for the measurements.

Fig. 2b shows the color and convergence plot after 20 iterations. It can be seen that using larger values for $\boldsymbol{Q}_k$ increases the rate of convergence but the divergent cases increased from 21.5% to 22.4%.

The effect of $\boldsymbol{R}$ values on the convergent D_1/D is shown in Fig. 3a. The figure shows that the percentage of the number of convergent D_1/D over the total number of D_1/D

almost around 80% as the $\boldsymbol{R}$ value increases from $0.000039B^2$ to $0.6B^2$, after that it begins to increase to 95% as the $\boldsymbol{R}$ increases to $3B^2$, then it almost keep around this percentage with larger values for $\boldsymbol{R}$. A possible reason is that the Kalman gain step becomes small as the $\boldsymbol{R}$ value increases.

The effect of $\boldsymbol{R}$ on standard deviations and mean values are shown in Fig. 3b. The figure shows that the standard deviation decreases as the $\boldsymbol{R}$ increases untill $\boldsymbol{R} = 1.5B^2$, then it increases slowly, also the mean value decreases as the $\boldsymbol{R}$ increases to $0.02B^2$, and then increases again. The $\boldsymbol{R}/B^2$ (Kalman) in the graph denoted suggested $\boldsymbol{R}$ for ordinary Kalman filter based on the average value of z and the 10% measurements noise, i.e $\boldsymbol{R} = (0.1z_{av})^2$, which is not the optimal case. One reason is that standard deviations and mean values are computed after one iteration, also the negative values of D are included. Slightly different results are obtained after more iterations, reason should be the non-linear model.

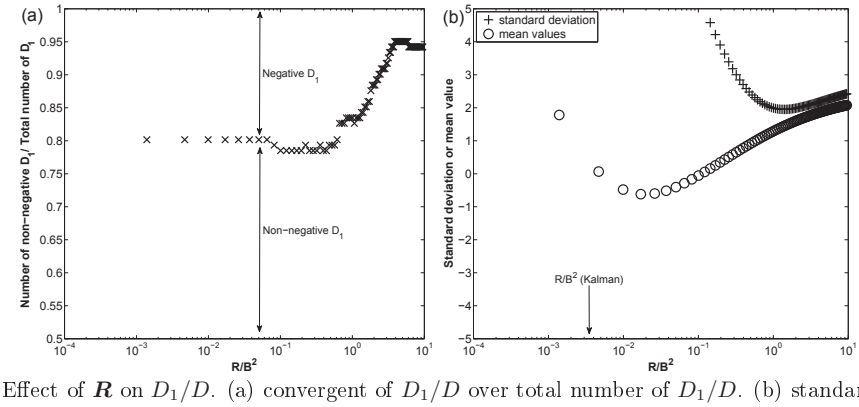

Fig. 3. Effect of $\boldsymbol{R}$ on D_1/D. (a) convergent of D_1/D over total number of D_1/D. (b) standard deviations and mean values, the standard deviation values over 5 are excluded from the graph. $\boldsymbol{Q} = 0$.

Fig. 4a shows the effect of different values of $\boldsymbol{Q}$ using $0.01 \leq p \leq 1$ and $\boldsymbol{R}$ as given in Eq. (16) on the convergent numbers of D_5/D over total number of D_5/D. It is clearly seen that the number of convergent D_5/D decreases as the p increases. Using large $\boldsymbol{Q}$ with small $\boldsymbol{R}$ affects the Kalman gain stability, this could be a possible reason.

Fig. 4b shows the effect of p on the standard deviations and mean values for the obtained D_5/D. The figure shows that standard deviation increases as p increases, and mean values play around 1.7 as the p increases. One reason could be that using large values of $\boldsymbol{Q}$ with small values for $\boldsymbol{R}$ increases the Kalman gain step. The $\boldsymbol{Q}$ value at $p = 0.71$, random walk, cf. (Brown, 1983), and at $p = 1$, the suggested variance as in Eq. (13), does not give significant effect on both standard deviations and mean values. A non-linear model might be a reason, so it is expected to have effect with more iterations. The p value is chosen for 0.01 that give smallest standard deviation and largest percentage of number of convergent D over total number of D to be one method (see Table 1).

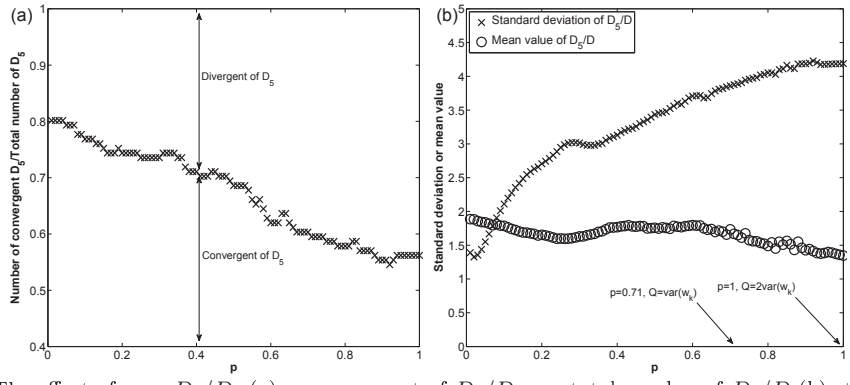

Fig. 4. The effect of p on D_5/D. (a) on convergent of D_5/D over total number of D_5/D (b) standard deviations and mean values of D_5/D. $\boldsymbol{R}$ is chosen as in Eq. (16).

5.2 Large $\boldsymbol{R}$ and $\boldsymbol{Q}$

By studying Eqs. (7) and (9), and Fig. 3 it is believed that choosing $\boldsymbol{R}$ large, decreases the risk of ending up with divergent results for D_k. Fig. 5a shows that increasing p for large values using $\boldsymbol{R}$ large increases the percentage of the number of convergent D_5 by 3%, this is an indication that using $p > 0$ with $\boldsymbol{R}$ large covers a wide range of initial parameters that converges.

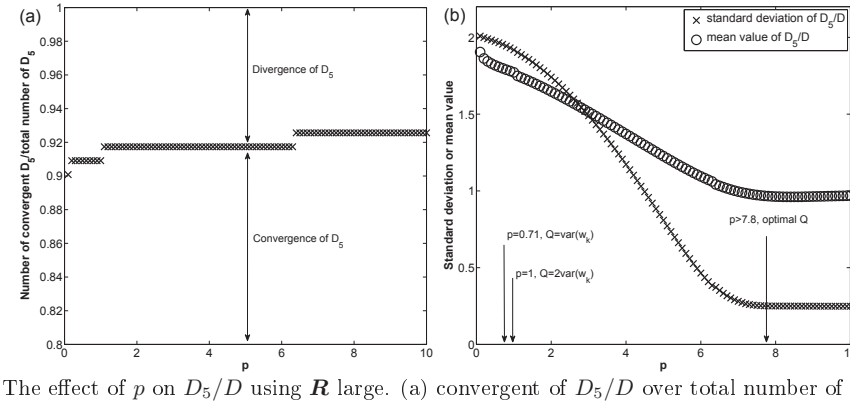

Fig. 5. The effect of p on D_5/D using $\boldsymbol{R}$ large. (a) convergent of D_5/D over total number of D_5/D (b) standard deviations and mean values of D_5/D. The large $\boldsymbol{R}$ is chosen as in Eq. (26).

The effect of $\boldsymbol{Q}$ on the standard deviations and mean values of the obtained D_5/D are shown in Fig. 5b. It can be seen that the standard deviation and mean value decrease as the p increases, untill optimal is obtained with $p > 7.8$. Also, increasing p speeds the rate of convergence. Again, this could be the effect of non-linearity of the model.

It can be concluded that using $\boldsymbol{R}$ and $\boldsymbol{Q}$ large increases the possibility of convergence for a wide range of D_0 and B_0 and speeds the convergence rate of parameters. To choose

$\boldsymbol{R}$ for large value, a vector v_s contains the largest variance value between measurement, z, and predicted , $h(x_0)$, for each initial parameters is chosen as

$$v_s = [v^{(1)}v^{(2)}....v^{(1681)}]^T, \tag{25}$$

where s is the number of initial parameters, i.e $s = 1, 2, ..., 1681$, and $v^{(i)}$ values are given by Eq. (15), then the $\boldsymbol{R}$ value is chosen as the maximum value in the whole initial parameters combinations as

$$\boldsymbol{R} = \max(v_s)I. \tag{26}$$

To choose $\boldsymbol{Q}$ large, the $\boldsymbol{Q}$ is chosen to be equal to $\boldsymbol{P}_0^-$ as in Eq. (23), since the $\boldsymbol{Q}$ represents the variance between the seeking parameters and instant parameters.

Fig. 6a shows that the divergent results after 1 iteration using large $\boldsymbol{R}$ and $\boldsymbol{Q} = 0$ decreased to 7.8% compared with the divergent results of 21.5% for different $\boldsymbol{R}$ values as shown in Fig. 2a. It also decreased to 7.9% after 20 iterations using large $\boldsymbol{R}$ and $\boldsymbol{Q}$ as shown in Fig. 6b compared to the divergent results of 22.4% for different $\boldsymbol{R}$ and $\boldsymbol{Q}$ values as shown in Fig. 2b.

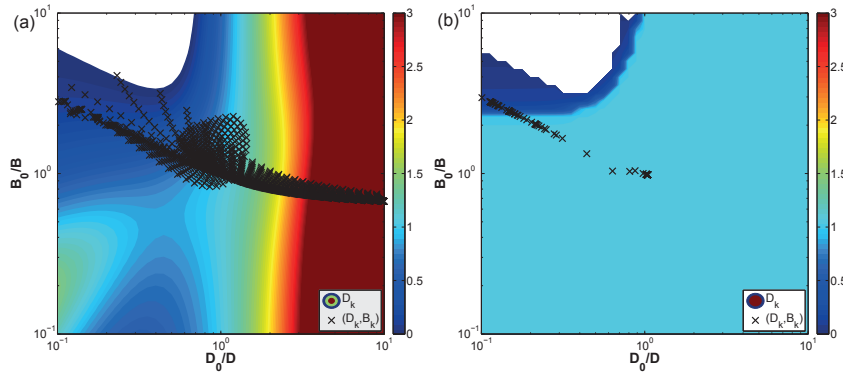

Fig. 6. Color plot for D_k merged with convergence plot between (D_k,B_k) for initial starting points D_0 and B_0 after (a) 1 iteration, for large $\boldsymbol{R}$ and $\boldsymbol{Q} = 0$, and (b) 20 iterations for large $\boldsymbol{R}$ and large $\boldsymbol{Q}$. $\boldsymbol{Q}$ is selected to be large and equal to $\boldsymbol{P}_0^-$ as in Eq. (23), while $\boldsymbol{R}$ is chosen as in Eq. (26). Noises are $\pm 5\%$ for the parameters and $\pm 10\%$ for the measurements.

It can be discussed that large values of $\boldsymbol{R}$ and $\boldsymbol{Q}$ decreases the percentage of divergent results of D_k, and also speeds the rate of convergence as shown in Fig. 2 and Fig. 6.

5.3 Different methods

The method with the selections of $\boldsymbol{Q}$ and $\boldsymbol{R}$, is compared with the second, the third, and the fourth methods that are explained in subsec. 3.1, and summarized in Table 1. The $\boldsymbol{R}$ in the second and third methods is chosen as the maximum difference between generated data, z, and generated data with the noises, $h(x)$ as in Eq. (16). The $\boldsymbol{P}_0^-$ for the second and third method is chosen as in Eq. (23), the same as in the suggested method.

Fig. 7a shows that 92.1% of the initial selected D_0/D and B_0/B give convergent results for diffusion coefficients. Around 98.3% of those values are converged to 1.042 after 50 iterations, while the 1.7% left (dark blue area in the color plot) almost converged to the same point after 180 iterations. The Kalman filter with $p = 0.01$ gives almost the same convergent area of D_{50}/D as the Kalman filter with $p = 0$ around 80%, but it speeds the rate of convergence as shown in Fig. 7c, while Kalman filter with $p = 0$ needs a large number of iterations for the parameters to converge as shown in Fig. 7b. The non-linear least squares speeds the rate of convergence but with 40.93% of the initial selected parameters that give convergent results for diffusion coefficients as shown in Fig. 7d.

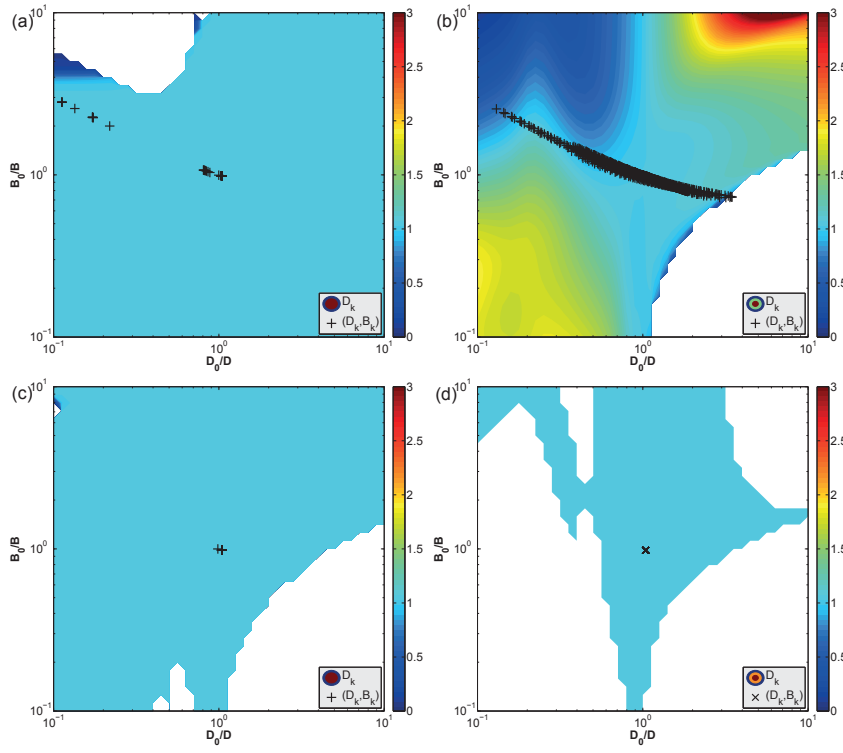

Fig. 7. Color plot for D_{50}/D merged with convergence plot between (D_{50}/D,B_{50}/B) for initial starting points D_0/D and B_0/B after 50 iterations for: (a) suggested Kalman filter with large $\boldsymbol{R}$ and large $\boldsymbol{Q}$, (b) Kalman filter with $p = 0$, (c) Kalman filter with $p = 0.01$, and (d) non-linear least squares method. For generated data with noises of $\pm 5\%$ for parameters and $\pm 10\%$ for measurements.

The suggested Kalman filter covers a wider range of the initial selected values for D_0 and B_0 that give convergent results for diffusion D_{50} than Kalman filter with $p = 0$, Kalman filter with $p = 0.01$, and non-linear least squares. This makes it an appropriate method to determine diffusion coefficient if the *a priori* information is rare or there is a large variation in the parameters, such as bone as an in-homogeneous material. Also, it speeds the rate of convergence. The Kalman filter with $p = 0.01$ might be a good choice if the *a priori*

information in the adjacent area of the seeking parameters are enough. Also, the non-linear least squares might be one choice but for small range of initial selected values for D_0 and B_0.

The effect of different ranges for D_0 and B_0 against the standard deviations and mean values for the four methods after 5 iterations is shown in Fig. 8. The ranges are selected to start from a small range and end with a large range as

$$\frac{1}{i\,D} < \text{selected initial ranges} < i\,D, \tag{27}$$

$$\frac{1}{i\,B} < \text{selected initial ranges} < i\,B, \tag{28}$$

where $i = 1.2, 1.6, 2, ..., 10$. The figure shows that the standard deviation and mean value increase as i increases. A reason for that could be that the number of initial parameters increases as the ranges increase. It can be noticed that Kalman filter with $p = 0.01$ gives the smallest standard deviation while the suggested method gives standard deviations closest to Kalman filter with $p = 0$. On the other hand, the mean values obtained by suggested method is found to be the smallest among the other three methods. This is an indication that the suggested method and Kalman filter with $p = 0.01$ might converge around the same speed. On the contrary, the non-linear least squares gives very large values for standard deviations for $i > 1.6$, these values are above 2 and excluded from the graph as shown in Fig. 8a, and gives large mean values for D_5/D as shown in Fig. 8b. A possible reason for that is the divergent result that obtained after 5 iterations, it has some large negative values for D_5/D.

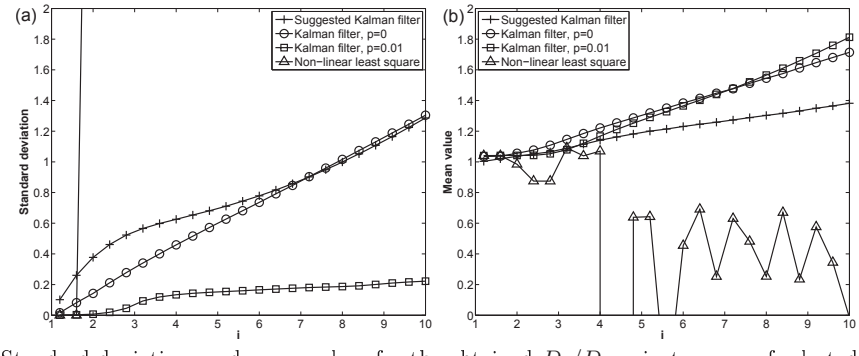

Fig. 8. Standard deviations and mean values for the obtained D_5/D against ranges of selected initial parameters for the four methods after 5 iterations, (a) standard deviations and (b) mean values. For generated data with noises of $\pm 5\%$ for parameters and $\pm 10\%$ for measurements.

Fig. 9 shows the standard deviations and mean values of the obtained D_k, $k = 1, 2, .., 100$ against number of iterations for large initial range, $i = 10$, for the four methods. The standard deviation values for D_k for the suggested Kalman filter decrease slowly up to 70

iterations, and the mean values increase as number of iterations increases to 70 iterations, and almost be stable after that. The reason for that is some of the obtained values of D_k were stuck to small values up to the 70 iterations, moving with small steps of $\boldsymbol{K}_k$ until they reached to good predicted values to move with larger steps.

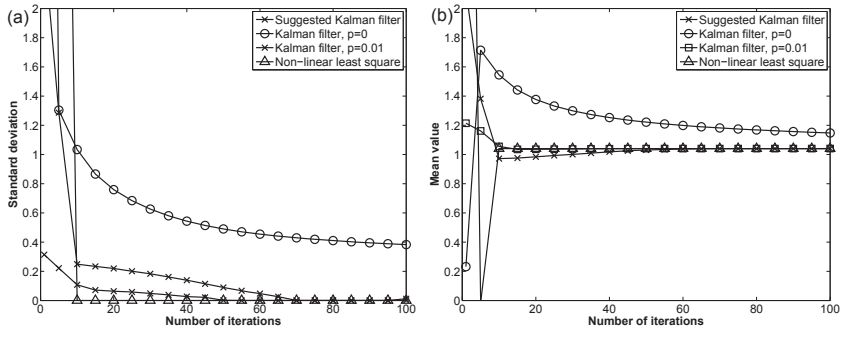

Fig. 9. Standard deviations and mean values for obtained D_k against number of iterations for the four methods after 5 iterations, (a) standard deviations and (b) mean values. For generated data with noises of $\pm 5\%$ for parameters and $\pm 10\%$ for measurements. (points over 2 and less than 0 are excluded from the graph).

The standard deviations and mean values using the Kalman filter with $p = 0$ decrease slowly as the number of iterations increases. This is expected since $\boldsymbol{R}$ in the second method was chosen to a small value and $\boldsymbol{Q}$ vanishes, which makes the Kalman gain is small. On the other hand, the standard deviations and mean values of D_k for Kalman filter with $p = 0.01$ and for non-linear least squares converge quicker than the others. This is an indication that methods 3 and 4 can be used effectivly if the *apriori* information fortunately adjacent to the seeking parameters.

The determination of diffusion coefficients for generated data with $\pm 5\%$ parameters noise and $\pm 50\%$, and $\pm 100\%$ measurements noise almost follow the same trend as in $\pm 5\%$ parameters noise and $\pm 10\%$ measurements noise. Table 2 shows the standard deviations, mean values, and the percentage of numbers of convergent D_{50}/D over total number of D_{50}/D (D.N%) for the selected range with $i = 10$, for the four methods.

The table shows that the suggested Kalman filter gives compromise results compared with the other methods. The most important difference is the percentage of the obtained D_{50}/D that give convergent results (around 92%), that is found to be large compared with the others, which means high possibilities to determine the diffusion coefficients from the selected initial range even it was a large range, and for measurements noise up to $\pm 100\%$. The table also shows that the suggested Kalman filter speeds the rate of convergence as well as Kalman filter with $p = 0.01$ and non-linear least squares but with higher D.N%. By comparing standard deviations and mean values as in the table, the standard deviations for Kalman filter with $p = 0$ give the largest values among the other methods, and the mean values are pretty a way from the convergent parameters. A reason for that is Kalman

Table 2: Standard deviations, mean values and D.N% for the obtained D_{50}/D for the four methods with noises of ±5% for parameters and ±10%, ±50%, and ±100% for measurements.

Random noise	Method	Standard deviation	Mean value	$D.N\%$
±10%	Suggested Kalman filter	0.09	1.03	92.09
	Kalman filter, $p = 0$	0.49	1.22	80.90
	Kalman filter, $p = 0.01$	0.03	1.04	80.19
	Non-linear least squares	8.71×10^{-09}	1.04	40.93
±50%	Suggested Kalman filter	0.06	0.93	91.96
	Kalman filter, $p = 0$	0.54	1.06	80.37
	Kalman filter, $p = 0.01$	0.003	0.94	80.67
	Non-linear least squares	6.19×10^{-16}	0.94	45.63
±100%	Suggested Kalman filter	0.03	1.69	92.03
	Kalman filter, $p = 0$	0.66	1.44	85.24
	Kalman filter, $p = 0.01$	0.22	1.66	85.66
	Non-linear least squares	0.064	1.69	42.47

filter with $p = 0$ converges to many different points with small Kalamn gain step, which means more iterations are needed for convergence. In sum, the suggested method can be applied effectively for both rare and sufficient information about the seeking parameters, and can be applied for a wide range of initial parameters.

The behavior of mean square error for a selected real bovine bone sample is found almost the same as the generated one in Fig. 1. The initial predicted parameters D_0 and B_0 are chosen to be 41×41 combinations, with $0.001 < D_0 < 0.1$ mm^2/min and $6 < B_0 < 600$ µS/mm, which construct a large combinations between the initial parameters. The initial predicted parameters error $\boldsymbol{P}_0^-$, covariance error for the parameters $\boldsymbol{Q}$, and covariance error for the measurements $\boldsymbol{R}$ are chosen based on both suggested method and these combinations. Fig. 10 shows the convergence plot for the two parameters D and B that obtained using the suggested Kalman filter for the real sample after 1, 10, 50, and 250 iterations.

The initial predicted parameters that give convergent results for D_k are found to be 92.2% from the combination, that converged around a specific line after some iterations as in 10 and 50 iterations (see Fig. 10). Around 92.5% of them converged to the seeking unknown parameters $D = 0.0144$ mm^2/min and $B = 73.602$ µS/mm after 50 iterations, while the 7.5% left converged to the same place almost after 250 iterations. Small Kalman gain steps at the 7.5% might be a possible reason for the slowly convergence. The convergence line is expected since the mean square error has smaller values along this line as shown in Fig. 1.

The conductivity versus time for analytical model Eq. (20) using D and B obtained by the suggested Kalman filter and experimental data for the real sample is shown in Fig. 11. The figure shows that the analytical function fits very well with the experimental data accompanied with mean square error of 0.85 (µS/mm)^2.

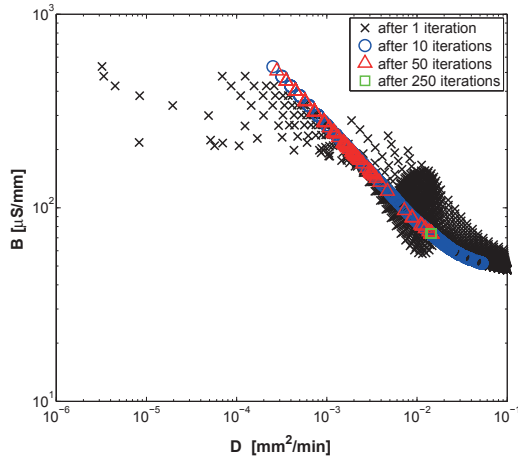

Fig. 10. Convergence between D_k and B_k obtained using suggested method for a real sample for 1, 10, 50, and 250 iterations

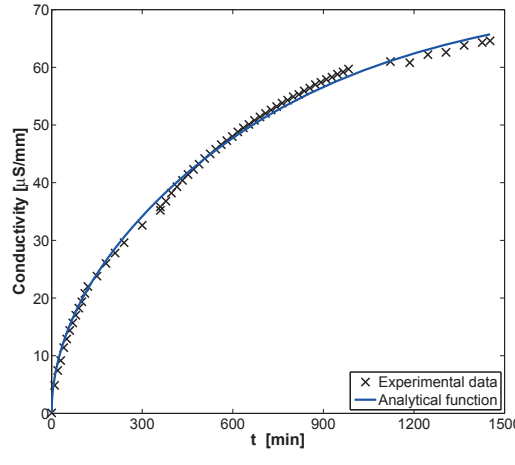

Fig. 11. Conductivity versus time for analytical and experimental for the real sample.

6 Conclusions

Four methods to choose appropriate initial parameters, covariance errors for parameters, and covariance errors for measurements, required for Kalman filter for determination of material parameters, is investigated in this work. The methods are applied to generated data with ±5% parameters noise and ±10%, ±50%, and ±100% measurements noise for known parameters. The suggested method covers a wider range of the initial suggested values for the parameters than the standard Kalman filters, and non-linear least squares, which enhances the possibilities of convergence around the seeking parameters. The suggested method speeds the rate of convergence compared with the other methods. Very good results are obtained for diffusion coefficient in bovine bone as a case study.

Acknowledgments

The following organizations are acknowledged: Erasmus Mundus Action 2 for financial support of both authors, Lund University for supporting P. Ståhle and Fayoum University for supporting the visit of A. Shokry.

Appendix A Non-linear least squares

The sum of the squared residuals is written

$$\Phi = (z-h)^{\mathrm{T}}(z-h). \tag{A-1}$$

By putting the derivative of Φ with respect to x to zero, a set of n equations is obtained,

$$\frac{\partial \Phi}{\partial x}=0 \quad \Rightarrow \quad \mathbf{H}(x)^{\mathrm{T}}\{z-h(x)\}=0\,. \tag{A-2}$$

Insertion of Eq. (3) into Eq. (A-2) gives the following,

$$\mathbf{H}^{\mathrm{T}}\{z-h(\hat{x}_k)\} \approx \mathbf{H}^{\mathrm{T}}\mathbf{H}(x-\hat{x}_k)\,. \tag{A-3}$$

Provided that the $n \times n$ matrix $\mathbf{H}^{\mathrm{T}}\mathbf{H}$ is non-singular, one obtains the following approximation,

$$x \approx \hat{x}_k + (\mathbf{H}^{\mathrm{T}}\mathbf{H})^{-1}\mathbf{H}^{\mathrm{T}}\{z-h(\hat{x}_k)\}. \tag{A-4}$$

For linear systems the Jacobian $\mathbf{H}$ is independent of x, which makes the solution in Eq. (A-4) exact.

Appendix B Kalman filter derivation

The variance of the errors of the parameters before, $\boldsymbol{P}_k^-$, and after, $\boldsymbol{P}_k$, the iterative update are

$$\boldsymbol{P}_k^- = \mathrm{Var}(x_k - \hat{x}_{k-1}), \quad \text{and} \quad \boldsymbol{P}_k = \mathrm{Var}(x_k - \hat{x}_k)\,. \tag{B-1}$$

The function $\mathrm{Var}(a)$ is an $l \times l$ matrix with the elements α_{ij} given by the vector $a = (a_1, ...a_l)^{\mathrm{T}}$ as follows, cf. (Courant and Hilbert, 1953)

$$\alpha_{ij} = \mathrm{E}(x_i x_j) - \mathrm{E}(x_i)\mathrm{E}(x_j)\,, \tag{B-2}$$

where $E(\vartheta)$ is the statistical mean value of the stochastic variable ϑ. Hence, the matrices $\boldsymbol{P}_k$ and $\boldsymbol{P}_{k-1}^-$ are symmetric with the dimension $n \times n$.

Using Eqs. (B-1) and (2), a relation between $\boldsymbol{P}_k^-$ and $\boldsymbol{P}_k$ is obtained as,

$$\begin{aligned}\boldsymbol{P}_{k+1}^- &= \mathrm{Var}(x_{k+1} - \hat{x}_k) = \mathrm{Var}(x + w_{k+1} - \hat{x}_k) = \mathrm{Var}(x_k - w_k + w_{k+1} - \hat{x}_k) \\ &= \mathrm{Var}(x_k - \hat{x}_k) + \mathrm{Var}(-w_k + w_{k+1}) = \mathrm{Var}(x_k - \hat{x}_k) + 2\mathrm{Var}(w_k) = \boldsymbol{P}_k + \boldsymbol{Q}_k.\end{aligned} \tag{B-3}$$

where $\boldsymbol{Q}_k = 2\mathrm{Var}(w_k)$ is an $n \times n$ matrix. Note that the covariance of the supposedly uncorrelated quantities $(x - \hat{x}_k)$ and w_k respectively vanishes.

On the other hand, substituting $\hat{x}_k$ in Eq. (B-1) by using Eq. (6), $\boldsymbol{P}_k$ can be expressed as

$$\boldsymbol{P}_k = \mathrm{Var}[x_k - (\hat{x}_{k-1} + \mathbf{K}_k\{z_k - h(\hat{x}_{k-1})\})]\,.$$

Replacing z_k according to Eq. (1) leads to

$$\begin{aligned}\boldsymbol{P}_k &= \mathrm{Var}(x_k - \hat{x}_{k-1} - \mathbf{K}_k\{h(x_k) + v_k - h(\hat{x}_{k-1})\}) \\ &= \mathrm{Var}(x_k - \hat{x}_{k-1}) - \mathbf{K}_k\mathrm{Cov}(h(x_k) - h(\hat{x}_{k-1}), x_k - \hat{x}_{k-1}) \\ &\quad - \mathrm{Cov}(x_k - \hat{x}_{k-1}, h(x_k) - h(\hat{x}_{k-1}))\mathbf{K}_k^{\mathrm{T}} + \mathbf{K}_k\mathrm{Var}(h(x_k) - h(\hat{x}_{k-1}))\mathbf{K}_k^{\mathrm{T}} \\ &\quad + \mathbf{K}_k\mathrm{Var}(v_k)\mathbf{K}_k^{\mathrm{T}}\,,\end{aligned} \tag{B-4}$$

where the function $\mathrm{Cov}(a, b)$ gives the covariance of the stochastic vectors a and b. The function $\mathrm{Cov}(a, b)$ is an $m \times m$ matrix with the elements α_{ij} given by the stochastic variables $a = (a_1, ...a_m)^{\mathrm{T}}$ and $b = (b_1, ...b_m)^{\mathrm{T}}$ as follows, cf. (Courant and Hilbert, 1953),

$$\alpha_{ij} = \mathrm{E}(a_i b_j) - \mathrm{E}(a_i)\mathrm{E}(b_j)\,. \tag{B-5}$$

It is used that the covariance between the elements of $h(x_i)$ and v_k for any i and k vanishes. The Taylor series in Eq. (3) giving $h(x_k) - h(\hat{x}_{k-1}) = \mathbf{H}_k(x_k - \hat{x}_{k-1})$ results in

$$\begin{aligned}\boldsymbol{P}_k &= \boldsymbol{P}_k^- - \mathbf{K}_k\mathbf{H}_k\boldsymbol{P}_k^- - \boldsymbol{P}_k^-\mathbf{H}_k^{\mathrm{T}}\mathbf{K}_k^{\mathrm{T}} + \mathbf{K}_k\mathbf{H}_k\boldsymbol{P}_k^-\mathbf{H}_k^{\mathrm{T}}\mathbf{K}_k^{\mathrm{T}} + \mathbf{K}_k\boldsymbol{R}_k\mathbf{K}_k^{\mathrm{T}} \\ &= (\boldsymbol{I} - \mathbf{K}_k\mathbf{H}_k)\boldsymbol{P}_k^-(\boldsymbol{I} - \mathbf{K}_k\mathbf{H}_k)^{\mathrm{T}} + \mathbf{K}_k\boldsymbol{R}_k\mathbf{K}_k^{\mathrm{T}}\,,\end{aligned} \tag{B-6}$$

where $\boldsymbol{R}_k$ is the covariance error of the measurements and an $N \times N$ matrix defined as follows

$$\boldsymbol{R}_k = \mathrm{Var}(v_k)\,. \tag{B-7}$$

Since the x_k and v_k are mutually uncorrelated, $\boldsymbol{P}_k$ becomes a diagonal matrix that contains errors between the parameters before and after an iteration, the $\boldsymbol{K}_k$ that minimizes the error can be obtained by taking the derivative of the trace $\mathrm{Tr}\,(\boldsymbol{P}_k)$ with respect to $\mathbf{K}_k$ and putting it equal to zero. Taking the trace of the first equality in Eq. (B-6) provides

$$\begin{aligned}\mathrm{Tr}(\boldsymbol{P}_k) = \mathrm{Tr}(\boldsymbol{P}_k^-) - \mathrm{Tr}(\mathbf{K}_k\mathbf{H}_k\boldsymbol{P}_k^-) - \mathrm{Tr}(\boldsymbol{P}_k^-\mathbf{H}_k^{\mathrm{T}}\mathbf{K}_k^{\mathrm{T}}) + \mathrm{Tr}(\mathbf{K}_k\mathbf{H}_k\boldsymbol{P}_k^-\mathbf{H}_k^{\mathrm{T}}\mathbf{K}_k^{\mathrm{T}}) \\ + \mathrm{Tr}(\mathbf{K}_k\boldsymbol{R}_k\mathbf{K}_k^{\mathrm{T}}).\end{aligned} \tag{B-8}$$

Using following identities for the matrix trace, cf. (Petersen and Pedersen, 2008)

$$\mathrm{Tr}(\boldsymbol{P}_k^-\mathbf{H}_k^{\mathrm{T}}\mathbf{K}_k^{\mathrm{T}}) = \mathrm{Tr}(\mathbf{K}_k\mathbf{H}_k\boldsymbol{P}_k^-)\,,\ \ \frac{\partial \mathrm{Tr}(\boldsymbol{AC})}{\partial \boldsymbol{A}} = \boldsymbol{C}^T \text{ and } \frac{\partial \mathrm{Tr}(\boldsymbol{AFA}^T)}{\partial \boldsymbol{A}} = 2\boldsymbol{AF}\,. \tag{B-9}$$

The last equality requires that the matrix $\boldsymbol{F}$ is symmetric. The derivative of Eq. (B-8) with respect to $\mathbf{K}_k$ can be written

$$\frac{\partial \mathrm{Tr}(\boldsymbol{P}_k)}{\partial \mathbf{K}_k} = -2\boldsymbol{P}_k^-\mathbf{H}_k^{\mathrm{T}} + 2\mathbf{K}_k\mathbf{H}_k\boldsymbol{P}_k^-\mathbf{H}_k^{\mathrm{T}} + 2\mathbf{K}_k\boldsymbol{R}_k. \tag{B-10}$$

The optimal $\mathbf{K}_k$ can be obtained by putting the right term in Eq. [B-10] to zero as next

$$\mathbf{K}_k = \boldsymbol{P}_k^-\mathbf{H}_k^{\mathrm{T}}(\mathbf{H}_k\boldsymbol{P}_k^-\mathbf{H}_k^{\mathrm{T}} + \boldsymbol{R}_k)^{-1}\,. \tag{B-11}$$

The $\boldsymbol{P}_k$ associated to the optimal $\mathbf{K}_k$ can be written as in Eq. [B-12] by substituting Eq. [B-11] into Eq. (B-6) as next

$$\boldsymbol{P}_k = (\boldsymbol{I} - \mathbf{K}_k\mathbf{H}_k)\boldsymbol{P}_k^- + \{-\boldsymbol{P}_k^-\mathbf{H}_k^{\mathrm{T}} + \mathbf{K}_k(\mathbf{H}_k\boldsymbol{P}_k^-\mathbf{H}_k^{\mathrm{T}} + \boldsymbol{R}_k)\}\mathbf{K}_k^{\mathrm{T}}.$$

Using Eq. (B-11) readily gives

$$\boldsymbol{P}_k = (\boldsymbol{I} - \mathbf{K}_k\mathbf{H}_k)\boldsymbol{P}_k^-\,, \tag{B-12}$$

and consequently

$$\boldsymbol{P}_{k+1}^- = (\boldsymbol{I} - \mathbf{K}_k\mathbf{H}_k)\boldsymbol{P}_k^- + \boldsymbol{Q}_k\,. \tag{B-13}$$

References

Ahn, K., Truong, D., 2009. Online tuning fuzzy pid controller using robust extended kalman filter. Journal of Process Control 19 (6), 1011–1023.

Antonov, S., Fehn, A., Kugi, A., 2011. Unscented kalman filter for vehicle state estimation. Vehicle System Dynamics 49 (9), 1497–1520.

Aoki, S., Amaya, K., Sahashi, M., Nakamura, T., 1997. Identification of Gurson′s material constants by using kalman filter. Computational Mechanics 19 (6), 501–506.

Bolzon, G., Fedele, R., Maier, G., 2002. Parameter identification of a cohesive crack model by kalman filter. Computer Methods in Applied Mechanics and Engineering 191 (25), 2847–2871.

Brown, R. G., 1983. Introduction to random signal analysis and Kalman filtering. Vol. 8. Wiley New York.

Corigliano, A., Mariani, S., Orsatti, B., 2000. Identification of Gurson−Tvergaard material model parameters via kalman filtering technique. I. theory. International journal of fracture 104 (4), 349–373.

Courant, R., Hilbert, D., 1953. Methods of Mathematical Physics (Interscience, New York, 1953). Vol. 63.

Kalman, R. E., 1960. A new approach to linear filtering and prediction problems. Journal of Fluids Engineering 82 (1), 35–45.

Lindberg, G., Shokry, A., Reheman, W., Svensson, I., 2014. Determination of diffusion coefficients in bovine bone by means of conductivity measurement. International Journal of Experimental and Computational Biomechanics 2 (4), 324–342.

Mitchell, H. L., Houtekamer, P., 2009. Ensemble kalman filter configurations and their performance with the logistic map. Monthly Weather Review 137 (12), 4325–4343.

Miyoshi, T., Kunii, M., 2012. The local ensemble transform kalman filter with the weather research and forecasting model: Experiments with real observations. Pure and applied geophysics 169 (3), 321–333.

Nakamura, T., Gu, Y., 2007. Identification of elastic−plastic anisotropic parameters using instrumented indentation and inverse analysis. Mechanics of materials 39 (4), 340–356.

Nakamura, T., Liu, Y., 2007. Determination of nonlinear properties of thermal sprayed ceramic coatings via inverse analysis. International journal of solids and structures 44 (6), 1990–2009.

Petersen, K. B., Pedersen, M. S., 2008. The matrix cookbook. Technical University of Denmark, 7–15.

Plackett, R. L., 1950. Some theorems in least squares. JSTOR.

Shi, Y., Fang, H., Yan, M., 2009. Kalman filter-based adaptive control for networked systems with unknown parameters and randomly missing outputs. International Journal of Robust and Nonlinear Control 19 (18), 1976–1992.

Siouris, G. M., Chen, G., Wang, J., 1997. Tracking an incoming ballistic missile using an extended interval kalman filter. Aerospace and Electronic Systems, IEEE Transactions on 33 (1), 232–240.

Vaddadi, P., Nakamura, T., Singh, R. P., 2003. Inverse analysis for transient moisture diffusion through fiber-reinforced composites. Acta materialia 51 (1), 177–193.

Vaddadi, P., Nakamura, T., Singh, R. P., 2007. Inverse analysis to determine hygrothermal properties in fiber reinforced composites. Journal of composite materials 41 (3), 309–334.

Weng, S.-K., Kuo, C.-M., Tu, S.-K., 2006. Video object tracking using adaptive kalman filter. Journal of Visual Communication and Image Representation 17 (6), 1190–1208.

Wu, C.-C., Lien, G.-Y., Chen, J.-H., Zhang, F., 2010. Assimilation of tropical cyclone track and structure based on the ensemble kalman filter (EnKF). Journal of the Atmospheric Sciences 67 (12), 3806–3822.

Paper C

A. Shokry, P. Ståhle and I. Svensson (2015)

Determination of spatially dependent diffusion parameters in bovine bone using Kalman filter

Submitted for international publication

Determination of spatially dependent diffusion parameters in bovine bone using Kalman filter

Abdallah Shokry[a,b], Per Ståhle[a] and Ingrid Svensson[c]

[a] *Division of Solid Mechanics, Lund University, 22100 Lund, Sweden*

[b] *Industrial Engineering Department, Fayoum University, 63514 Fayoum, Egypt*

[c] *Department of Biomedical Engineering, Lund University, 22100 Lund, Sweden*

Abstract

Although many studies have been made for homogeneous constant diffusion, bone is an in-homogeneous material. It has been suggested that bone porosity decreases from the inner boundaries to the outer boundaries of the long bones. The diffusivity of substances in the bone matrix is believed to increase as the bone porosity increases. In this study, an experimental set up is used where bovine bone samples, saturated with potassium chloride (KCl), were put into distilled water and the conductivity of the water was followed. Chloride ions in the bone samples escaped out in the water through diffusion and the increase of the conductivity was measured. A one-dimensional, spatially dependent mathematical model describing the diffusion process is used. The diffusion parameters in the model are determined using a Kalman filter technique. The parameters for spatially dependent at endosteal and periosteal surfaces are found to be $(12.8 \pm 4.7) \times 10^{-11}$ and $(5 \pm 3.5) \times 10^{-11}$ m^2/s respectively. The mathematical model function using the obtained diffusion parameters fits very well with the experimental data with mean square error varies from 0.06×10^{-6} to 0.183×10^{-6} $(\mu\mathrm{S/m})^2$.

1 Introduction

Diffusion can be defined as the process by which matter is transported from one part of a system to another as a result of random molecular motion (Crank, 1975). The commonly used mathematical representation of the diffusion process that can be used to find the diffusion parameter is the so-called Fick′s law. Based on this mathematical representation, many researchers were able to derive and use models based on diffusion in many different fields (Margetis, 2009; Yildirim et al., 2011; Cayan et al., 2009; Naceri, 2009).

One of the fields where Fick′s laws can be applied is for representing diffusion in blood cell membranes. More specifically, such diffusion involves the diffusion of nutrients and oxygen from high concentrations in the blood vessels to less concentrations in the blood cells. For example, models including diffusion, have been presented in studies of bone healing where bone is repaired after fracture (Chou and Müftü, 2013; Gomez-Benito et al., 2005; Ambard and Swider, 2006; Adam, 2002; Sapotnick and Nackenhorst, 2012). Other models have been presented for bone remodeling, in which old bone tissue is replaced by a new one (Fernández et al., 2012; Stadelmann et al., 2009; Adachi et al., 2006). Stress or strain driven diffusion have been suggested to play an important role in the transportation of substances from the inner surface, endosteal, that covers medullar canal in the long bone to the outer, periosteal, bone surface. A one-dimensional model for strain driven transport of bone nutrients has been presented by Banks-Sills et al. (2011). This study was followed up by another study (Lindberg et al., 2013) where a two-dimensional model describing the stress driven diffusion was presented.

Several studies have investigated the bone structure and the apparent diffusion coefficient using magnetic resonance imaging (Balliu et al., 2009; Capuani, 2013; Ababneh et al., 2009). The latter method is very suitable for obtaining information about the structural properties of the bone. A less complex method for determining the diffusion coefficient has been introduced by Lindberg et al. (2014). They used an experimental set up where the increased conductivity in distilled water due to the diffusing chloride ions escaping from saturated bone samples was measured over time. Further, the diffusion parameter was determined from fitting the parameters in an analytical model according to the experimental data using a Kalman filtering technique. Kalman filters could be used as a recursive method in order to extract unknown parameters from noisy experimental measurements. In previous studies, despite the very complex structure of bone, the diffusion parameter was assumed to be independent of the position in the bone wall. The diffusion of solutes that promote bone growth are crucial for creating a good environment for bone remodeling and bone healing. Therefore, it is important to get a better understanding of the diffusion process and determine the parameters involved. Bone has been found to have hierarchically decreasing porosity from inner boundaries to outer boundaries of cortical bone (Cowin, 1999; Cowin et al., 2009). Since it is believed that diffusivity increases as bone porosity increases, the observed variation in bone porosity supports the hypothesis that the diffusion parameter may decrease linearly from inner boundaries to outer boundaries of bone.

In this study, a one-dimensional model for linear diffusion in the radial direction, as-

suming linear spatially dependent diffusivity will be presented. Dominantly, the diffusion of nutrients and signal substances are transported in the radial direction from the marrow and blood vessels to the periosteal bone surface. Two diffusion parameters for the bone sample based on the new model will be determined from experimental results using a Kalman filter technique.

2 Materials and Methods

2.1 Experimental Setup

The diffusion of potassium chloride in the mid-shaft of a long bovine bone was studied. The samples were taken from the central part between the ends of a femur bone of a Holstein-cattle (marked with black rectangle in Fig. 1a) at scattered angular positions around the bone cross-section, since previous research has found that the position (anterior, posterior, medial, lateral) around the periphery of the bone has no significant effect on the diffusion properties (Lindberg et al., 2014).

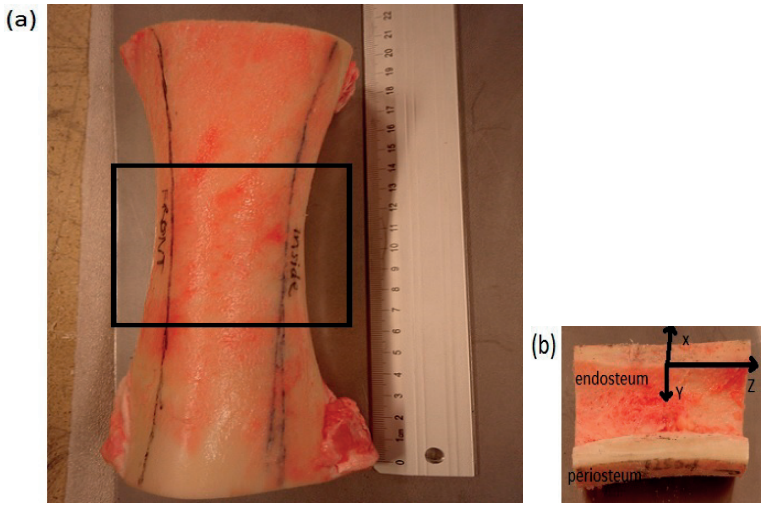

Fig. 1. Images of the the Holstein-cattle femur bone. (a) long bone with a black rectangle indicates position of samples. (b) a midsection of the diaphysis cut along the long axis showing the endosteum and periosteum . Note the incorporated coordinate system in the picture .

The femur bones were cut into pieces according to Fig. 1b, cut free from flesh and quickly rinsed in running water. The bone pieces were then cut into smaller samples and again quickly rinsed in water. The dimensions of the bone samples are given in Table 1. Note that the size in the radial direction, L, corresponds to the wall thickness of the bone.

The samples were stored at around -4 °C in a freezer for a few days up to a couple of weeks. Just before the measurements they were placed in room temperature for one

Table 1: Sample dimensions in mm. L, h and b correspond to the sizes in radial, tangential and axial directions, in respectively.

Sample	1	2	3	4	5
L (mm)	7.0	9.05	7.9	6.6	7.0
h (mm)	19.7	21.2	20.5	22.5	20.1
b (mm)	13.6	16.1	16.5	14.3	15.3

hour. The samples were then submerged into polyester resin for a curing time of one hour. The endosteal surface and the periosteal surface were covered by a layer of rubber, after the curing the rubber was peeled off. Thus, the surfaces with axial and tangential normal directions were sealed, leaving only the periosteal and endosteal surfaces open as shown in Fig. 2.

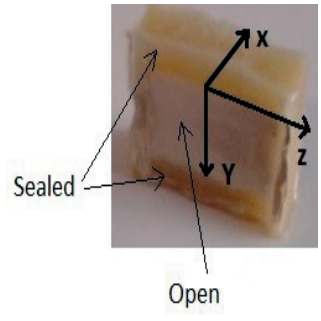

Fig. 2. Bone sample 1 with polyester closing axial (z) and tangential (y) directions. The radial direction (x) is kept open. The coordinate system is in accordance with the system shown in Fig. 1b.

The samples were then put in a saturated potassium chloride, KCl, solution for 24 hours, which is supposed to be sufficiently long for the KCl ions to diffuse into the samples so that a fairly constant concentration is achieved (see Appendix A for details). After flushing in distilled water for around 5 seconds, the samples were finally submerged in 100 ml of distilled water which allows the potassium and chloride ions to diffuse through the bone to the surface where they escape into the surrounding water. The conductivity in the surrounding water was measured once per second using a SevenEasy S30 conductivity meter from Mettler Toledo. The instrument has an accuracy of $\pm 0.5\%$ of the measured value. The equipment was calibrated at 25 °C but during operation (presumably due to stirring) the temperature rose a couple of centigrades but remained in the interval 28 ± 3 °C.

2.2 Analytical Model

Bousson et al. (2001) and Baron (2012) studied the porosity of human long bones from females of different age. The measurements were taken at three different positions in the

bone wall: at the periosteal surface, at the endosteal surface and in between the two surfaces. They found that porosity decreases from the endosteal surface to the periosteal surface with a linear regression, as shown in Fig. 3.

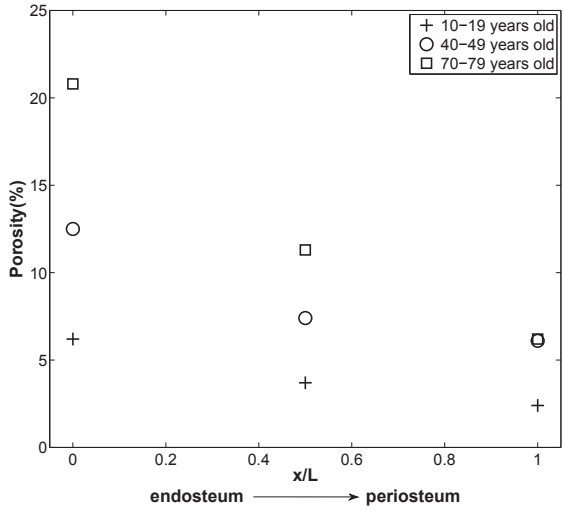

Fig. 3. Porosity versus cortical bone thickness in females. Porosity is calculated as the mass of porous filled with water over the mass of cortical bone (Baron, 2012)

The diffusivity also in bovine cortical bone is believed to be related to the porosity in a similar way, i.e., that a small porosity gives a low diffusivity and a large porosity gives a high diffusivity. This motivates the hypothesis of a linear position dependence of the diffusivity in bovine cortical bone. With a linear dependence is introduced in the analytical model, a better agreement between calculated values and experimental results is expected.

For diffusion parameters depending linearly on x the following relation is used,

$$D(x) = D_o(1 - \frac{x}{L}) + D_1\frac{x}{L}\,, \tag{1}$$

with $D_o > 0$ and $D_1 > 0$, where D_o and D_1 are the diffusion parameters at the endosteal and periosteal surfaces respectively.

The specimen is a rectangular prism placed in a Cartesian coordinate system. The endosteal and periosteal surfaces are on opposite sides of the specimen with normals along the x-axis (c.f. the coordinate system shown in Fig. 2). The specimen occupies the region $0 \leq x \leq L$, where $x = 0$ at the endosteal surface and $x = L$ at the periosteal surface. The size of the specimen in y- and z-directions, h and b, varies from around $2L$ to around $3L$, c.f. Table 1.

The diffusivity is assumed to be a function of the x-coordinate and insignificantly depending of the position in the $y - z$ plane, i.e., the diffusivity parameters $D = D(x)$. It is

assumed that the ions escape from the specimen through the endosteal and the periosteal surfaces only. A consequence is that the diffusion becomes uniaxial. Therefore, the concentration is a function of x and the time, t, only. It is assumed that the change of the concentration inside the bone follows Fick′s law in its one-dimensional form which states

$$\frac{\partial C(x,t)}{\partial t} = \frac{\partial}{\partial x}\left(D(x)\frac{\partial C(x,t)}{\partial x}\right), \tag{2}$$

where $C(x,t)$ represents the concentration in the specimen.

Initially, the concentration is supposed to be constant in the interior of the specimen, i.e.,

$$C(x,0) = C_0, \qquad \text{for} \quad 0<x<L \quad \text{at} \quad t=0. \tag{3}$$

During the measurements, the specimen is placed in a beaker and the potassium chloride accumulates in the water. Since the ions are diluted in the large volume of water, it is believed that the concentration in the beaker is very little affected by potassium chloride so that the concentration at the boundaries of the sample may be assumed to be constantly zero. The boundary conditions at $x = 0$ and $x = L$, therefore, become

$$C(0,t) = C(L,t) = 0, \qquad \text{for} \quad t\geq 0\,. \tag{4}$$

A variable separation is employed to solve the second order linear partial differential Eq. (2) by assuming that,

$$C(x,t) = X(x)T(t)\,. \tag{5}$$

Inserted into Eq. (2), this gives

$$\frac{1}{X}\frac{\partial}{\partial x}\left(D(x)\frac{\partial X}{\partial x}\right) = \frac{1}{T}\frac{\partial T}{\partial t}\,. \tag{6}$$

Since the right side is a function only of t and the left side is a function only of x, both sides are represented by a constant, here for convenience, selected to be $-\lambda^2$. Eq. (6) is now split into two ordinary differential Eqs.:

$$\frac{1}{T}\frac{\mathrm{d}T}{\mathrm{d}t} = -\lambda^2\,, \tag{7}$$

$$\frac{1}{X}\frac{\partial}{\partial x}\left(D(x)\frac{\partial X}{\partial x}\right) = -\lambda^2\,, \tag{8}$$

where λ is an arbitrary real constant. The solution of the first order Eq. (7) is readily obtained as

$$T = ke^{-\lambda^2 t}\,, \tag{9}$$

where k is an arbitrary constant.

Eq. (8) is of second order and with non-constant parameters. On expanded form it is written,

$$D(x)\frac{\mathrm{d}^2X}{\mathrm{d}x^2} + D'(x)\frac{\mathrm{d}X}{\mathrm{d}x} + \lambda^2 X = 0\,, \tag{10}$$

where $D'(x)$ is the derivative of $D(x)$ with respect to x. The coefficient of the leading term is removed by substituting $X(x)$ with $U(\xi)$ using

$$\xi(x) = \frac{2L}{D_1 - D_0}\sqrt{D(x)} \quad \text{for } 0{\leq}x{\leq}L\ . \tag{11}$$

One obtains from Eqs. (1) and (11) that, Eq. (10) now becomes

$$\frac{\mathrm{d}^2U(\xi)}{\mathrm{d}\xi^2} + \frac{1}{\xi}\frac{\mathrm{d}U(\xi)}{\mathrm{d}\xi} + \lambda^2 U(\xi) = 0\,, \tag{12}$$

which is identified as Bessel's differential Eq.. The solution is

$$U(\xi) = R_1 J_0(\lambda\xi) + R_2 Y_0(|\lambda\xi|) \quad \text{for } \xi(0){\leq}\xi(x){\leq}\xi(L)\,, \tag{13}$$

where R_1 and R_2 are two arbitrary real constants, and J_0 and Y_0 represent the zero:th order Bessel functions of the first and the second kind (Arfken, 2001).

By using the boundary conditions Eq. (4), and the definition Eq. (11), the following matrix is obtained:

$$\begin{bmatrix} J_0(\lambda\xi(0)) & Y_0(|\lambda\xi(0)|) \\ J_0(\lambda\xi(L)) & Y_0(|\lambda\xi(L)|) \end{bmatrix} \begin{bmatrix} R_1 \\ R_2 \end{bmatrix} = \begin{bmatrix} 0 \\ 0 \end{bmatrix}, \tag{14}$$

with the root $\lambda = \lambda_n$. A non-trivial solution requires

$$J_0(\lambda\xi(0))\,Y_0(|\lambda\xi(L)|) - J_0(\lambda\xi(L))\,Y_0(|\lambda\xi(0)|) = 0\,. \tag{15}$$

The roots $\lambda = \lambda_n$ of Eq. (15) are used to generate a complete system of orthogonal functions in the region $0 < x < L$. The solution c_n for $\lambda = \lambda_n$, using Eqs. (5, 9, 13) becomes

$$c_n(x,t) = \left[J_0(\lambda_n\xi(0))\,Y_0(|\lambda_n\xi(x)|) - J_0(\lambda_n\xi(x))\,Y_0(|\lambda_n\xi(0)|)\right] e^{-\lambda_n^2 t} \tag{16}$$

that fulfills the boundary conditions. Without loss of generality, k in Eq. (9) has been put to unity. Adopting the assumed linearity in Eq. (2), a general solution is obtained as

$$C(x,t) = \sum_{n=1}^{\infty} Q_n c_n(x,t)\,, \tag{17}$$

where Q_n are arbitrary constants. The initial conditions Eq. (3) require that the Q_n coefficients fulfill the condition

$$C_0 = \sum_{n=1}^{\infty} Q_n c_n(x,0)\,. \tag{18}$$

An implication of the orthogonality of the functions $c_n(x,t)$ is that the integral $\int_0^L c_n(x,t)c_s(x,t)\mathrm{d}x$ vanishes if $n \neq s$. Thus, both sides of Eq. (18) are multiplied by $c_n(x,0)$ and integrated over the specimen length, L, which gives

$$Q_n = C_0 \frac{\int_0^L c_n(\eta,0)\mathrm{d}\eta}{\int_0^L c_n^2(\eta,0)\mathrm{d}\eta}\,. \tag{19}$$

With the complete solution of Eqs. (16, 17, 19) that now is established, the amount, M, of ions that escape from the specimen may be calculated as follows,

$$M = bh\int_0^L (C_0 - C(x,t))\mathrm{d}x = bh\sum_{n=1}^{\infty} Q_n \int_0^L \{c_n(x,0) - c_n(x,t)\}\,\mathrm{d}x\,. \tag{20}$$

Inserting (19) and using that $c_n(x,t) = c_n(x,0)e^{-\lambda_n^2 t}$ gives

$$M = bh\sum_{n=1}^{\infty} Q_n \int_0^L c_n(x,0)\mathrm{d}x\,(1 - e^{-\lambda_n^2 t}) = bh\,C_0 \sum_{n=1}^{\infty} \frac{\left(\int_0^L c_n(x,0)\mathrm{d}x\right)^2}{\int_0^L c_n^2(x,0)\mathrm{d}x}(1 - e^{-\lambda_n^2 t})\,, \tag{21}$$

where b is the width and h is the height of the specimen cross section. The conductivity of the liquid in the beaker is assumed to be proportional to the density of dissolved potassium and chloride ion pairs that has escaped from the sample. Initially, at t=0, there is a small but measurable conductivity ζ_0 present and this is also accounted for. The conductivity, ζ, is described as

$$\zeta = \zeta_0 + B'\,M, \tag{22}$$

where B' is the conversion factor of the unit of conductivity per mole of ions in the beaker.

The result is evaluated through the Eqs. (16, 21, 22), and the integrals of Eq. (21) are given in Appendix B.

For convenience, non-dimensional variables are introduced as follows:

$$p_n = \frac{2\lambda_n L}{\sqrt{D_0}} \quad \text{and} \quad m{=}1 - \frac{D_1}{D_0}. \tag{23}$$

The calculation of eigenvalues fails for small values of m, whereas the argument, $\lambda_n\xi(x)$ of the Bessel functions become unlimited (see Appendix C for a more detailed description). The Eq. to be solved is

$$\zeta_i = \zeta_0 + \frac{B}{L}\sum_{n=1}^{\infty} \frac{F_o}{F_1 + F_2 + F_3}\{1 - \exp(-\frac{p_n^2 D_0}{4L^2}t_i)\}\,, \tag{24}$$

where ζ_i is the conductivity and t_i is the time of the i:th measurement, ζ_0 is taken as the initial conductivity at $t_i = 0$, $B = B'C_0bh$, p_n is given in Appendix C, and the integrals F_0 to F_3 are given in Appendix B.

2.3 Kalman Filter Technique

During the experiment, measurements are obtained in a time sequence. The result is collected in a vector, $z = \{z_1, ...z_N\}^{\mathrm{T}}$, with N measurements of the conductivity.

These measurements may be predicted using Eq. (24), now written in the form of a vector with a number of N predictions $\zeta = \{\zeta_1, ...\zeta_N\}^{\mathrm{T}}$. The prediction vector is a function of β, i.e., $\zeta = \zeta(\beta)$, where $\beta = \{D_0, B, m\}^{\mathrm{T}}$ are the unknown model parameters, being the diffusivity constant D_0 at the endosteal surface, the conductivity parameter B, and the non-dimensional gradient parameter m, cf. Eqs. (1), (23) and (24).

Measurements always include systematic and non-systematic errors due to instrumentation, the indirect observations, probe sensitivity, temperature fluctuations, etc. Also, inevitably, there is more or less differences between the model and the physical processes. Under ideal conditions the model would be perfect in the sense that $z = \zeta(\beta)$, according to Eq. (24). However, apart from systematic insufficiency of the model also non-systematic noise, is expected.

Here an inverse analysis is performed to obtain the material parameters β. The Eq. (24) is linear in B but non-linear in D_0 and m which complicates the inverse analysis. Here a Kalman filter is used iteratively to obtain sufficiently accurate estimates of β. The method is derived from the method of least-squares with the improved convergence rate while it takes advantage of an *apriori* information regarding the non-systematic noise. Both noise that arise during the measurements and a random variation of the material parameters are considered by the Kalman filter.

The estimated material parameter vector β_k is updated using the following algorithm:

$$\beta_{k+1} = \beta_k + \mathbf{K}_k\{z - \zeta(\beta_k)\}\,, \tag{25}$$

where $\mathbf{K}_k$ is a $3 \times N$ matrix denoted the Kalman gain. The $\mathbf{K}_k$ is updated at every iteration cycle as follows,

$$\mathbf{K}_k = P_k\mathbf{H}_k^{\mathrm{T}}(\mathbf{H}_k P_k \mathbf{H}_k^{\mathrm{T}} + R)^{-1}\,, \tag{26}$$

where P_k is a 3×3 matrix that contains the covariance errors for the parameters, which is updated according to

$$P_{k+1} = (\boldsymbol{I} - \mathbf{K}_k\mathbf{H}_k)P_k + Q\,. \tag{27}$$

The parameters Q and R are used to counteract the uncertainty that is introduced by the noises (Brown, 1983). The general form of the Kalman filter uses a priori available information regarding the noise to determine Q and R. However, in the present analysis Q and R are used as tuning parameters to streamline the iterations. The matrix $\mathbf{H}$ is an $N \times 3$ Jacobian matrix defined as follows,

$$\mathbf{H} = \begin{bmatrix} \dfrac{\partial\zeta_1}{\partial D_0} & \dfrac{\partial\zeta_1}{\partial B} & \dfrac{\partial\zeta_1}{\partial m} \\ \vdots & \vdots & \vdots \\ \dfrac{\partial\zeta_N}{\partial D_0} & \dfrac{\partial\zeta_N}{\partial B} & \dfrac{\partial\zeta_N}{\partial m} \end{bmatrix}\,. \tag{28}$$

To simplify calculation of $\zeta(\beta)$ based on 27 combinations for the initial guess $\beta_0 = [D_{00} \quad B_0 \quad m_0]^T$ of β, a Lagrangian interpolation with equal distances between three different initial values of each of D_{00}, B_0 and m_0 is used. The following interpolation function is used to approximate ζ:

$$\zeta(\beta) = \sum_{p=1}^{3}\sum_{q=1}^{3}\sum_{r=1}^{3}\left[\left(\prod_{u=1\neq p}^{3}\frac{D_0 - D_{00}^u}{D_{00}^p - D_{00}^u}\right)\left(\prod_{v=1\neq q}^{3}\frac{B - B_0^v}{B_0^q - B_0^v}\right)\left(\prod_{w=1\neq r}^{3}\frac{m - m_0^w}{m_0^r - m_0^w}\right)\zeta(\beta_0)^{pqr}\right], \tag{29}$$

where $\zeta(\beta_0)^{pqr} = \zeta(D_0, B, m)$ in Eq. (24), and the parameters D_0, B, and m assume the values $D_{00}^p = \{D_{00}^{min}, \frac{1}{2}(D_{00}^{min} + D_{00}^{max}), D_{00}^{max}\}$, $B_0^q = \{B_0^{min}, \frac{1}{2}(B_0^{min} + B_0^{max}), B_0^{max}\}$, and $m_0^r = \{m_0^{min}, \frac{1}{2}(m_0^{min} + m_0^{max}), m_0^{max}\}$ respectively for each of $p, q, r = \{1, 2, 3\}$.

In the present study non-standard choices Q and R are used for best performance by choosing

$$Q = \begin{bmatrix} (D_{00}^{max} - D_{00}^{min})^2 & 0 & 0 \\ 0 & (B_0^{max} - B_0^{min})^2 & 0 \\ 0 & 0 & (m_0^{max} - m_0^{min})^2 \end{bmatrix}, \tag{30}$$

$$R = \max(\theta^i)I \tag{31}$$

c.f. Shokry (2015), where max and min denoted to the maximum and minimum values for the initial suggested parameters, i.e. D_{00}^{max} is the maximum initial suggested value for the parameter D_0, and θ^i is a vector that contains the maximum square differences between measurements, z, and predictions for the 27 combinations, $\zeta(\beta_0)$, i.e $\theta^i = (z - \zeta(\beta_0^i))^2$.

The P_0 is related to the error between the seeking and suggested parameters. Since P_0 describes the uncertainty of parameters, the initial value of P_0 is selected to be large, equal to Q in Eq. (30).

3 Results and Discussions

The model is checked by applying initial and boundary conditions as given in Eqs. (3) and (4). D_0 is assumed to a value that agrees with the findings of Lindberg et al. (2014), while m is tested for three values, close to 0, 0.5 and 0.9. The $m \simeq 0$ means that a diffusion parameter independent of the position in the bone wall is expected. Fig. 4 shows the concentration inside the specimen as given in Eq. (17) over a unit length for number of terms $n = 1$. It can be seen that the model fulfills the initial and boundary conditions for different m values. Also, it can be noticed that the model with $m = 0.5$ and 0.9 is not symmetric as in the independent position model with $m = 0$.

The initial state values $\beta_0 = [D_{00} \quad B_0 \quad m_0]^T$ were selected to be 27 cubic Lagrange sets that used to obtain the non-linear predicted conductivity, $\zeta(\beta)$, as in Eq. (29).

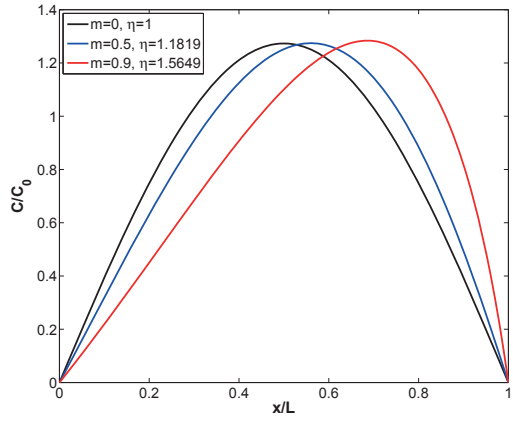

Fig. 4. Concentration versus unit length for n=1. ($D = 2 \times 10^{-11}\mathrm{m}^2/\mathrm{s}$, unit length, $t = 0$ and $m = 10^{-5}, 0.5$, and 0.9). See Appendix C for more information about η.

Lindberg et al. (2014) found that the average constant diffusion of bovine bone is 0.011 ± 0.0069 mm^2/min with a good consistency of n equal to 10000 terms. Since the samples in this study also come from bovine bone, the initial state range of the state values was firstly suggested to be from 0.001 to 0.101 with mid point 0.051 mm^2/min for D_{00} and from 80 to 180 with mid point 130 μS/mm for B_0 and from 0.05 to 0.45 with mid point 0.25 for m_0. The mean square error (MSE) between the experimental and the analytical that were obtained by Kalman filter was computed according to:

$$MSE = \frac{1}{N}\sum_{j=1}^{N}(z_j - \zeta(\beta_k)_j)^2. \tag{32}$$

The 27 combinations between the suggested initial parameters for sample 4 converged to one place after 60 iterations with MSE of 418.2 $(\mu\mathrm{S/mm})^2$. A new and smaller initial state range was suggested according to the converged point, by decreasing the initial state values of D_{00}, a better MSE was obtained. Since Kalman filter works well with small ranges (especially when interpolation is used), a repeated processes of decreasing the initial state ranges were applied until a good fitting was obtained between the analytical model and experimental data. Table 2 contains all the suggested initial state ranges for sample 4, the obtained parameters using Kalman filter, the MSE, and the convergence points (CP) for each initial state range.

Fig. 5 shows the derived values from the analytical model using the extracted parameters that were obtained by using the Kalman filter for the five suggester initial state ranges. The parameter fitting is done using the experimental data from sample 4 which also is presented in Fig. 5.

As shown in Table 2 and Fig. 5, the combinations of D_0, B and m were converged to five different points for the five different ranges. The MSE was found to be large

Table 2: The suggested initial state ranges for sample 4, obtained D_0, B, m, MSE and CP for each range using Kalman filter .

Initial ranges	D_0[mm^2/min]	B [μS/mm]	m	MSE [(μS/mm)^2]	CP
$0.001 \leq D_{00} \leq 0.101$ $80 \leq B_0 \leq 180$ $0.05 \leq m_0 \leq 0.45$	0.00277	197.530	0.762	418.20	1
$0.001 \leq D_{00} \leq 0.041$ $80 \leq B_0 \leq 180$ $0.05 \leq m_0 \leq 0.45$	0.00187	167.110	0.585	67.04	1
$0.001 \leq D_{00} \leq 0.021$ $80 \leq B_0 \leq 180$ $0.05 \leq m_0 \leq 0.45$	0.00213	138.797	0.501	28.98	1
$0.001 \leq D_{00} \leq 0.011$ $80 \leq B_0 \leq 180$ $0.05 \leq m_0 \leq 0.45$	0.00625	80.058	0.682	0.386	1
$0.004 \leq D_{00} \leq 0.008$ $76 \leq B_0 \leq 86$ $0.6 \leq m_0 \leq 0.7$	0.00568	82.377	0.641	0.067	1

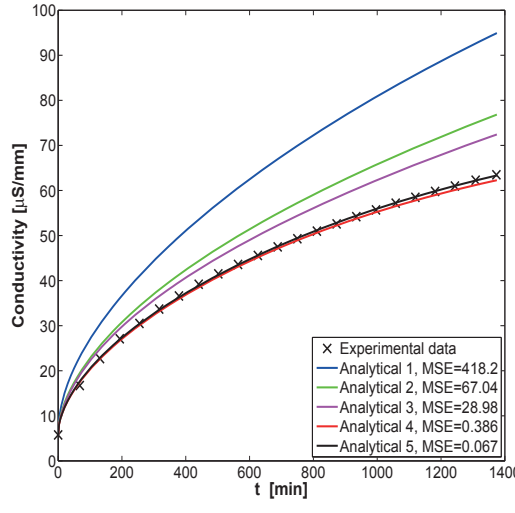

Fig. 5. Analytical results using the parameters obtained from the Kalman filtering using the five initial state ranges. Experimental results for sample 4 is also presented in the figure.

(418.20 (μS/mm)^2) for the largest range and to be small (0.067 (μS/mm)^2) for the smallest range. This is expected since interpolation function was used. Fig. 6 shows the convergence of combinations for the fifth initial state range for sample 4 for four different iterations, which converged to one place after 50 iterations.

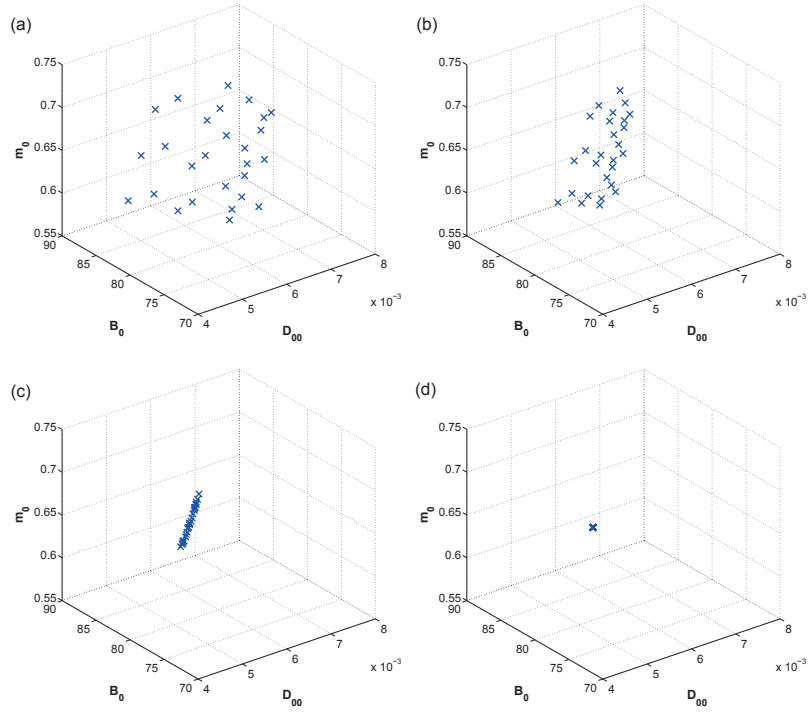

Fig. 6. Convergence between D_0 [mm^2/min], B [μS/mm], and m for the fifth initial state range for sample 4 after (a) 1 iteration, (b) 3 iterations, (c) 10 iterations, and (d) 50 iterations.

The figure shows that the 27 initial combinations started to converge after the first iteration as shown in Fig. 6a. The convergence started to be around specific area after a little iterations as shown in Fig. 6b, and around specific line after more iterations as shown in Fig. 6c. Finally, they converged around only one point after 50 iterations as shown in Fig. 6d. A possible reason, is that the Kalman filter minimizes the MSE between the states, and the value of the MSE started to decrease from the converged area to the converged point passed with the converged line.

The best fitting between analytical results obtained by Kalman filter and experimental data accompanied with the least MSE is found to be the point where the 27 sets were converged in the fifth initial state range, as shown in Fig. 5.

The same processes are repeated for bone samples 1, 2, 3, and 5. Knowing that bone is an inhomogeneous material, the results obtained for sample 4 suggests that the initial state ranges start from the fourth range. The combinations of the 27 sets converged to two

different points for the fourth initial state range for some samples, few numbers of the 27 sets (from 3 to 5 sets) are converged to the wrong place while the rest converged to the right place. A possible reason for that is some of the sets might converge to a wrong place due to the interpolation. Fig. 7 shows analytical results using the obtained parameters by Kalman filter and experimental data for samples 1 and 2.

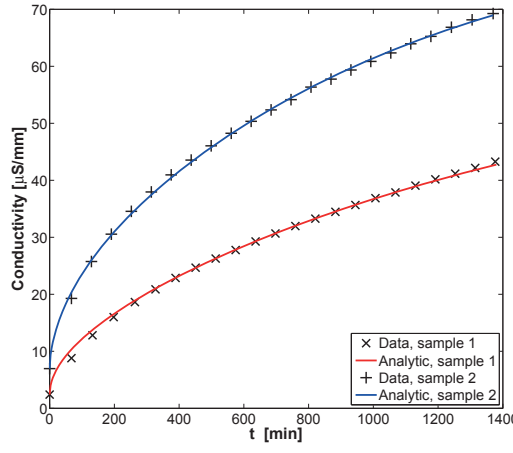

Fig. 7. Experimental data and results from analytical model and experimental data for spatially dependent diffusion parameters for samples 1 and 2.

The values of the parameters obtained by Kalman filtering of the experimental data for the five bovine bone samples are summarized in Table 3. The values of the parameter D_1 for the samples are derived using Eq. (23) and they are also presented in the table together with the MSE of the calculations, cf. Eq. (32).

Table 3: Values of D_0, B , m, D_1 and MSE that obtained by Kalman filtering

Sample	D_0 [mm^2/min]	B [μS/mm]	m	D_1 [mm^2/min]	MSE [(μS/mm)^2]
1	0.00485	75.329	0.814	0.0009	0.183
2	0.01051	83.372	0.512	0.0051	0.127
3	0.00807	71.073	0.529	0.0038	0.094
4	0.00568	82.377	0.641	0.0020	0.067
5	0.00949	47.523	0.599	0.0038	0.055

The values of the diffusion parameters D_0 and D_1 vary between the samples and this can be explained by the inhomogeneity of the bone material. D_0 ranges from 0.00485 to 0.01051 mm^2/min while D_1 ranges from 0.0009 to 0.0051 mm^2/min, however, the value of the diffusion parameter D in the middle of the bone wall, $D = (D_0+D_1)/2$, is in good agreement with the previous work for constant diffusion. In previous work, it has been shown that the diffusion constant for bone is varying between 2.78×10^{-11} and 42.9×10^{-11} m^2/s

based on different studies (Li et al., 2009; Wang et al., 2006; Lindberg et al., 2014). Table 4 contains the range of the values of the diffusion parameter that were obtained in these studies. However, the values could not be directly compared since different bones and solutes were used in the studies. Li et al. (2009) measured diffusion coefficients of five exogenous fluorescent tracers (sodium fluorescein, dextran-3k, dextran-10k, parvalbumin, and ovalbumin) in murine tibiae in situ. Wang et al. (2006) studied the diffusion coefficients of fluorescent dye (sodium fluorescein) in mice in situ. Lindberg et al. (2014) calculated the diffusion coefficient of KCl ions escaped from bovine cortical bone samples into distilled water.

Table 4: Values of the diffusion parameters from different studies

D [m^2/s]	(Li et al., 2009)	(Wang et al., 2006)	(Lindberg et al., 2014)	Average diffusion for suggested model
from	4.4×10^{-11}	27×10^{-11}	2.78×10^{-11}	4.79×10^{-11}
to	34.1×10^{-11}	39×10^{-11}	42.9×10^{-11}	13.01×10^{-11}

The distribution of the spatially dependent diffusion parameters for the five samples as functions of a normalized coordinate in the bone wall could bee seen in Fig. 8. The figure shows that D decreases when the coordinate increase, which may indicate that the bone becomes more dense and less porous with coming closer to the periosteal surface.

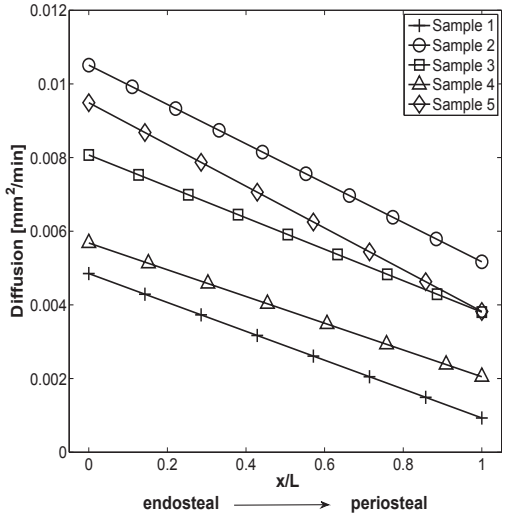

Fig. 8. Spatially dependent diffusion parameters versus positions of the bone wall for the five samples. The markers are merely identifying the specified samples.

The results obtained for spatially dependent diffusion through the bone wall (see Fig. 8) agree well with the findings obtained by Baron (2012) regarding porosity in the bone wall (see Fig. 3), with a strong believe that diffusivity decreases as bone porosity decreases.

4 Conclusions

A hypothesis based on previous research (Baron, 2012) is suggested as a method for considering diffusion as spatially dependent parameters in bovine bone. Here, a one-dimensional model for spatially dependent diffusion parameters is introduced. Diffusion parameters are introduced using the analytical model Eq. (24), where the material parameters are determined by Kalman filtering of experimental data. The diffusion parameters are found to be $(12.8 \pm 4.7) \times 10^{-11}$ and $(5 \pm 3.5) \times 10^{-11}$ m^2/s at the endosteal and periosteal surfaces respectively. The average diffusion value in the middle of the bone wall are in well agreement with previous work (Li et al., 2009; Wang et al., 2006; Lindberg et al., 2014), taking different bone and solutes into considerations. The mean square error varies from 0.06×10^{-6} to 0.183×10^{-6} $(\mu\mathrm{S/m})^2$. The suggested one-dimensional model for spatially dependent diffusion parameters succeeded to introduce a complete behavior for the concentration inside the bovine bone samples with very good accuracy. Also, the results show that the behavior of concentration inside the bone wall can be considered as linear dependent position.

Acknowledgments

The following organizations are acknowledged: Erasmus Mundus Action 2 for financial support of both authors, Lund University for supporting P. Ståhle and Fayoum University for supporting the visit of A. Shokry.

Appendix A Diffusivity of KCl ions

Diffusion parameters were chosen to be in consistent with the values given in Table 4 to check the concentration content inside the bone samples for different times. Since high diffusivity takes a smaller time than low diffusivity, the diffusion parameters were selected to be lower than the lowest value in Table 4, which enhances the required enough time for ions to diffuse from bone sample. Fig. A-1 shows the concentration inside bone sample for five different times for only one term (the first term in the series of Eq. (17)) for $m \simeq 0$ and $m = 0.9$.

The results indicate that 24 hours might be enough time for ions to diffuse from the bone samples, knowing that a higher value of D will give a faster diffusion and a shorter time for ions to leave the bone samples.

Appendix B Coefficients F_0, F_1, F_2, and F_3

The following assumption is made in order to use the recursive Bessel function properties that required to solve the integrated parts in the mathematical model:

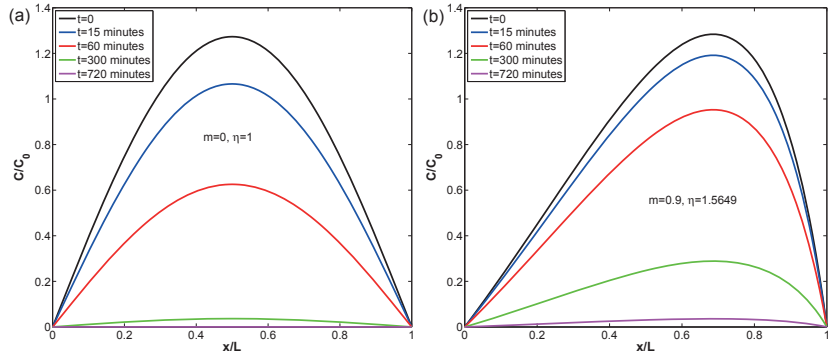

Fig. A-1. Concentration content inside bone sample after five different times for unity length, $D = 2 \times 10^{-11}\mathrm{m}^2/\mathrm{s}$, and $t = 0$, 15, 60, 300 and 720 minutes. (a) $m = 10^{-5}$. (b) $m = 0.9$. See Appendix C for more information about η. Note that the concentration is derived using only one term in the series expansion.

$$\tau_n = \frac{P_n}{m}\sqrt{1 - \frac{mx}{L}}. \tag{B-1}$$

Then the final form of the integrated parts can be written as:

$$\left(\int_0^L c_n(x,0)\mathrm{d}x\right)^2 = F_0 \tag{B-2}$$

where F_0 is given by:

$$F_0 = \left(-\frac{2L}{P_n}\sqrt{1-m}\left[J_0\left(\frac{P_n}{m}\right)Y_0\left(\frac{P_n}{m}\sqrt{1-m}\right) - J_0\left(\frac{P_n}{m}\sqrt{1-m}\right)Y_0\left(\frac{P_n}{m}\right)\right] + \frac{4Lm}{\pi P_n^2}\right)^2, \tag{B-3}$$

and

$$\int_0^L c_n^2(x,0)\mathrm{d}x = F1 + F2 + F3 \tag{B-4}$$

where F_1, F_2, and F_3 are given by:

$$\begin{aligned} F_1 = &-\left(\frac{Lm}{P_n^2}\right)Y_0^2\left(\frac{P_n}{m}\right)\left\{\left[\left(\frac{P_n}{m}\sqrt{1-m}\right)^2\left(J_0^2\left(\frac{P_n}{m}\sqrt{1-m}\right)\right.\right.\right. \\ &\left.\left.\left. + J_1^2\left(\frac{P_n}{m}\sqrt{1-m}\right)\right)\right] - \left[\left(\frac{P_n}{m}\right)^2\left(J_0^2\left(\frac{P_n}{m}\right) + J_1^2\left(\frac{P_n}{m}\right)\right)\right]\right\}, \end{aligned} \tag{B-5}$$

$$F_2 = \left(\frac{2Lm}{P_n^2}\right) J_0\left(\frac{P_n}{m}\right) Y_0\left(\frac{P_n}{m}\right) \left\{ \left[\left(\frac{P_n}{m}\sqrt{1-m}\right)^2 J_0\left(\frac{P_n}{m}\sqrt{1-m}\right) \right.\right.$$
$$\left. Y_0\left(\frac{P_n}{m}\sqrt{1-m}\right)\right] + \left[\left(\frac{P_n}{m}\sqrt{1-m}\right)^2 J_1\left(\frac{P_n}{m}\sqrt{1-m}\right) Y_1 \right. \tag{B-6}$$
$$\left.\left(\frac{P_n}{m}\sqrt{1-m}\right)\right] - \left[\left(\frac{P_n}{m}\right)^2 \left(J_0\left(\frac{P_n}{m}\right) Y_0\left(\frac{P_n}{m}\right) + J_1\left(\frac{P_n}{m}\right) Y_1\left(\frac{P_n}{m}\right)\right)\right] \Big\},$$

$$F_3 = -\left(\frac{Lm}{P_n^2}\right) J_0^2\left(\frac{P_n}{m}\right) \left\{ \left[\left(\frac{P_n}{m}\sqrt{1-m}\right)^2 \left(Y_0^2\left(\frac{P_n}{m}\sqrt{1-m}\right)\right.\right.\right.$$
$$\left.\left.\left. + Y_1^2\left(\frac{P_n}{m}\sqrt{1-m}\right)\right)\right] + \left[\left(\frac{P_n}{m}\right)^2 \left(Y_0^2\left(\frac{P_n}{m}\right) + Y_1^2\left(\frac{P_n}{m}\right)\right)\right] \Big\}, \tag{B-7}$$

Appendix C Roots of λ

The condition of non-trivial solution to find the roots of λ can be rewritten in the next form:

$$J_0\left(\frac{P}{m}\right) Y_0\left(\left|\frac{P}{m}\right| \sqrt{1-m}\right) - J_0\left(\frac{P}{m}\sqrt{1-m}\right) Y_0\left(\left|\frac{P}{m}\right|\right) = 0 \tag{C-1}$$

The roots for λ of Eq. (C-1) are obtained numerically. It is, however, known that the roots are $2n\pi$ for a constant D, i.e. for $m = 0$, cf. (Crank, 1975). With the attempt to find a first order perturbation of P_n for small m the result is written on the form

$$P_n = 2n\pi(1 - \frac{m}{4}\eta) \tag{C-2}$$

where n is the number of the root and η is a factor that corrects the result for a constant diffusion coefficient. The results for $n = 1$ and 10 and for different degrees of variation of $D(x)$ with $m = 0.9$,$0.7, 0.5, 0.1, 0.01$ are given in Table C-1.

Table C-1: η values for different m

m	0.9	0.7	0.5	0.1	0.01
$\eta(n = 1)$	1.5649	1.3121	1.1819	1.0277	1.0027
$\eta(n = 10)$	1.5200	1.2924	1.1717	1.0264	1.0022

The result reveals that the error using a perturbed value according to Eq. (C-2) with $\eta = 1$ leads to an error of less than 18.2% for $m < 0.5$.

References

Ababneh, Z. Q., Beloeil, H., Berde, C. B., Ababneh, A. M., Maier, S. E., Mulkern, R. V., 2009. In vivo lipid diffusion coefficient measurements in rat bone marrow. Magnetic resonance imaging 27 (6), 859–864.

Adachi, T., Osako, Y., Tanaka, M., Hojo, M., Hollister, S. J., 2006. Framework for optimal design of porous scaffold microstructure by computational simulation of bone regeneration. Biomaterials 27 (21), 3964–3972.

Adam, J., 2002. The effect of surface curvature on wound healing in bone: Ii. the critical size defect. Mathematical and computer modelling 35 (9), 1085–1094.

Ambard, D., Swider, P., 2006. A predictive mechano-biological model of the bone-implant healing. European Journal of Mechanics-A/Solids 25 (6), 927–937.

Arfken, G. B., 2001. hans J. Weber. Mathematical methods for Physicists. Harcourt/Academic Press.

Balliu, E., Vilanova, J., Peláez, I., Puig, J., Remollo, S., Barceló, C., Barceló, J., Pedraza, S., 2009. Diagnostic value of apparent diffusion coefficients to differentiate benign from malignant vertebral bone marrow lesions. European journal of radiology 69 (3), 560–566.

Banks-Sills, L., Ståhle, P., Svensson, I., Eliaz, N., 2011. Strain driven transport for bone modeling at the periosteal surface. Mathematical biosciences 230 (1), 37–44.

Baron, C., 2012. Using the gradient of human cortical bone properties to determine age-related bone changes via ultrasonic guided waves. Ultrasound in medicine & biology 38 (6), 972–981.

Bousson, V., Meunier, A., Bergot, C., Vicaut, É., Rocha, M. A., Morais, M. H., Laval-Jeantet, A.-M., Laredo, J.-D., 2001. Distribution of intracortical porosity in human midfemoral cortex by age and gender. Journal of Bone and Mineral Research 16 (7), 1308–1317.

Brown, R. G., 1983. Introduction to random signal analysis and Kalman filtering. Vol. 8. Wiley New York.

Capuani, S., 2013. Water diffusion in cancellous bone. Microporous and Mesoporous Materials 178, 34–38.

Cayan, F. N., Pakalapati, S. R., Elizalde-Blancas, F., Celik, I., 2009. On modeling multi-component diffusion inside the porous anode of solid oxide fuel cells using Fick′s model. Journal of Power Sources 192 (2), 467–474.

Chou, H.-Y., Müftü, S., 2013. Simulation of peri-implant bone healing due to immediate loading in dental implant treatments. Journal of biomechanics 46 (5), 871–878.

Cowin, S. C., 1999. Bone poroelasticity. Journal of biomechanics 32 (3), 217–238.

Cowin, S. C., Gailani, G., Benalla, M., 2009. Hierarchical poroelasticity: movement of interstitial fluid between porosity levels in bones. Philosophical Transactions of the Royal Society A: mathematical, physical and engineering sciences 367 (1902), 3401–3444.

Crank, J., 1975. The mathematics of diffusion. Oxford: Clarendon.

Fernández, J., García-Aznar, J., Martínez, R., 2012. Numerical analysis of a diffusive strain-adaptive bone remodelling theory. International Journal of Solids and Structures 49 (15), 2085–2093.

Gomez-Benito, M., Garcia-Aznar, J., Kuiper, J., Doblaré, M., 2005. Influence of fracture gap size on the pattern of long bone healing: a computational study. Journal of theoretical biology 235 (1), 105–119.

Li, W., You, L., Schaffler, M. B., Wang, L., 2009. The dependency of solute diffusion on molecular weight and shape in intact bone. Bone 45 (5), 1017–1023.

Lindberg, G., Banks-Sills, L., Ståhle, P., Svensson, I., 2013. A two-dimensional model for stress driven diffusion in bone tissue. Computer methods in biomechanics and biomedical engineering 18 (5), 457–467.

Lindberg, G., Shokry, A., Reheman, W., Svensson, I., 2014. Determination of diffusion coefficients in bovine bone by means of conductivity measurement. International Journal of Experimental and Computational Biomechanics 2 (4), 324–342.

Margetis, D., 2009. Homogenization of reconstructed crystal surfaces: Fick′s law of diffusion. Physical Review E 79 (5), 052601.

Naceri, A., 2009. An analysis of moisture diffusion according to Fick′s law and the tensile mechanical behavior of a glass-fabric-reinforced composite. Mechanics of Composite Materials 45 (3), 331–336.

Sapotnick, A., Nackenhorst, U., 2012. A combined FIC-TDG finite element approach for the numerical solution of coupled advection−diffusion−reaction equations with application to a bioregulatory model for bone fracture healing. International Journal for Numerical Methods in Engineering 92 (3), 301–317.

Shokry, A., 2015. A methodology for using kalman filter to determine material parameters from uncertain measurements . arXiv:1502.03576v1 [cond-mat.mtrl-sci].

Stadelmann, V. A., Terrier, A., Gauthier, O., Bouler, J.-M., Pioletti, D. P., 2009. Prediction of bone density around orthopedic implants delivering bisphosphonate. Journal of biomechanics 42 (9), 1206–1211.

Wang, L., Wang, Y., Han, Y., Henderson, S., Majeska, R., Weinbaum, S., Schaffler, M., 2006. In situ measurement of solute transport in the bone lacunar-canalicular system. The FASEB Journal 20, A418.

Yildirim, A., Öner, M. D., Bayram, M., 2011. Fitting Fick′s model to analyze water diffusion into chickpeas during soaking with ultrasound treatment. Journal of Food Engineering 104 (1), 134–142.

Paper D

A. Shokry, G. Lindberg, G Kharmanda, and P. Ståhle (2015)

Superposition principles for calculation of diffusion and elastic parameters of sparsely porous materials

Submitted for international publication

Superposition principles for calculation of diffusion and elastic parameters of sparsely porous materials

Abdallah Shokry[a,b], Gustav Lindberg[a], Ghias Kharmanda [a] and Per Ståhle[a]

[a] *Division of Solid Mechanics, Lund University, 22100 Lund, Sweden*

[b] *Industrial Engineering Department, Fayoum University, 63514 Fayoum, Egypt*

Abstract

Effective material parameters are calculated using a derived continuum mechanically based superposition principle. Exact expressions are obtained for materials with sufficiently low pore densities, ensuring that pore to pore interaction is insignificant. The superposition method that is obtained, simplifies the calculations which may be performed manually for a moderate number of pores and are suitable to use in connection stochastic methods for cases with very many pores.

To establish the method, shape factors that are two for the diffusion coefficient and one for the elastic modulus, have to be found numerically. The shape factors, that depend on the individual pore shapes are calculated for a few characteristic pores.

A cross section of bovine bone is taken as an example. In the evaluation the superposition principle is compared with full scale finite element calculations. The evaluation shows that pores are sufficiently sparse if the ratio of pore volume to total volume is less than around 20%. The changes of the material parameters because of the present pores are compared. The study shows that the superposition methods predicts the change of the diffusion coefficient with a result differs from that of full scale numerical calculations with only around 10%. A similar accuracy is obtained for the elastic modulus.

1 Introduction

Bone is a complex material, with a multiphasic, heterogeneous and anisotropic microstructure. One of the main goals of this work is to define the relationship between bone porosity and both diffusion coefficient and elastic modulus. The idea of making computational simulations is to define the different biomechanical relationships, that are difficult to obtain experimentally or clinically. The porosity in bone can vary continuously from 5 to 95%, most bone tissues have either very low or very high porosity. Accordingly, it is usually distinguished between two types of bone tissue. The first type is the trabecular or cancellous bone with 40-95% porosity, usually found in cuboidal bones, flat bones and at the ends of long bones. The pores are interconnected and filled with marrow, while the bone matrix has the form of plates and struts called trabeculae. The second type is the cortical or compact bone with 5-20% porosity and different types of pores (Winkelstein, 2012; Marcus et al., 2013).

The porosity is related to the diffusivity and the elastic modulus. The diffusivity is important for maintaining a proper supply of nutrients and for removing waste products, while the elastic modulus determines the quality and the reliability of bone strength. Some useful models were presented to study the properties of bone tissues in the presence of pores based on the poroelasticity theory, in which the mechanical properties of a material is affected by the movement of the fluid in the pores (Biot, 1941; Rice and Cleary, 1976; Showalter, 2000; Cowin, 2003). In bone tissue, the transport of fluids and solutes is a concern for the bone formation and remodelling. The diffusion coefficients of different solutes in cortical bone of mammals were investigated using different techniques (Patel et al., 2004; Wang et al., 2005; Li et al., 2009; Lindberg et al., 2014). Further, the diffusion coefficients of water in tubercular bone tissue for human are studied by Marinozzi et al. (2014a) and Marinozzi et al. (2014b). Knowing diffusion coefficients in bone is important to understand the transportation process of substances in the cell level, and to make realistic models for bone remodelling and bone healing.

The mechanical properties such as elastic modulus of bone are affected by the pore sizes and densities. To investigate the interrelationships between the pore size and the bone strength, several experiments are required. The relationship between the pore size and the elastic modulus may be established analytically or experimentally. The elastic modulus decreases as the pore size increases (Schaffler and Burr, 1988; Baron et al., 2007; Grimal et al., 2011). It is believed that the different properties of bone, strength and damage resistance, can be predicted with good accuracies using knowledge of the effect of both pore size and shape on the bone strength.

In this work, the diffusion coefficients and the elastic modulus of a mammal bone sample with irregular pores are analysed by carrying out a superposition principle and finite element calculations using ABAQUS software (ABAQUS, 2014). A mathematical formulations relating between the porosity and both of the diffusivity and the elastic modulus in cortical bone are presented. A correction factor is obtained for a few number of pores for different pore sizes based on the finite element calculations. Next, a generalisation of the irregularly distributed pores in a region of the bone sample is carried out to

define the diffusion coefficient and the elastic modulus, based on the correction factor of the selected pores.

2 Diffusion theory

Bone is a heterogeneous material, and the diffusion coefficient D becomes a function of the spatial coordinates. In the present study, described in this paper, an effective diffusion coefficient is determined for a large area of bone containing small pores, which makes it possible to use the easy accessible Fick′s law with good precision for describing the flow through the heterogeneous bone structure.

Inside the pores, the diffusion coefficient is set to D_w, where w stands for water, and far away from the pores, the diffusion coefficient is set to D_b, where b is for bone. The flow J is driven by the concentration gradient. This analytical model describes a one-dimensional flow, although locally close to the pores the flow will be highly affected in several directions. This is handled by introducing two parameters, θ and κ that are determined by finite element calculations, and with this, the effective flow over the region can be determined.

A Cartesian coordinate system $x_i \equiv x_1,x_2,x_3$ is introduced. Tensor notation including the summation rule is applied. Undefined indicies $i, j,$ etc. $= 1, 2, 3$. The flux vector J_i of a selected substance in the bone environment becomes, due to differences in concentration of matter,

$$J_i = -Dc_{,i} \,, \tag{1}$$

where $c_{,i}$ is the gradient vector of the concentration. Indices $,i$ denote partial differentiation with respect to x_i, i.e. $c_{,i} = \partial c/\partial x_i$. The material parameter D is the diffusion coefficient of the substance-bone system. Also matter is conserved giving that

$$\frac{\partial c}{\partial t} = -J_{i,i} \,. \tag{2}$$

It is believed that the concentration of matter at the boundaries does not change over time, and so a steady-state, $\partial c/\partial t = 0$, is assumed. The consequence is that the flux through the structure will be divergence free, i.e.

$$(Dc_{,i})_{,i} = 0 \,. \tag{3}$$

The governing Eq. (3) are solved for the boundary conditions

$$c_{,2} = 0 \tag{4}$$

at $0 < x_1 < h$ and $x_2 = 0$ and $x_2 = w$. Further,

$$c = 0 \tag{5}$$

at $x_1 = 0$ and $0 \leq x_2 \leq w$, and

$$c = c_1, c_2, c_\alpha, c_\beta \text{ or } \Delta c \tag{6}$$

at $x_1 = h$ and $0 \leq x_2 \leq w$.

At first, a thin slice of bone structure is studied, see Fig. 1. The slice contains a small section (with the height h_0) where a pore, or something else that affects the effective diffusion coefficient, is located. In this small section, the effective diffusion coefficient is set to D_0, and becomes a function, e.g., of the relation between the size of the pore and the section, and of the shape of the pore and the diffusion coefficient D_w inside of it. With D_0 an effective diffusion coefficient D_1 for the entire slice can be calculated.

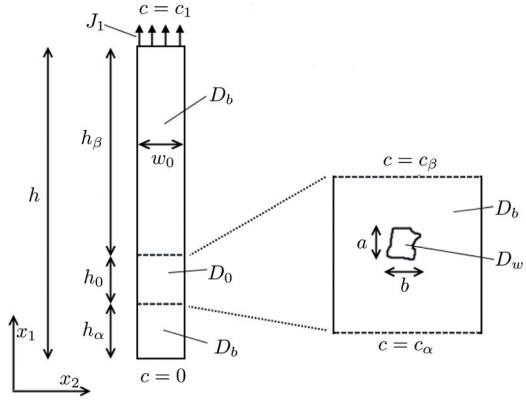

Fig. 1. A thin section containing an area $h_0 \times w_0$ with a pore.

The flux through the strip remains constant and according to the conventions used in Fig. 1, the relations

$$J_1 = -D_1 \frac{c_1}{h} \tag{7}$$

and

$$J_1 = -D_0 \frac{\Delta c}{h_0} \,, \tag{8}$$

apply. By combining Eqs. (7) and (8) D_1 is described as

$$D_1 = D_0 \frac{h \Delta c}{h_0 c_1} \,. \tag{9}$$

The unknown concentration difference Δc covers the arbitrary located small section containing the pore and is described by

$$\Delta c = c_\beta - c_\alpha \tag{10}$$

and it is also seen in Fig. 1 that

$$h = h_0 + h_\alpha + h_\beta \,. \tag{11}$$

The flux over the part of the slice with height h_β is described by

$$J_1 = -D_b \frac{c_1 - c_\beta}{h_\beta} \,. \tag{12}$$

In the same way the concentration c_α can be written as

$$c_\alpha = -\frac{J_1 h_\alpha}{D_b} \,. \tag{13}$$

By using Eqs. (10) and (11), Eq. (12) now looks like

$$J_1 = -D_b \frac{c_1 - \Delta c - c_\alpha}{h - h_0 - h_\alpha} \tag{14}$$

and by replacing c_α according to Eq. (13), the flux reads

$$J_1 = -D_b \frac{c_1 - \Delta c}{h - h_0} \,. \tag{15}$$

The unknown distances h_α and h_β together with c_α and c_β are now eliminated. Eq. (15) can be re-arranged into

$$\Delta c = \frac{J_1}{D_b}(h - h_0) + c_1 \,. \tag{16}$$

If this is inserted into Eq. (9), D_1 can be written as

$$D_1 = D_0 \frac{h\left(\frac{J_1}{D_b}(h - h_0) + c_1\right)}{h_0 c_1} \,. \tag{17}$$

If $J_1 h$ is replaced by $-D_1 c_1$ according to Eq. (7), then c_1 can be eliminated from Eq. (17) which then take the appearance of

$$D_1 = \frac{D_0}{h_0}\left(\frac{-D_1}{D_b}(h - h_0) + h\right) \,. \tag{18}$$

After some re-arranging, the final expression for the effective diffusion coefficient for the thin slice of bone structure is given as

$$D_1 = D_b \left(1 - \left(1 - \frac{D_b}{D_0}\right)\frac{h_0}{h}\right)^{-1} \,. \tag{19}$$

Now a wider part of bone structure is considered, see Fig. 2.

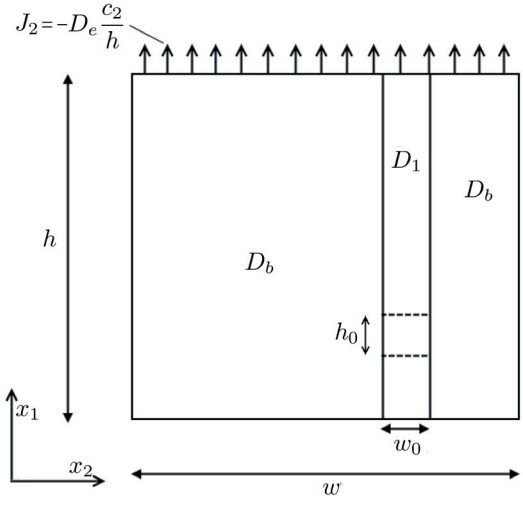

Fig. 2. Same as Fig. 1 embedded in a larger bone section.

By introducing an effective diffusion coefficient D_e for the entire structure, the averaged flow J_2 through the structure is described as

$$J_2 = -D_e \frac{c_2}{h} \,. \tag{20}$$

By looking at Fig. 2 it is also obvious that the total amount of matter that passes the cross-section of the structure is

$$J_2 w = -D_b \frac{c_2}{h}(w - w_0) - D_1 \frac{c_2}{h} w_0 \,. \tag{21}$$

If Eqs. (20) and (19) are used to eliminate and D_1, then Eq. (21) reads

$$D_e = D_b \left(1 + \left[\frac{1 - D_b/D_0}{1 - (1 - D_b/D_0)\frac{h_0}{h}} \right] \frac{h_0 w_0}{hw} \right) . \tag{22}$$

The derived scaling $h_0 w_0 / hw$ relates the rectangular area, $h_0 w_0$, to the area of the full body, hw. The only relevant quantities defining D_e are the height ratio, h_0/h, the area ratio, $h_0 w_0 / hw$ and the ratio of the diffusivity constants, D_b/D_0.

A similar relation for non-rectangular shapes as Eq. (22) is assumed as well. By introducing the area of the pore, A_p, the $h_0 w_0$ in Eq. (22) can be replaced with θA_p, where θ is a correction factor. The correction θ is supposed to cover all remaining interactions between the bone and the pore, such as shape, orientation of the pore with respect to the flux etc. Further, the dependence of the height ratio h_0/h (cf. Eq. (22)) can be replaced with a/h using a correction factor κ. The pores are assumed to contain a fluid with the diffusion coefficient, D_w. With the diffusion coefficient D_0 replaced with D_w, the following approximation of the effective diffusion coefficient is obtained as

$$D_e = D_b\left(1 + \frac{\theta s}{(1-\kappa s\frac{a}{h})}\frac{A_p}{hw}\right) \tag{23}$$

where

$$s = 1 - D_b/D_w\,. \tag{24}$$

The expression in Eq. (23) is expected to be asymptotically exact for infinitesimal values of A_p/hw. The numerical values θ and κ are established for different pore shapes using finite element calculations. The obtained result D_e/D_b is expanded as a power series in $\sqrt{A_p/hw}$ as follows

$$(\frac{D_e}{D_b} - 1)\frac{hw}{sA_p} = \alpha_1 + \alpha_2\left(\frac{A_p}{hw}\right)^{\frac{1}{2}} + \alpha_3\frac{A_p}{hw} + \alpha_4\left(\frac{A_p}{hw}\right)^{\frac{3}{2}} + O\left(\left(\frac{A_p}{hw}\right)^2\right)\,, \tag{25}$$

where α_1 to α_4 are constants that are fitted to the numerical finite element result for 10 to 11 different pore sizes A_p. The last term is big O which gives the limiting behaviour of remaining terms. Different pore shapes and orientations with respect to the remote fluxes are computed and the results are, for each shape and orientation, fitted to the series expansion Eq. (25) to obtain numerical values for the coefficients, α_1 to α_4. By rewriting Eq. (23) as a power series in $\kappa s a/h$ the expression becomes

$$(\frac{D_e}{D_b} - 1)\frac{hw}{sA_p} = \theta(1-\kappa s\frac{a}{h})^{-1} = \theta\left(1 + \kappa s\frac{a}{h} + (\kappa s\frac{a}{h})^2 + (\kappa s\frac{a}{h})^3 + O((\kappa s\frac{a}{h})^4)\right) \tag{26}$$

and one can now identify θ and κ by comparing Eqs. (25) and (26) and using the coefficients α_1 and α_2.

The effective diffusion coefficient is defined as

$$D_e = -\frac{J_a h}{\Delta c}, \tag{27}$$

where Δc is the prescribed concentration at $x_1 = h$ and J_a is the average total flux through the body calculated as

$$J_a = \frac{1}{w}\int_0^w J_2 \mathrm{d}x_2 \;\text{ at }\; x_1 = h\,. \tag{28}$$

The effective diffusivity coefficient D_e can be calculated for bodies with large geometries and multiple pores. It is obvious from the analysis above that as long as the individual pores do not interact, the result is found using a superposition giving

$$D_e = D_b\left(1 + \frac{s}{hw}\;\sum_{i=1}^{N}\frac{\theta^{(i)}A_p^{(i)}}{1 - s\kappa^{(i)}\frac{a^{(i)}}{h}}\right), \tag{29}$$

where summation is performed for N pores. The hypothesis here is that $\theta^{(i)}$ and $\kappa^{(i)}$ can be taken as the result for a similar shape.

3 Elastic theory

In this section, a method to compute how present pores influence the elastic modulus of the bone is presented. The same geometries and pores as above, are assumed. To follow the conventional tensor notation, the stresses are written σ_{ij}, the strains ϵ_{ij} and the displacements u_i. The stresses are given by Hooke's law as

$$\sigma_{ij} = \frac{E}{1+\nu}(\epsilon_{ij} + \frac{\nu}{(1-2\nu)}\delta_{ij}\epsilon_{kk}) \tag{30}$$

and the strains ϵ_{ij}, that are assumed to be small, are defined by

$$\epsilon_{ij} = \frac{1}{2}(u_{i,j} + u_{j,i})\,. \tag{31}$$

The equations of equilibrium, $\sigma_{ij,j} = 0$, after insertion of Eqs. (30) and (31) give the equation

$$u_{i,jj} + \frac{1}{1-2\nu}u_{j,ij} = 0. \tag{32}$$

Eq. (32) governs the linear elastic behaviour of the body. For nominal stress in the x_1 direction the boundary conditions are

$$u_1 = 0 \quad \text{at} \quad 0 \leq x_2 \leq w \quad \text{and} \quad x_1 = 0 \tag{33}$$

and

$$u_1 = \Delta u \quad \text{at} \quad 0 \leq x_2 \leq w \quad \text{and} \quad x_1 = h. \tag{34}$$

Normal tractions on remaining edges $x_2 = 0$, $0 < x_1 < h$ and $x_2 = w$, $0 < x_1 < h$ vanish. Finally, shear tractions on all edges vanish.

The average tractions at $x_1 = h$ are calculated as

$$\sigma_a = \frac{1}{w}\int_0^w \sigma_{22}\mathrm{d}x_1. \tag{35}$$

The effective modulus of elasticity is defined as

$$E_e = \sigma_a \frac{h}{\Delta u}\,. \tag{36}$$

The presence of pores will weaken the structure, whereas the stiffness of the pore material, being a fluid, is assumed to be insignificant. Here compressive stresses are assumed to be insignificant. It seems reasonable that the weakening may be ignored outside a region surrounding the pore, provided that this region can be selected large enough. It is also assumed that the linear extent of this region scale with the width of the pore b perpendicular to the loading direction. The scaling is proposed to be quadratic with the linear extent b of the pore (cf. Eq. (23)). To include the ability to deal with pure crack the square of the

linear extent in the direction perpendicular to the remote loading direction is selected as the scaling parameter. This leads to the hypothetical approximation

$$E_e = E_b\left(1 - \theta_E \frac{b^2}{hw}\right) \tag{37}$$

for loading in the x_1 direction. The constant θ_E is a shape dependent coefficient that includes other details apart from the width b into the equation. The expression in Eq. (37) is supposed to be asymptotically exact for infinitesimal values of $b/\sqrt{hw}$. To obtain the constant θ_E, numerical values of E_e for single pore geometries for different pore sizes are calculated using the finite element method. A power expansion for small pores gives the expression,

$$(\frac{E_e}{E_b} - 1)\frac{hw}{b^2} = \alpha_1 + \alpha_2 \frac{b}{\sqrt{hw}} + \alpha_3 \frac{b^2}{hw} + \alpha_4 \left(\frac{b}{\sqrt{hw}}\right)^3 + O\left(\left(\frac{b}{\sqrt{hw}}\right)^4\right). \tag{38}$$

The values α_1 to α_4 are fitted to the numerical values E_e for different pore shapes and orientations in the remote stress. The numerical value θ_E is identified as the coefficient α_1.

For a large body with multiple pores, the effective modulus of elasticity, E_e, may be calculated using the same superposition principle as for the diffusion case. The calculation is performed as

$$E_e = E_b\left(1 - \frac{1}{hw}\sum_{i=1}^{N} \theta_E^{(i)} \left(b^{(i)}\right)^2\right), \tag{39}$$

where summation is performed for N pores. Also here the hypothesis is that the $\theta_E^{(i)}$ can be taken from pores with similar shape.

4 Numerical Analysis

The finite element computations have been performed using the ABAQUS computer program (ABAQUS, 2014). The program offers the possibility to compute elastic deformation and steady-state diffusion. Eq. (3) is the governing equation for diffusion and Eq. (32) is the governing equation for deformation. The boundary value problem is solved for the region $0 \leq x_1 \leq h$ and $0 \leq x_2 \leq w$ using a free mesh composed of trilateral 6-node and quadrilateral 8-node isoparametric elements. Full integration is used. Same element mesh is used for both the diffusion and the deformation problems. A representative case is shown in Fig. 3.

The ratio of the linear extent of adjacent elements are never more than 2 and normally around 1.2. A typical mesh is built up of eight to ten thousand nodes and two to three thousand six-node and eight-node isoparametric plane elements.

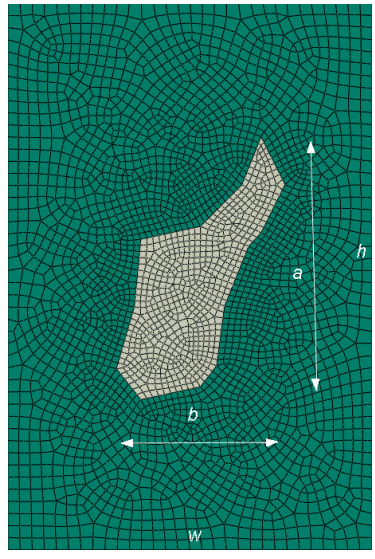

Fig. 3. A typical mesh. Here for pore C' and with $h/a = w/b = 2$. The pore is the central grey area.

5 Results and discussions

A single CT scan image of a bone sample is used, see Fig. 4a. The image is produced by Persson et al. (2013). The image shows a region from an around $1 \times 1 \times 3$ cm^3 bone specimen from a bovine ulna. The x_1-axis is in the radial direction of an cross section shaped as an annular ring and the x_2-axis is along the tangential direction of the bone cross section. The longitudinal direction along the ulna is perpendicular to the plane of the image in Fig. 4a. The x_1-axis goes from the endosteum edge towards the periosteum edge.

The four pores marked A to D are assumed to represent the variety of shapes that are present in a general segment of the bone cross section. Images showing the geometrical details of the selected pores are shown in Fig 4b. It may be noted that only the shapes are considered.

For each shape a series of results for different but small pore sizes are needed. The sizes are assigned for the different calculations by scaling the available shapes. Around eight to eleven different sizes are used. Further, each shape is used for two different, perpendicular orientations of the pore with respect to the remote diffusion and loading. All together around 80 diffusion cases and equally many elastic cases are calculated.

The linear extent of the pores is b perpendicular to the direction of the nominal that is in the vertical direction in Fig 4a, and a in the vertical direction and obviously along the nominal flux. The ratio a/b are from 0.38 for pore A to 0.85 for pore D, see Table 1. The unit of length is in pixels, where the pixel size is close to 4 μm. Table 1 also includes a set of pores A' to D' that are identical to the pores A to D but they are rotated 90° clockwise

with respect to the direction of the nominal flux with a/b are from 2.67 for pore A' to 1.17 for pore D'.

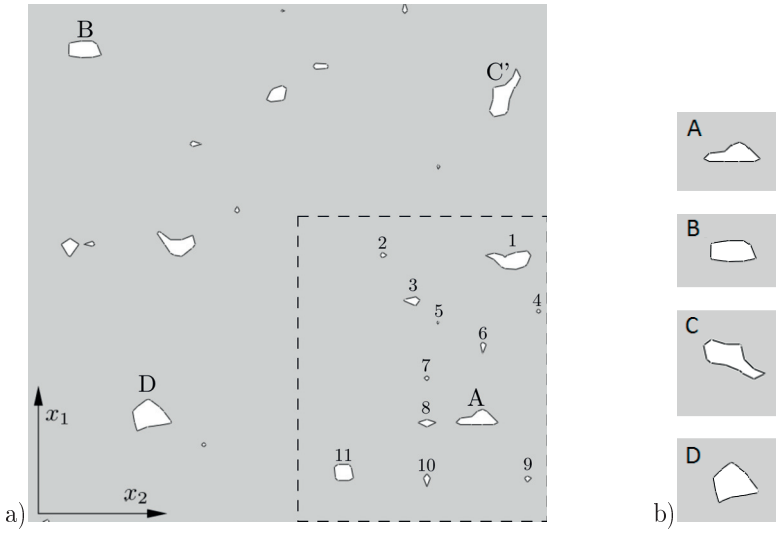

Fig. 4. a) Image of the studied bone sample (Persson et al., 2013). The pores A, B, C, and D are used as reference cases. Evaluation is then performed on the region with numbered pores in the lower right corner of the image (marked with a rectangle). b) details of pores A, B, C, and D.

Table 1: Data for the pores A to D and their counterparts A' to D' that are rotated 90°. Length scale is in units of pixel size.

Case	a	b	a/b	A_p
A	3	8	0.38	12
B	3	6	0.50	15
C	6	9	0.67	21
D	6	7	0.85	24
D'	7	6	1.17	24
C'	9	6	1.50	21
B'	6	3	2.00	15
A'	8	3	2.67	12

5.1 Diffusion coefficient results

The calculations are performed for a ratio of the diffusion coefficient in water versus that in bone of $D_w/D_b = 20000$. The distribution of the normalised concentration inside the computed region is shown in Fig. 5. The geometry corresponds to that one found in Fig.

3. The pore is displayed as the dashed curve in Fig. 5. The extent of the geometry is $h \times w$. The side ratio of the geometry is the same as the ratio of the pore size meaning that $a/b = h/w$. Fig. 5 shows the distributed concentration for pore C'. The extent of the area of the pore versus that of the geometry is $A_p/hw = 0.09$. One readily observes how the flux in the neighbourhood of the pore diverts from uniaxial flux and approaches the pore.

The colours represent constant concentration. The increased diffusion rate in the neighbourhood of the pore, reveals itself as an increase of the distances between the colour contours. The flux direction is perpendicular to the concentration levels as indicated by the inserted arrows. The nominally vertical diffusion is observed to be diverted towards the pore. Obviously the increased diffusion rate also increases in a region surrounding the pore. Closer to the all four edges of the geometry, the diffusion is less affected by the presence of the pore. The affected region seems to be a few times the extent of the pore (see Fig. 5).

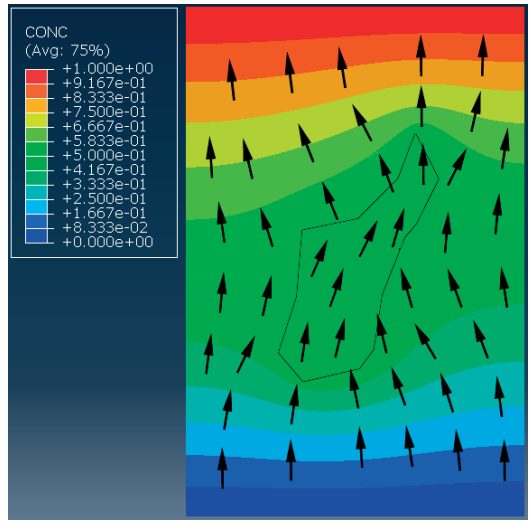

Fig. 5. Distribution of the concentration. The nominal flux is vertical. The dashed region is pore C' with an around 20000 times larger diffusivity than the surrounding bone.

The calculated normalized average flux, $J_a h/(D_b \Delta c)$, where Δc is the difference in concentration between $x_1 = 0$ and $x_1 = h$ for different flow directions and different pore sizes, is displayed in Fig. 6. The nominal flux, i.e. the flux for $\sqrt{A_p/hw} = 0$ is $Jh/(D_b \Delta c) = 1$. Fig. 6 shows that the flux as expected increases with increasing pore sizes. As an example, when the area of the pore is 30% of the area of the computed area, the flux is in the region of around 5% to 80% larger than the nominal flux in the absence of a pore. When the area of the pore is 40% of the computed area, the flux is as much as two times the nominal flux.

The quantity $\tilde{\theta} = (\dfrac{D_e}{D_b} - 1)\dfrac{hw}{sA_p}$, where D_e is defined according to Eq. (27) is shown in

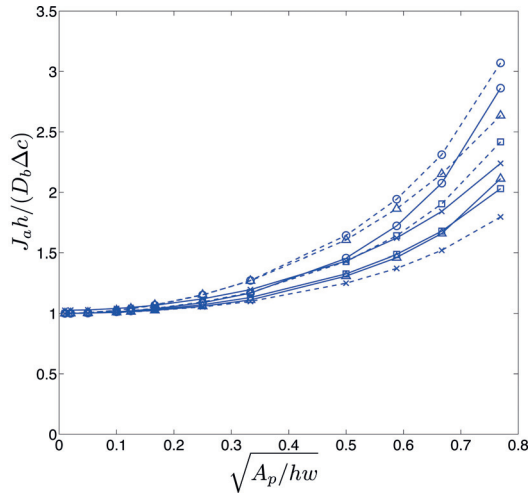

Fig. 6. Normalised average flux $J_a h/(D_b \Delta c)$ for pores A (□) , B (○), C (△) and D (×) (solid lines) and A' to D' with markers as the corresponding pores A to D (dashed lines) as a function of the pore size $\sqrt{A_p/hw}$.

Fig. 7 as a function of the pore size, i.e. $\tilde{\theta} = \tilde{\theta}(\sqrt{A_p/hw})$. As expected the result depends on the shape of the pore. The parameter θ, according to Eq. (23), is obtained as

$$\theta = \lim_{\frac{A_p}{hw} \to 0} \tilde{\theta}\,. \tag{40}$$

To achieve a reliable results, the numerical values for $\tilde{\theta}$, that are vitiated with scatter that is exceptionally strong for small pores, are replaced with the series expansion Eq. (25). A Matlab function that employs the least square fit is used to find the coefficients, α_1 to α_4.

The coefficients $\theta = \alpha_1$ and $\kappa = \dfrac{\alpha_2}{\theta s}$ are given in Table 2.

Table 2: θ and κ values for the pores A to D and A' to D'.

Case	A	B	C	D	A'	B'	C'	D'
$\theta = \alpha_1$	1.60	1.50	3.80	2.00	4.50	3.00	2.20	2.60
$\kappa = \dfrac{\alpha_2}{\theta s}$	-1.10	-.05	-0.11	-0.11	-0.01	-0.16	-0.02	-0.09

The result is summarized in Fig. 8. A clear trend is observed from the present calculations. The θ increases as the aspect ratio a/b increases but with some scatter. The result from a series of six rectangular pores is examined. As in pores A to D', The diffusivity for the rectangular pores is measured in the x_1 and x_2 directions. The series has a smaller scatter which indicates that there are more influential details regarding the shape than merely the aspect ratio (c.f. Fig. 8).

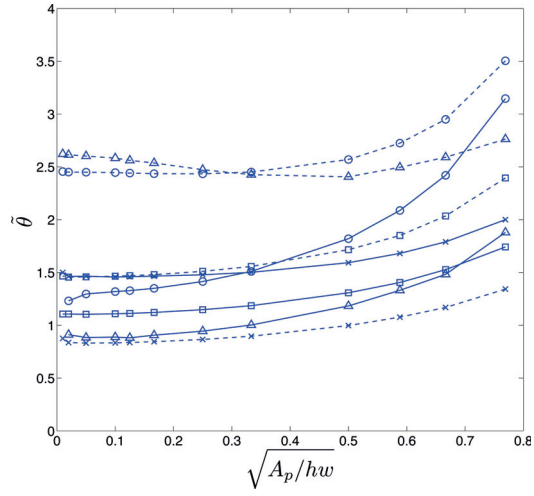

Fig. 7. Influence of factor $\tilde{\theta}$ for pores A (□) , B (○), C (△) and D (×) (solid lines) and A' to D' with markers as the corresponding pores A to D (dashed lines) as a function of the pore size $\sqrt{A_p/hw}$.

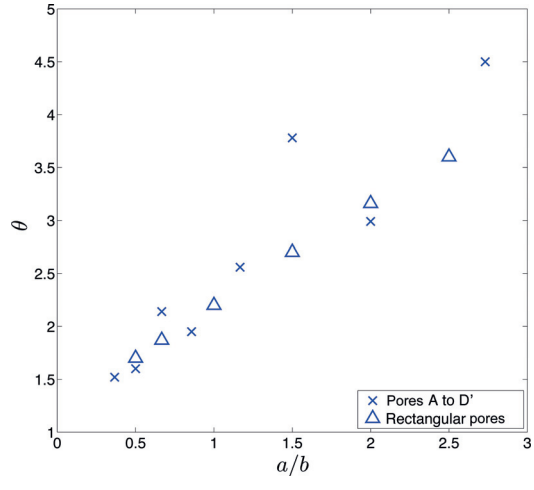

Fig. 8. θ versus the shape ratio a/b for pores A to D and A' to D' (makers ×). The θ for six rectangular pores with $a/b = 2.5, 2, 1.5, 1, 0.67, 0.5$ are also included (markers △).

5.2 Elastic modulus results

Calculation of the elastic modulus of a region containing a single pore is performed along the same lines as for the diffusion analysis. The modulus of elasticity of the bone is E_b and Poisson's ratio is $\nu = 0.3$. The displacement difference of two opposed edges, separated by the distance h, is Δu. Plane stress is assumed. The material in the pore is assumed to lack stiffness, meaning that the body is treated as a hollow section.

The distribution of the normalised largest principal stresses $\sigma_1 h/E_b\Delta u$ for pore C', for which $a/b = 1.5$, is shown in Fig. 9. The figure shows that stresses are high at two points on the edges of the pore. Here the stress is expected to be high but is probably overestimated because of the rather course mesh that is used in the vicinity of the pore. The reason for the course mesh is that the pore geometry is given by only 21 pixels and therefore the details of the pore geometry are unknown.

The stress distribution along the edges of the body is fairly homogeneous and close to the nominal value $\sigma_1 h/E_b\Delta u = 1$, which shows that the disturbance of the remote uniaxial stress field is more or less localised to a limited region around the pore.

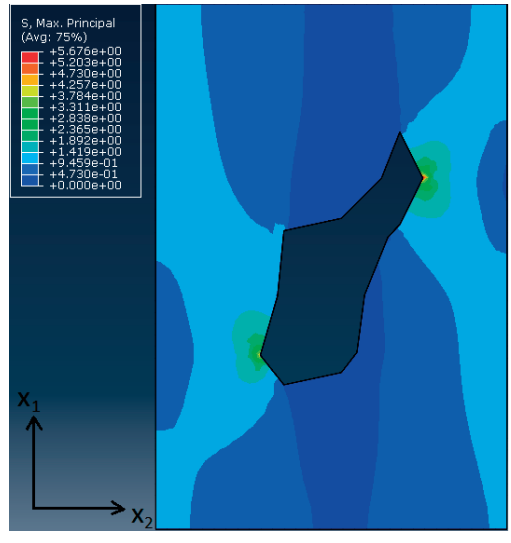

Fig. 9. Distribution of the largest principal stress $\sigma_1 h/E_b\Delta u$ for pore C' with $a/b = 1.5$. The nominal loading is in the x_1 direction.

The average stress for different loading directions and different pore sizes is shown in Fig. 10. With the nominal stress $\sigma_b = E_b\Delta u/h$, the effective stress versus nominal stress ratio $\sigma_e/\sigma_b = E_e/E_b$. The effective stress σ_e is obtained from the finite element calculations. As expected, the figure shows that the stress decreases as the pore size increases. For small pores ($\sqrt{A_p/hw} < 0.3$) the result seems to follow a power whereas for larger pore sizes the resulting stress (and stiffness) decays approximately linear towards zero at $\sqrt{A_p/hw} = 1$,

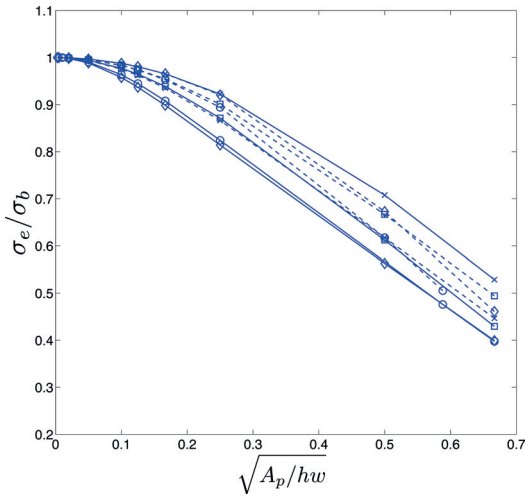

Fig. 10. Computed average normalised stress σ_e/σ_b for pores A (□) , B (○), C (△) and D (×) (solid lines) and A' to D' with markers as the corresponding pores A to D (dashed lines) for different pore sizes $\sqrt{A_p/hw}$. σ_b is the stress in bone without a pore.

i.e. when the pore is crossing the entire computed body.

The obtained $\tilde{\theta}_E$ for different $\sqrt{A_p/hw}$ values is shown in Fig. 11. As shown in the figure, the resulting $\tilde{\theta}_E$ is dependent on the pore shape. Further, $\tilde{\theta}_E$ decreases as the pore size increases which is an expected consequence of the switch off behaviour of the stress size dependence described in previous paragraph.

The obtained θ for the eight pores A to D' versus the ratio a/b is shown in Fig. 12. A couple of diverging results are observed. Both are for the slender pores A and C when the nominal stress is along the longest side of the pore, which is b for both. It is known from crack mechanics that energy released at the introduction of a crack vanishes for a crack that is parallel with the loading direction and reaches a maximum if the crack is perpendicular to the loading direction. The exact result for a crack is $\theta_E = \pi/2$. The known result $\theta_E = 8/\pi$ for a circular pore is added to Fig. 11. The result is obtained by using the the analytical solution for an infinite stretched plane body with a circular hole cf. (Muskhelishvili, 1953) For pores with $a > b$ the nominal stress is parallel with the longer direction a while the Eq. (37), that defines the θ_E, only involves the side length b. This inadvertence might influence the results in the way observed.

6 Qualifying examples

The method is qualified by applying the superposition technique on a real cases for diffusion coefficient and elastic modulus. The porous region of the image in Fig. 4 is chosen. The region is recognised as the region with numbered pores A and 1 to 11, marked with the

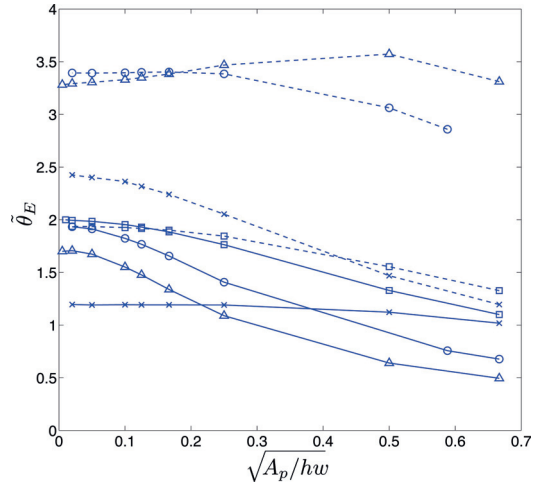

Fig. 11. Influence factor $\tilde{\theta}_E$ for pores A (□) , B (○), C (△) and D (×) (solid lines) and A' to D' with markers as the corresponding pores A to D (dashed lines) for different pore sizes $\sqrt{A_p/hw}$.

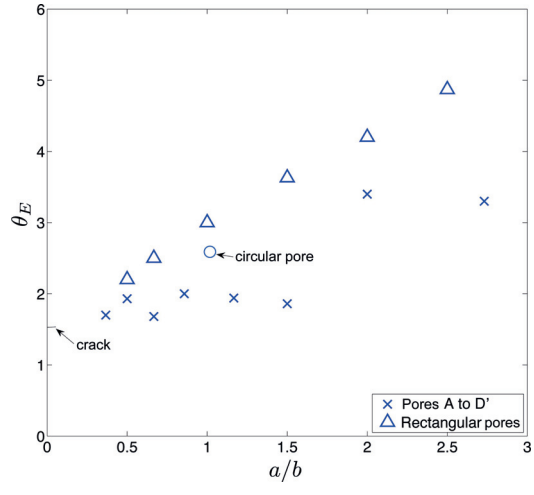

Fig. 12. θ_E versus the shape ratio a/b for pores A to D' with markers (×). The θ_E for six rectangular pores with side ratios $a/b = 2.5, 2, 1.5, 1, 0.5, 0.67$ are also presented here with markers (△). The side length is a in the direction of the load. The known limit result as $a/b \to 0$, i.e. for a pure crack, is $\theta_E = \dfrac{\pi}{2}$ as indicated.

rectangle. Regarding diffusion, a finite element calculation was performed using 17682 8-noded isoparametric elements. The resulting diffusion coefficient was found to be $D_{e,\mathrm{FEM}} = 1.033D_b$ in the radial (x_1) direction, and $1.071D_b$ the tangential (x_2) direction. This is compared with the superposition technique represented by the Eq. (29) with the result $D_{e,sup} = 1.030D_b$, and $1.068D_b$ in radial and tangential directions respectively. The focus here is on the correction of the diffusion coefficient of the bone D_b. The relative correction due to the superposition technique versus the finite element calculations for diffusion in the radial direction is $0.03/0.033 = 0.91$. In the tangential direction the corresponding figure is $0.068/0.071 = 0.96$, i.e. in the radial and tangential directions the superposition technique gives an 9% and 4% smaller correction than the finite element technique. The reason might be that there is an interaction between the pores that is not fully captured.

For the elastic modulus part, the finite element calculation was performed using 16579 8-noded isoparametric elements. The resulting elastic modulus was found to be $E_{e,\mathrm{FEM}} = 0.895E_b$ in the radial direction and $0.955E_b$ in the tangential direction. The superposition technique gives $E_{e,sup} = 0.889E_b$ in the radial direction and $0.948E_b$ in the tangential direction. The ratio of the correction due to the superposition technique is 6% for the radial direction and 16% for the tangential direction, larger than the correction obtained from the the finite element method. The reason for these differences regarding diffusion coefficient and elastic modulus is for the presence somewhat unclear.

The error that is made by assuming that the pores are small leads to an underestimated θ for the diffusion case and an overestimated θ_E for the elastic case. This would lead in the direction of the obtained result and could at least partly explain the results.

7 Conclusions

Superposition principles are derived that employ dimensional scaling of material parameters. The result, that is asymptotically exact for infinitesimal pores, is used to formulate a method for simplified calculations of material parameters for diffusion and deformation of sparsely porous materials. The diffusion coefficient of Fick′s law and the elastic modulus of Hooke′s law are studied.

The method is evaluated on bovine ulnae regarding both the diffusion and deformation. The superposition results are compared with full scale finite element results. Specifically, the change of the diffusion coefficient and the change of the elastic modulus because of the presence of pores, are compared with the corresponding finite element results. The result of the superposition principle for diffusion deviate from 4 to 9% from the finite element result. The corresponding deviations for the elastic modulus are 6 to 16%. The method seems to fulfil the requirements that the pores should be sparse when ratio of pore volume and total volume is less than 20%.

References

ABAQUS, V., 2014. 6.14 documentation. Dassault Systemes Simulia Corporation.

Baron, C., Talmant, M., Laugier, P., 2007. Effect of porosity on effective diagonal stiffness coefficients (c_{ii}) and elastic anisotropy of cortical bone at 1mhz: a finite-difference time domain study. The Journal of the Acoustical Society of America 122 (3), 1810–1817.

Biot, M. A., 1941. General theory of three-dimensional consolidation. Journal of applied physics 12 (2), 155–164.

Cowin, S. C., 2003. A recasting of anisotropic poroelasticity in matrices of tensor components. Transport in porous media 50 (1-2), 35–56.

Grimal, Q., Rus, G., Parnell, W. J., Laugier, P., 2011. A two-parameter model of the effective elastic tensor for cortical bone. Journal of biomechanics 44 (8), 1621–1625.

Li, W., You, L., Schaffler, M. B., Wang, L., 2009. The dependency of solute diffusion on molecular weight and shape in intact bone. Bone 45 (5), 1017–1023.

Lindberg, G., Shokry, A., Reheman, W., Svensson, I., 2014. Determination of diffusion coefficients in bovine bone by means of conductivity measurement. International Journal of Experimental and Computational Biomechanics 2 (4), 324–342.

Marcus, R. M., et al., 2013. Osteoporosis. Oxford, Academic Press.

Marinozzi, F., Bini, F., Marinozzi, A., 2014a. Water uptake and swelling in single trabeculæ from human femur head. Biomatter 4 (1).

Marinozzi, F., Bini, F., Quintino, A., Corcione, M., Marinozzi, A., 2014b. Experimental study of diffusion coefficients of water through the collagen: Apatite porosity in human trabecular bone tissue. BioMed research international 2014.

Muskhelishvili, N., 1953. Some Basic Problems of the Mathematical Theory of Elasticity. P. Noordhoff Ltd. Groningen, Holland.

Patel, R., O'Leary, J., Bhatt, S., Vasnja, A., Knothe Tate, M., 2004. Determing the permeability of cortical bone at multiple length scales using fluorescence recovery after photobleaching techniques. In: Proc 51st Annual ORS Meeting. Vol. 141.

Persson, C., Isaksson, P., Ståhle, P., 2013. CT images. Researchgate, URL http://dx.doi.org/10.13140/RG.2.1.3961.8082.

Rice, J. R., Cleary, M. P., 1976. Some basic stress diffusion solutions for fluid-saturated elastic porous media with compressible constituents. Reviews of Geophysics 14 (2), 227–241.

Schaffler, M. B., Burr, D. B., 1988. Stiffness of compact bone: effects of porosity and density. Journal of biomechanics 21 (1), 13–16.

Showalter, R., 2000. Diffusion in poro-elastic media. Journal of mathematical analysis and applications 251 (1), 310–340.

Wang, L., Wang, Y., Han, Y., Henderson, S. C., Majeska, R. J., Weinbaum, S., Schaffler, M. B., 2005. In situ measurement of solute transport in the bone lacunar-canalicular system. Proceedings of the National Academy of Sciences of the United States of America 102 (33), 11911–11916.

Winkelstein, B. A., 2012. Orthopaedic Biomechanics. CRC Press, FL, USA.